Sensitivity of Tropical Cyclones in the Southwest Indian Ocean to the Topography of Madagascar

Zachary Christensen

Supervisors: Prof. Chris Reason, Dr. Ross Blamey and Dr. Rondrotiana Barimalala

This dissertation is submitted in fulfillment of the requirements for the degree.

of

Master of Science

in

Ocean and Atmospheric Science

Department of Oceanography

University of Cape Town University

Plagiarism Declaration

I understand the nature of plagiarism and am aware of the University of Cape Town's policy on this. I certify that this master's dissertation reports original work by me during my time at the University of Cape Town.

Signed by candidate

Zachary Christensen

Signed by: 3a8a4bf6-727c-4149-a155-b6145ad9e2e5

Acknowledgments

I would like to first thank my supervisor, Professor Chris Reason, for his immense patience and guidance in this master's thesis. I would also like to thank Dr. Blamey and Dr. Barimalala for their help in working through the challenges of Python and for conversations regarding how to tell a proper story. I am also immensely grateful to my friends and coworkers who helped encourage and support me through this process. Finally, I would like to thank my mom and dad, whose never-ending support and motivation have pushed me to become a better person and strive for the best in life.

Abstract

In this study, simulations from the Weather Research and Forecasting (WRF) model are used to investigate the sensitivity of tropical cyclone (TC) characteristics in the Southwest Indian Ocean (SWIO) to the presence of Madagascar topography. This is achieved through running two sensitivity experiments where the topography is i) flattened to a uniform plateau of 300 m height (FLAT run) or ii) ocean grid points completely replace Madagascar with sea surface temperatures (SST) interpolated from the neighboring South Indian Ocean (SEA). These are then compared to the control run (CNTRL), where the topography is unchanged. Each run receives the same boundary conditions at the surface and lateral boundaries from the Climate Forecast System Reanalysis version 2. In terms of model evaluation, the background climatology of the CNTRL run compares reasonably well with the modern European Centre for Medium-Range Weather Forecasts reanalysis data (ERA5). The model outputs are then run through the TRACK-1.5.2 program to identify and track TCs. It is found that the TC characteristics in CNTRL are reasonable when compared to those found in observations, which are provided by the International Best Track Archive for Climate Stewardship. Based on WRF being able to adequately represent the track and regional atmospheric circulation, the analysis of TC genesis and tracks in the three WRF runs indicates that these weather systems are sensitive to the Madagascan mountains. Each sensitivity run showed cyclonic high-pressure anomalies across southern Madagascar and enhanced low-level easterly winds, possibly from an enhanced South Indian Ocean high pressure system, causing TCs to track further westward into Mozambique when the mountains are either flattened or removed completely. Additionally, the SEA shows considerably more TCs generated in the far west of the basin, which are stronger than CNTRL and tend to follow a more zonal track towards and onto the mainland. These differences relate to Madagascar being replaced by warm SST with increased latent heat release. The results suggest that the island of Madagascar plays an important role in the tracks, intensity, and numbers of TCs found in the real world in the Mozambique Channel (MC) region.

Table of Contents

Figure Captions and Tables

List of Acronyms and Abbreviations

AEJ-S	African Easterly Jet (Southern Hemisphere)
AL	Angola low
BH	Botswana high
CFSRV2	Climate Forecast System Reanalysis version 2
DJFM	December January February March
ENSO	El Niño Southern Oscillation
ERA5	European Centre for Medium-Range Weather Forecasts Reanalysis V5
GCM	Global Climatology Models
GPH	Geopotential Height
IBTrACS	International Best Track Archive for Climate Stewardship
ITCZ	Intertropical Convergence Zone
MC	Mozambique Channel
MCT	Mozambique Channel Trough
NCAR	National Center for Atmospheric Research
NOAA	National Oceanic and Atmospheric Administration
OLR	Outgoing Longwave Radiation
RSMC	Regional Specialized Meteorological Centre
SICZ	South Indian Convergence Zone
SIHP	South Indian High Pressure
SST	Sea Surface Temperature
STJ-S	Subtropical Westerly Jet (Southern Hemisphere)

SWIO	Southwest Indian Ocean
TC	Tropical cyclones
TRB	Tropical Rain Belt
UTC	Coordinated Universal Time
VWS	Vertical Wind Shear
WRF	Weather Research and Forecasting

Chapter 1

1. Introduction

Over the last 50 years, the World Meteorological Office has found that tropical cyclones (TCs) produced, on average, around 43 deaths and about US$ 78 million in damages on a daily basis worldwide (World Meteorological Organization, 2022). These large, compact, circular convective systems are found to bring extreme destruction and hazardous impacts to communities through flooding, extreme winds, tornadoes, lighting, and storm surges. These natural disasters are even more devastating for economically disadvantaged communities whose infrastructure cannot withstand these intense convective systems.

Countries like Madagascar and Mozambique are greatly influenced by the rain and storm surges a TC creates in the SWIO. Madagascar, which is located in the middle of the TC average track, has been affected by a number of large-scale systems, causing extensive damage and fatalities (Jury, 1993; Naeraa and Jury, 1998; Reason and Keibel, 2004; Klinman and Reason, 2008; Chang-Seng and Jury, 2010). Mozambique, however, is found to be marginally blocked from direct TC trajectories, with landfall being less frequent due to the storm's interactions with Madagascar's terrain (Jury and Pathack, 1991; Jury, 1993; Vitart et al., 2003; Reason and Keibel, 2004). While it is rarer for TCs formed in the Mozambique Channel (MC) to make landfall, it has happened before. For instance, TC Dera in March 2001 resulted in significant property damage and flooding in Mozambique after already dealing with the aftermath of the previous TC impact earlier in that season (Reason, 2007). Due to their economic hardship, many of these countries rely heavily on agriculture for food and profit (Brown, 2009). Powerful storm surges, winds, and heavy rain accompanying TCs can then lead to widespread mudslides and crop mortality, resulting in property destruction and famine across the country (Naeraa and Jury, 1998; Brown, 2009). Within an average season, TCs within the SWIO are found to track on a southwestward trajectory, returning to the SWIO once they interact with Madagascar's steep topography. Over the last 50 years, only 5% of storms were found to make landfall in Southern Africa, with even fewer moving further

inland due to the 1–1.5-km plateau and relatively dry surface conditions within the region (Reason and Keibel, 2004). However, within the last few decades, storms such as TC Eline (February 2000), TC Favio (February 2007), and TC Idai (March 2019) have been influenced by Madagascar's topography before moving into Mozambique and causing significant damage to the surrounding communities. TC Eline alone was shown to track through most of southern Africa for about four weeks before dissipating in southern Namibia. This TC was found to displace more than 500,000 people altogether and led to roughly 1,000 deaths (Reason and Keibel, 2004). Previous studies have found similar severe weather systems such as TC Eline have contributed to significant rainfall and storm surges, impacting millions of people from these communities (e.g., Reason and Keibel, 2004; Klinman and Reason, 2008; Moses and Ramotonto, 2018; Rapolaki and Reason, 2018)

With the significant damage to property and life TCs bring, very little research has been done on understanding TC trajectories and their sensitivities towards terrain such as Madagascar. However, Madagascar has been seen to influence the regional scale climate variables such as the Mozambique Channel Trough (MCT) and its impacts on southern African rainfall (e.g., Barimalala et al., 2018; 2020). These studies showed how Madagascar's terrain plays a major role in the moisture transport into southern Africa, acting as a blocking feature toward direct zonal flow (Barimalala et al., 2018; 2020). With significant regional circulation features such as the MCT being affected by Madagascar, a better understanding of the terrain's influence on large-scale, organized, convective systems, such as TCs, is needed.

It remains unclear how the terrain of Madagascar influences the trajectory of TCs in the SWIO. Most studies have focused on individual storm analysis using regional numerical models to understand the primary regional climatic factors leading to the TC trajectory (Jury et al., 1993; Naeraa and Jury, 1998; Reason and Keibel, 2004; Klinman and Reason, 2008). However, this idealized study uses regional numerical modeling to understand TC sensitivities toward Madagascar's terrain over a period of 16 seasons. Analyzing these TC tracks over a longer time period will allow for a better understanding of how this terrain of Madagascar might affect TC tracks within the SWIO and the MC.

Chapter 2

2. Literature Review

2.1 Tropical Cyclone Definition

In this chapter, TC characteristics, seasonality trends, and large-scale factors leading to their development in the SWIO are discussed. Where relevant, comparisons are made with TCs in other regions.

On a global scale, TCs are defined as well-constructed, nearly circular, warm-cored convective systems that circulate over warm tropical water and low-pressure areas (World Meteorological Office, 2022). A TC creates a cyclonic low-pressure rotation that is clockwise in the Northern Hemisphere and counterclockwise in the Southern Hemisphere forming a warm core or eye wall at the center of the storm (Fink and Speth, 1998). Although the structure can extend up to 1000 km in diameter, it usually falls anywhere between 200 to 500 km on average, reaching a minimum central pressure of around 950hPa (Pezza and Simmonds, 2005; World Meteorological Office, 2022)

Although tropical cyclones are the generic name, they are formally called typhoons in the Northwest Pacific and hurricanes in the North Atlantic or Northeast Pacific. Monitored mostly by the National Hurricane Center or the Central Pacific Hurricane Center and organized based on the Saffir–Simpson scale (National Hurricane Operations Plan, 2022). Typhoons are categorized based on the Regional Specialized Meteorological Centre (RSMC) Tokyo's Tropical Cyclone Intensity Scale. Finally, those located in the Southwest Pacific, South Indian, and North Indian Oceans are referred to as tropical cyclones. In the SWIO, RSMC of La Réunion uses the Météo-France Tropical Cyclone Wind Scale. This scale ranges from a Tropical Disturbance (>50 $km \cdot h^{-1}$ or >13 $m \cdot s^{-1}$) to a very intense tropical cyclone (>212 $km \cdot h^{-1}$or > 60 $m \cdot s^{-1}$). These storms are categorized using a 1-min or 10-min surface-based maximum sustained wind speed based on the

wind scale that is used in the region. The RSMC utilized the 10-minute surface maximum wind speed and identified anything above 17 $m \cdot s^{-1}$ or 61.2 $km \cdot h^{-1}$ as a tropical storm, giving it an official name.

2.2 Global Life Cycle of Tropical Cyclones

2.2.1 Genesis

A TC life cycle can be broken down into formation, development, and dissipation, requiring specific environmental conditions. Pielke (1990) and Gray (1968) suggested the necessary criteria that need to be met for cyclogenesis anywhere in the tropical oceans as:

(i) Significant values of negative low-level relative vorticity.

(ii) Location at least 4-5° from the equator so that Coriolis is strong enough to create poleward motion.

(iii) Weak vertical shear allows for vertical convection and the development of a low-level core and upright vortex.

(iv) SST exceeding 26°C and deep thermocline (60 meters or more).

(v) Atmospheric instability in the lower and mid-levels.

(vi) Significant relative humidity values throughout the surface and middle troposphere, allowing for increased moisture content.

However, more recent literature has discussed exceptions from these criteria (Watterson et al., 1995; Schreck et al., 2014; Pillay and Fitchett, 2021). Studies have found once specifying to the Southern Hemisphere, ideal conditions amongst variables such as SST can rise to about 27-28°C, with the minimum running at 24°C (Dare and McBride, 2011; Defforge and Merlis 2017; Pillay and Fitchett, 2021). This analysis has found that the regions where TCs are found may each have slightly different conditions for TC genesis.

2.2.2 Tracks

Typically, after genesis, TCs track westward under the influence of the easterly trade winds and then, when the Coriolis effect becomes sufficiently strong, curve poleward (Rossby, 1949; Gray, 1998) (**Fig. 2.1**).

2.2.3 Lysis

Finally, the dissipation of TCs begins once the storm loses its energy source as it tracks, which is typically after landfall. These factors can cause slow or rapid dissipation in wind strength, destroying the warm central core of the TC (Weatherford, 1989; Emanuel, 2003). While there are examples of TCs crossing islands and maintaining their strength or recurving back from the land to the ocean before intensifying once again, significant topography often rapidly weakens landfalling storms. For example, TCs tracking over southern or central Mozambique usually are found to weaken substantially after encountering the Drakensberg Mountains in northern South Africa or the Chimanimani Mountains in eastern Zimbabwe (Takong and Abiodun, 2022)

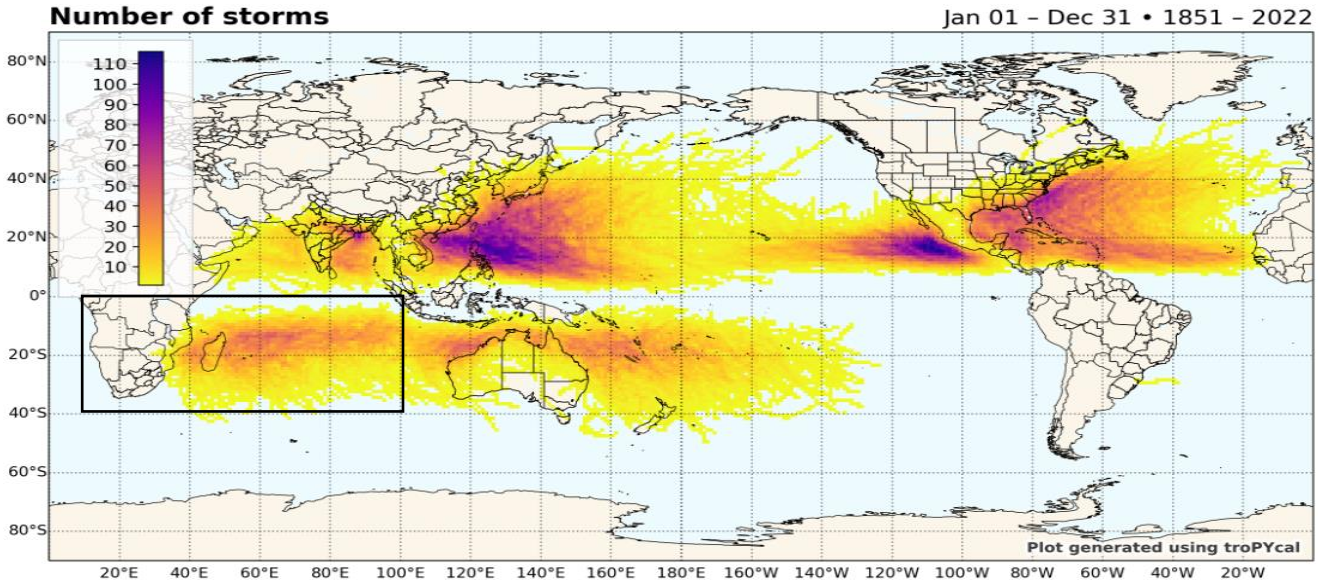

Figure 2.1: Total TC density per 1° grid box worldwide. Data provided by IBTrACS data sets. The black box outlines the SWIO domain utilized within this study.

2.3. Tropical Cyclones in the Southwest Indian Ocean

2.3.1 Regional Seasonality of Tropical Cyclone Tracks

The observed best-track data used to study seasonal and decadal trends of a TC within the SWIO is pulled from the International Best Track Archive for Climate Stewardship (IBTrACS; Knapp et al., 2010). The National Oceanic and Atmospheric Administration (NOAA) first developed this observed track data by combining the best track data sets worldwide from organizations such as Tropical Cyclone Warning Centers, the World Meteorological Office, and the RSMCs. This data compiles the latitude and longitude points of every storm track globally. Each storm then has additional data, such as maximum wind speed and minimum central pressure, collected and stored at a 6-hour interval in coordinated universal time (UTC). **Figure 2.2** is used to show the observed trends of TCs from 1979 to the present; although IBTrACS was collected as early as 1851, this data set was cut due to the common use of satellites past 1979, allowing organizations to track storm progression more accurately.

TCs in the SWIO (0 – 40°S; 30 – 100°E) (**Fig. 2.1; Black Box**) occur on average 12 – 13 times per season (west of 100°E), with the majority of TCs forming from tropical depressions into TCs and lasting on average about nine days (**Table 1**) (Jury et al., 1999; Fink and Speth, 1998; Mavume et al., 2010). The cyclone seasons typically take place during the austral summer (November-April), with seasonal peaks happening around January 1st to March 31st (**Fig. 2.3**) (Jury et al., 1999; Vitart et al., 2003; Mavume et al., 2009). TC genesis is found to mostly occur east of Madagascar (50 – 100°E, 5 – 15°S), with only 10% originating in the MC, causing many studies to omit these storms in their climatological data sets (e.g., Jury, 1993; Jury et al., 1999; Chang-Seng and Jury, 2010; Ash and Matyas, 2012).

TCs post genesis are found to follow a westward trajectory pattern towards land due to enhanced zonal flow brought on by easterly trade winds (Vitart et al., 2003). As they approach land (i.e., Madagascar), a TC tends to follow a poleward (southeastward) trajectory, recurving back towards the SWIO, quickly dying off once interacting with the strong westerly trade winds 30°S (Parker and Jury, 1999; Vitart et al., 2003; Chang-Seng and Jury, 2010) (**Fig. 2.2**). Those found to cross into or form within the MC are seen to track southward before recurving southeastward out of the

channel (e.g., Jury and Pathack, 1991; Chikoore et al., 2015; Matyas, 2015) (**Fig. 2.2**). More recently, storms such as TC Eline and TC Favio have been found to continue inland, penetrating landfall. However, these rare storm occurrences were found to be due to specific environmental conditions, such as enhanced westerly zonal steering flow and high-pressure systems south of Madagascar, leading to these storms' tracking further inland (Vitart et al., 2003; Reason and Keibel, 2004; Klinman and Reason, 2008)

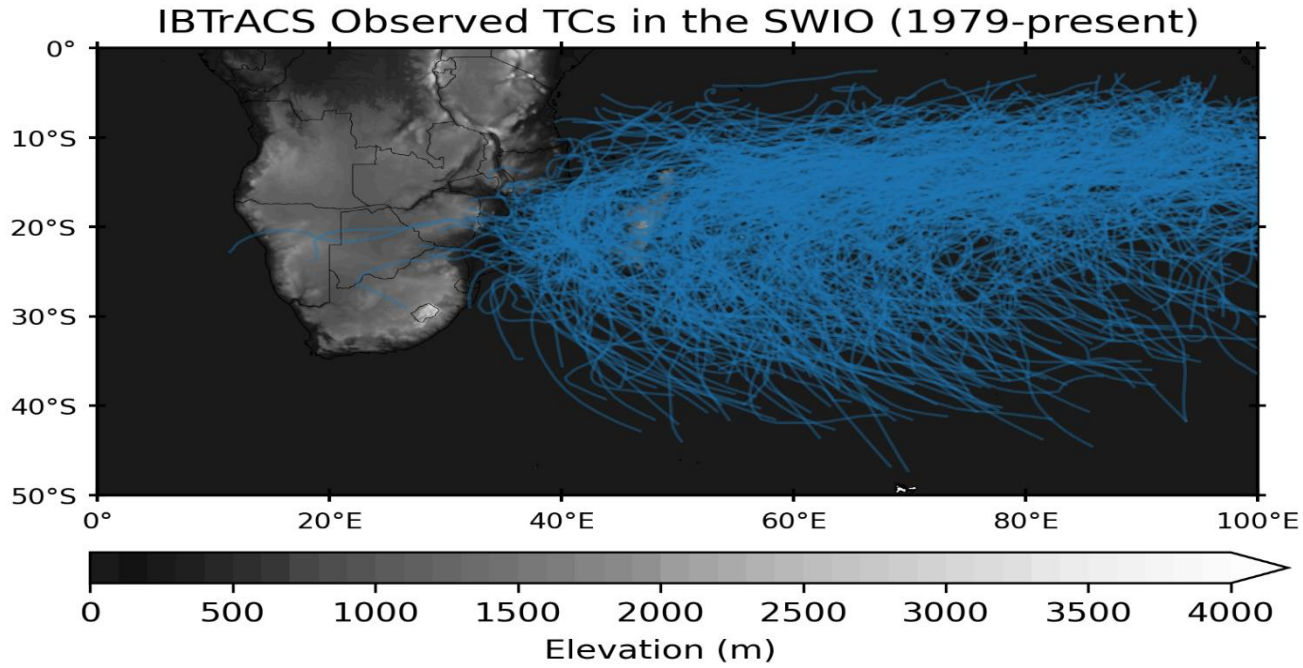

Figure 2.2: All IBTrACS storm tracks (1979–2023) tracking through the SWIO. (Generated from IBTrACS archive data)

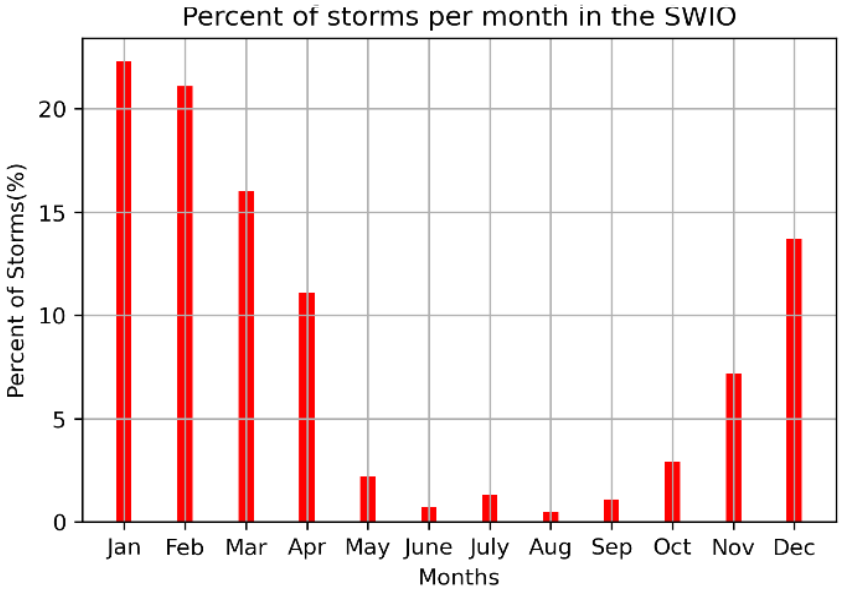

Figure 2.3: Percentage of IBTrACS storm formation (1979–2023) organized by the month they occurred. (Generated from IBTrACS archive data)

Duration of TC	Number of Days
Maximum	44
Minimum	0.25
Average	9

Table 1: IBTrACS storms (1979–2023) within the SWIO. The maximum, minimum, and average number of days TCs lasted from genesis to dissipation. (Generated from IBTrACS archive data)

2.4 Regional Circulation Influence on Tropical Cyclones

2.4.1 Tropical Rain Belt over Southern Africa

The Intertropical Convergence Zone or ITCZ is conventionally understood as the convergence of the low-level northeast and southeast trade winds and was seen as the primary system contributing to the distribution of rainfall in Central and West Africa. (Nicholson, 2009; Schneider et al., 2014; Byrne et al., 2018). As noted by Nicholson (2009) and Žagar et al. (2011), the Tropical Rain Belt (TRB) does not always spatially coincide with the ITCZ over land, but from a global perspective, they are tightly coupled and follow the seasonal progression of the sun. The TRB was found to be the primary contributor to West African precipitation contrary to the ITCZ and, therefore, will be used to describe the dominant seasonal movement in rainfall throughout the remaining sections. During the boreal summer, the TRB is found at its furthest point of 15°N, running parallel to the equator and tracking through central and southern Sahel. Proceeding into the austral summer, starting in November, the TRB starts to progress southwards towards southern Africa, reaching its furthest point at 15-18°S during mid-February (Nicholson and Grist, 2003; Reason et al., 2006). During its peak season (February), the TRB penetrates somewhere near southeastern Zambia, central Mozambique, and central Madagascar bringing a strong easterly moisture flux toward land (Nicholson and Grist, 2003; Reason et al., 2006; Suzuki, 2011; Reason, 2017) (**Fig. 2.4**). Through the southern African continent, the TRB is found to separate near central Africa and southeastern Zambia, forming a meridional arm that is developed through the presence of the Angola low (AL).

This arm pushes northward through the Congo basin before existing north of the Gulf of Guinea coast (Reason, 2017) (**Fig. 2.4**).

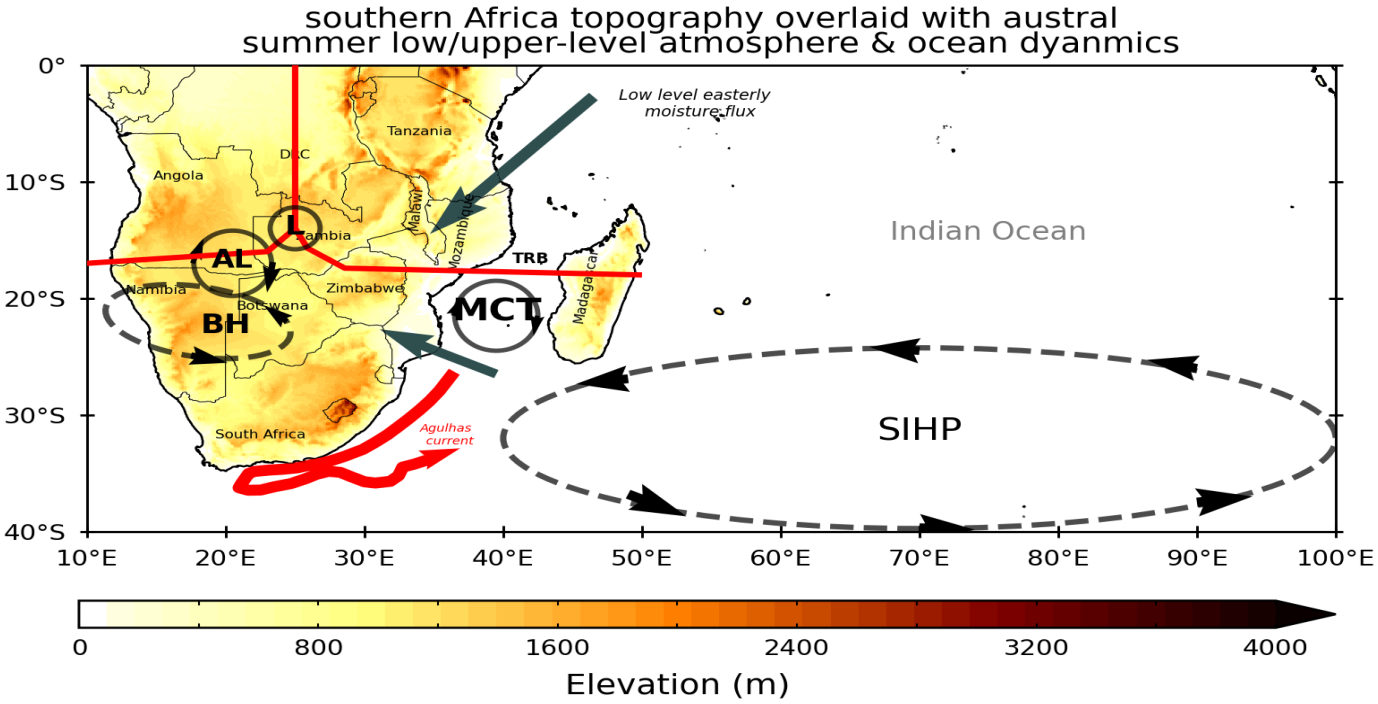

Figure 2.4: Schematic showing the primary oceanographic and atmospheric features important to moisture and wind variability in the SWIO and southern Africa during the austral summer. The grey arrows off either side of Madagascar represent low-level easterly moisture flux, MCT denotes the Mozambique channel trough, the SIHP denotes the South Indian high pressure, the red curved arrow featured off South Africa denotes the Agulhas current, the AL and BH denote the Angola low and Botswana high, and finally, symbol (L) denotes a low pressure with the red line running through Madagascar and into southern Africa to represent the Tropical Rain Belt (TRB).

The TRB intensity and location have been found to have strong influences on the southern African climate, specifically inland rainfall and moisture flux from the SWIO, leading to wet summer seasons (Cook et al., 2004; Reason et al., 2006; Suzuki, 2011). During the peak TC season (February), the TRB sits at its most southern point (18°S), increasing the probability of TC genesis within the region through optimal convective variables. Surrounding the rain belt, more than 50% of TCs are found to form within 600 km brought on by cyclogenesis features such as high relative vorticity, tropospheric humidity, low vertical wind shear (VWS), and enhanced easterly moisture flux (Gray, 1968; Jury and Pathack, 1991; Jury, 1993; Berry and Reeder, 2014). Studies have

shown that TC cases can vary depending on the intensity and location of the TRB during different seasons (e.g., Arivelo and Lin, 2016). The strength of the TRB can then fluctuate seasonally due to the variability of features such as the cross-equatorial monsoons, southern oscillation index, quasi-biennial oscillation, Tropical Easterly Jet, and African Westerly Jet. As a result, variations in the intensity and location of TRB can be found to influence cyclogenesis seasonally, allowing for more or less storm developments throughout a given season. (Jury and Pathack, 1991; Jury, 1993; Nicholson, 2009; Matyas, 2015; Arivelo and Lin, 2016).

2.4.2 South Indian High Pressure

The South Indian high pressure (SIHP) or Mascarene High pressure is a semi-permanent, synoptic-scale weather system that contributes to large variations in subtropical convection (**Fig. 2.4**) (Manatsa et al., 2014; Xulu et al., 2020). Created through the southern branch of Hadley cell, enhanced monsoonal heating and subsequent air-sea interactions (Seager et al., 2003). These features then result in strong southeasterly trade winds running roughly at 25°S and a westerly jet stream at about 35°S, creating this strong anticyclonic feature (Xulu et al., 2020). This high-pressure system extends through the south Indian Ocean from 25–35°S to 40–110°E seasonally, standing between the tropical and temperate belts (**Fig. 2.5**) (Manatsa et al., 2014; Xulu et al.,

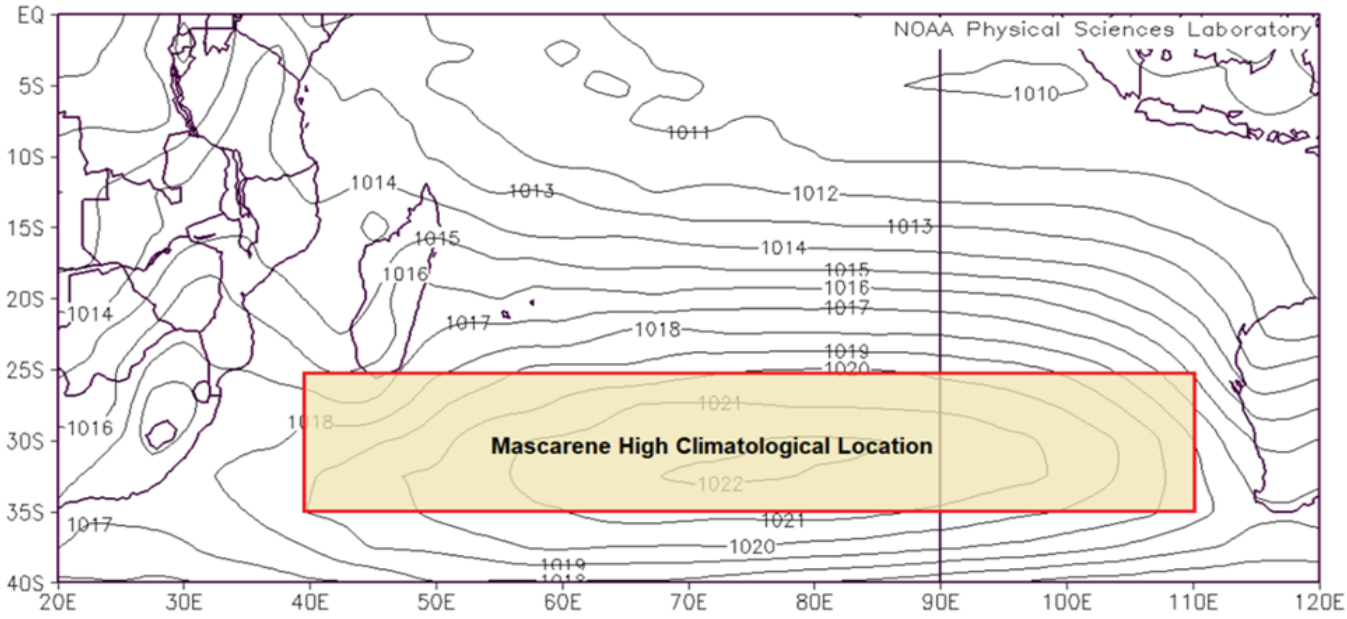

Figure 2.5: Average (mean) MH migration over the SWIO (Generated from NOAA Physical Science Laboratory). (Sourced from Xulu et al., 2020)

2020). Found to reach its furthest distance from southern Africa during the TC peak season (February), at 80°E, and being found to aid in cyclogenesis within the SWIO (Arivelo and Lin, 2016) (**Fig. 2.4**).

During the austral summer (winter), the SIHP is displaced southeastward (northwestward), creating decreased (increased) zonal easterly trade winds as well as decreased (increased) moisture flux pulled from the latent heat release of the Agulhas current surrounding southern Africa; this, along with the equatorward (poleward) displacement, leads to variations in the intensity of features such as the South Indian Convergence Zone (SICZ) and Indian Ocean Dipole leading to a dryer or wetter season within southern Africa. (Manatsa et al., 2014; Ogwang et al., 2015; Xulu et al., 2020). Additionally, features such as the AL also contribute to inland moisture flux and regional convection. In seasons with a strong AL and intense SIHP, a larger north-to-south pressure gradient is created, allowing for an increase in moisture flux and easterly flow inland (Xulu et al., 2020). This shift in moisture gradients and enhanced trade wind can then influence TC trajectories and formations, allowing for strong-than-average seasons and increased zonal trajectories based on the SIHP migration (Xulu et al., 2020; Vitart et al., 2003)

2.4.3 Mozambique Channel Trough

The MCT is a low-pressure system centered over the southwestern part of the MC with peaks during the austral summer (Cook et al., 2004; Munday and Washington, 2017) (**Fig. 2.4**). The system originates due to strong easterly moisture flux from the SIHP interacting with the topography of Madagascar and deflecting towards the southern edge of the island leading to a wind trough moving over the channel and feeding into the South Indian Ocean Convergence Zone. The troughs structure first appears in early December, having a peak intensity in February. The system is fueled by a substantial central SST increase within the MC, a zonal migration (southeastward) of the SIHP, and a strong cross-equatorial monsoonal westerly aiding in enhanced moisture towards the trough (Barimalala et al., 2018; 2020).

Connections between moisture flux and southern African climate have been investigated, allowing for a better understanding of MCT's influence on increased inland convection (Munday and Washington, 2017; 2018). Studies such as Barimalala et al. (2018) utilized a numerical modeling experiment to analyze the MCT impact on southern African rainfall. Through similar

methodologies to this study (Chapter 3), moisture transport and rainfall correlation to the trough was found, showing a weak MCT simulated through flatting or sea interpolation of Madagascar's topography. The weakening of the trough allowed for an increase in zonal moisture transport into the mainland, leading to increased rainfall. However, through the control run, a strong MCT increased moisture flux and precipitation through Madagascar and the outer ocean, decreasing inland rainfall and indicating that the topography and MCT strength had significant implications on inland and oceanic moisture flux. These findings were found to go against those of Munday and Washington (2017), correlating the influx of moisture from a weak MCT to connect to a weak AL and vis versa (Barimalala et al., 2018) The MCT influx of moisture transport could allow for a higher probability of TC land impact. Studies have found indications of storm intensification in connection with the trough's moisture flux, allowing storms such as TC Dera to intensify upon entering the channel (Reason, 2007). This might indicate that variations in the trough allow for variations in TC intensification or inland movement throughout the MC (e.g., Chikoore et al., 2015; Matyas, 2015; Barimalala et al., 2018; 2020)

2.4.3 Sub-tropical Westerly Jet

The Subtropical Westerly Jet (STJ-S) is an upper-tropospheric (200hPa) circulation of westerly winds found in both the Northern and Southern Hemispheres (Krishnamurti, 1961; Bluestein, 1992; Archer and Caldeira, 2008). The STJ-S resides around 30-35°S, running through the eastern Indian Ocean into the central Pacific Ocean (Gallego et al., 2005). The jet is found to form from the outer flow of tropical convection that is then transported using angular momentum toward the subtropics through the Hadley cell circulation leading to the STJ-S seasonal intensity and location (Held and Hou, 1980). During the austral winter (June-September), the STJ-S peaks due to enhanced moisture transport from the Hadley circulation and then weaken during the austral summer (December-April), allowing for the poleward easterly jet to strengthen (Gallego et al.,2005). Along with seasonal intensity, the STJ-S is found to have latitudinal movement due to enhancements of atmospheric features such as El Niño-Southern Oscillation (ENSO) and Southern Annular Mode (L'Heureux and Thompson, 2006). Studies such as Astier et al. (2015) found that the STJ-S was seen to have an equatorward displacement during the austral summers that experienced a positive ENSO. This displacement leads to a stronger wind shear located over the channel and creates detrimental conditions for cyclogenesis (Astier et al., 2015). Therefore,

although conditions such as a high La Niña are optimal for cyclogenesis, the lateral movement of the STJ-S is still an influential factor in TC genesis within the SWIO.

2.4.4 African Easterly Jet (Southern)

The African Easterly Jet in the Southern Hemisphere (AEJ-S) is a mid-tropospheric (600hPa) easterly jet sitting over southern Africa between 5-15°S (Nicholson and Grist, 2003; Adebiy and Zuidema, 2016). First discussed by Nicholson and Grist (2003), both the African Easterly jet in the Northern Hemisphere and AEJ-S were found to form in similar ways with a local reversal of the surface temperature gradient leading to an easterly wind flow. The AEJ-S formation was found to originate from the gradient formed between the dry subtropical Namib-Kalahari and semi-wet Congo Basin (Nicholson and Grist, 2003). The AEJ-S seasonal peaks around September, October, and November, reaching a max speed of 8 $m \cdot s^{-1}$ within the core of the jet (Nicholson and Grist, 2003; Adebiyi and Zuidema, 2016). More recent studies, such as Kuete et al. (2020), used reanalysis data sets to further understand the physical mechanism that makes up and influences the AEJ-S. The study found that as the AEJ-S strengthens (weakens) in intensity, the moisture convergence decreases (increases) within the southern African region. This, in turn, could affect mesoscale convection and moisture flux within central and southern African regions (Jackson et al., 2008).

2.5 Historical Modeling of Tropical Cyclones

2.5.1 Regional Climate Models

Regional modeling techniques are a utilized tool in the analysis of TC studies. Historically, Global Climatology models (GCM) have been used to analyze TC developments, with one of the first tracking proposed by Broccoli and Manabe (1990). Progression of GCM allowed for coarser resolution models (~100km) to be developed, allowing for higher precision in TC tracks. Although more accurate, the 100km resolution model did not account for problems in TC intensity (eye wall development) and location, with many tracking too far eastward in the SWIO (Bengtsson et al., 1995). Modern global scale models have significantly improved TC tracking and analysis, with models running at much higher resolutions, such as 10 km, allowing for a more accurate TC core

(Manganello et al., 2012). Although high resolutions GCM is preferred in the track of TC development and large-scale atmospheric factors, economically cautious organizations/countries needing atmospheric analysis use more regional-scaled modeling techniques (Walsh and Watterson, 1997; Landman et al., 2005). WRF is the most used regional model and is utilized in both short-term forecasting and large-scale climate modeling (e.g., Weisman et al., 2008; Potty et al., 2012; Mearns et al., 2012). Regional modeling is an ideal analysis of storm tracking. However, many have discussed limitations in resolution size, boundary forcings, and physical parameters (Giorgi and Mearns, 1999; Manganello et al., 2012; Cha and Wang, 2013). These factors, if not properly scaled to the region, can cause significant variability in the formation, intensity, and track location of TCs (Manganello et al., 2012; Cha and Wang, 2013)

2.6 Regional Climate Factors Leading to Inland Tracking

Currently, little to no studies have been found regarding TCs sensitivity toward the Madagascar terrain; however, studies have investigated the effects of regional climate variables regarding their sensitivity on TC trajectories toward land (Jury et al., 1999; Vitart et al., 2003; Reason and Keibel, 2004; Ash and Matyas, 2012; Fitchett and Grab, 2014). Vitart et al. (2003) first investigated the interannual variability of zonal steering flow, examining the impacts of stronger or weaker zonal flows in regard to trajectories of TC as they tracked westward. The zonal flow was calculated by vertically averaging the zonal wind from 200 to 850hPa, using data obtained from the National Centers for Environmental Prediction reanalysis output. This study used a statistical method to analyze storm seasons from 1950-2000 that either ran at one standard deviation above or below the average zonal flow to observe changes in storm trajectories toward land. A Kolmogorov–Smirnov test showed that zonal flow, at one standard deviation below the average (negative or westward flow), allowed a TC to progress on a strong zonal trajectory toward land. However, one standard deviation above (positive or eastward flow) showed decreased zonal tracks with enhanced storm defection off Madagascar. Additionally, Vitart et al. (2003) indicated through an atmospheric general circulation model that TCs were found to track more zonally as well as have an increased TC genesis during a La Niña year compared to other ENSO years. This optimal environment is due to a drop in VWS over the SWIO brought on by warm La Niña conditions in the southern Pacific. Additional studies also have found this connection between La Niña

conditions allows for a stronger environment for zonal trajectory towards land through higher-than-average SST promoting zonal flow. (Jury et al., 1999; Reason and Keibel, 2004).

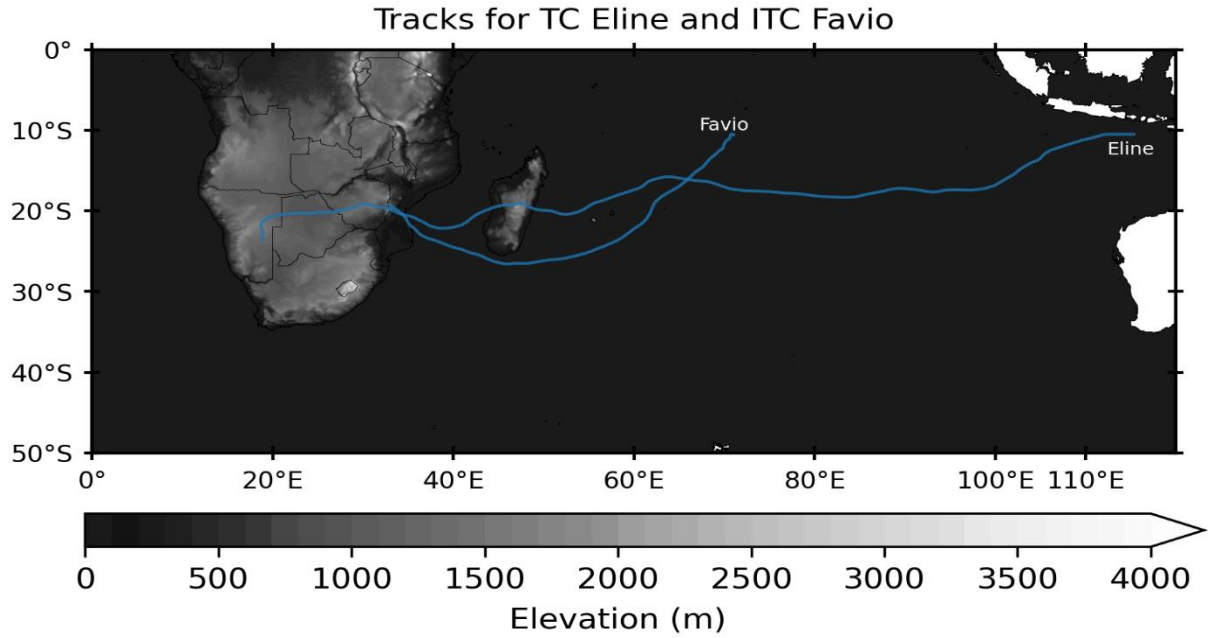

Figure 2.6: The observed trajectories of TC Favio (February 2007) and TC Eline (February 2000). (Generated from IBTrACS archive data)

Individual storm case studies, such as TC Eline and TC Favio, have also shown regional climate features to contribute to their unusual inland trajectory. In February 2000, TC Eline exhibited an unusual east-to-west trajectory, tracking into a significant portion of southern Africa before dissipating in southern Namibia (**Fig. 2.6**). TC Eline's trajectory was found to be highly unusual due to most storms originating in the SWIO tending to track to the southwest before recurving southeastward towards the poles. However, this strong zonal trajectory was found to be brought on by three large-scale climatic features that have been previously identified in literature to allow for a continued westward trajectory toward land (Olivier, 1993). The first was found to be an unusually strong lower to midlevel high-pressure anomaly located south of the MC several days before TC Eline initially arrived. This high-pressure ridge prevented storm tracks from moving further south, increasing the likelihood of a zonal trajectory towards land and reducing the possibility of TCs recurving back into the SWIO. The next parameter was a precisely located trough aligned northwest-southeast across the inland of southern Africa. This feature enabled an inland moisture concentration that allowed TC Eline to slowly continue into southern Africa, even once penetrating further inland. Finally, stronger-than-average easterly winds were found to create

a negative zonal flow allowing for optimal conditions for zonal progression inland. These features, along with a positive La Niña and enhanced SST, were to be conducive to the optimal environment leading to zonal progression and TC Eline's trajectory over Madagascar and into southern Africa (Jury et al., 1999; Vitart et al., 2003; Reason and Keibel, 2004).

In February 2007, TC Favio was also found to demonstrate an unusual zonal trajectory, having considerable influence on Madagascar and Mozambique (**Fig. 2.6**) (Klinman and Reason, 2008). The storm's trajectory was primarily influenced by factors comparable to TC Eline track towards land, with the first being a high-pressure anomaly at the mid-level winds (500hPa) southeast of Madagascar. With the anomalies strengthening and northeastward movement toward the island's southeastern edge, the progression of southwesterly recurve for storms decreased, causing TC Favio to push northward toward the MC. On top of the high-pressure anomaly, an uncommon negative zonal steering flow progressed during the days of TC Favio's movement next to Madagascar, leading to a stronger zonal and inland trajectory than was not seen during the rest of the season (Vitart et al., 2003). Finally, the storm experienced an unusual SST (27–28°C) over the MC, allowing for an increase in the storm as it tracked toward Mozambique. Additionally, ENSO was investigated for a factor leading towards zonal movement; however, TC Favio was during a weak El Niño year, causing these factors to have a large significance on its zonal trajectory toward land.

Although TC Eline and TC Favio were found to progress in different seasonal environments, both showed to be strongly impacted by high-pressure anomalies, negative zonal steering flow, and unusual SST. These factors have then been seen to be a strong influence on TC zonal tracking toward land in many studies and could be used to investigate other zonally tracking TCs in future studies (Jury et al., 1999; Vitart et al., 2003; Reason and Keibel, 2004; Klinman and Reason, 2008; Chang-Seng and Jury, 2010)

2.7 Summary

Historically, TCs have been defined globally in terms of their genesis, tracking, and dissipation. These storms are found to typically form approximately 4-5° away from the equator, experience

weak VWS, require SST above 26°C on a global scale and need enhanced moisture to feed into the system as they progress. While there are some similarities in the characteristics of TCs worldwide, it has been observed that the TC could have more regional characteristics optimizing genesis within their domain.

Within the SWIO, storms typically originate from mid-December and progress until mid-April, with peaks during February. These storms are then tracked and recorded by multiple organizations and put into the IBTrACS database for further analysis. Through studies, many climatic variables are then found to influence TC genesis along with their trajectories, such as El Niño and La Niña, zonal mean flow, TRB, reduced VWS, and increased moisture availability, promoting storm development. Additionally, factors such as the SIHP, MCT, STJ-S, and AEJ-S allow for changes in moisture distribution, easterly wind flow, and VWS, leading to storm intensity and trajectory changes.

These features can then be studied using multiple model techniques, allowing for an investigation of TC development and structure on both global and regional scales. However, regional models, such as the WRF model, are particularly favored for climatological studies due to their cost-effectiveness and ability to provide high-resolution analysis over a longer period.

This chapter examined various regional factors that play a role in influencing the paths of TCs toward land. Variables like VWS, zonal flow patterns, anomalies in high-pressure systems, and broader features such as the ENSO exert considerable influence on storm trajectories towards land. This is particularly evident when further investigating specific instances of TCs like TC Eline and TC Favio.

Chapter 3

3. Data and Methods

3.1 Boundary Conditions

The Climate Forecast System Reanalysis Model Version 2 (CFSRV2), and the National Oceanic and Atmospheric Administration—Optimum Interpolation Sea Surface Temperature, are used in this study to provide the initial boundary conditions and SST for the WRF runs (Saha et al., 2010; 2014; Reynolds et al., 2007). CFSRV2 is a third-generation reanalysis model developed by the National Center for Atmospheric Research (NCAR) (Saha et al., 2010; 2014). The CFSRV2 was an improvement in almost all aspects compared to the original CFSR through enhanced model configurations and atmospheric outputs (Saha et al., 2014). Additionally, the original CFSR ran from 1979-2009, with CFSRV2 expanding into 2017 by using the original CFSR outputs as an initial boundary condition for version 2. The reanalysis pulls from a multitude of historical and observation data sets, assimilating them into the numerical model. This model is built by coupling four climate models: atmospheric (resolution, 38 km), oceanographic, land surface, and sea ice, to create a high-resolution reanalysis dataset output (Saha et al., 2010; 2014). The model is then run at 0.5° horizontal resolution, outputting every 6 hours at 0000, 0600, 1200, and 1800UTC.

3.2 WRF Model Description

Regional scale models such as WRF are useful for studying weather and climate processes or phenomena over domains at a higher resolution than is feasible for global models. They also offer the opportunity to make idealized simulations to test the sensitivity of such phenomena to particular forcing factors, such as the SST or the topography, as is the case in this thesis. For example, WRF has previously been successfully used to study the sensitivity of southern African rainfall and atmospheric circulation to the presence of the Limpopo and Zambezi River valleys by

comparing long-term runs with these valleys included in the topography to those with these valleys blocked by imposed topography in the model (Barimalala et al., 2021).

For tropical storm studies, WRF has been successfully used to simulate particular regional cases, such as TC Chedza (Rapolaki and Reason, 2018) or TC Dineo (Meyiwa, 2019), using model resolutions of about 10km. For global models, Roberts et al. (2020) showed that high resolution is needed to produce TC frequency, intensity, and spatial distribution at reasonable accuracy through the High-Resolution Model Intercomparison Project. However, very substantial computational demand is required, and therefore lower resolution modeling (60-200km) is primarily used in GCM climatological studies. However, a significant advantage of regional models like WRF is that it allows researchers who do not have the resources or computational power of very large climate centers like NCAR or the United Kingdom Meteorological Office to produce model climatology with sufficiently high resolution and accuracy to be useful for TC applications (e.g., Potty et al., 2012; Cha and Wang, 2013; Kim et al.,2015). Therefore, the WRF application is found to be appropriate for the needs of this thesis.

WRF is a regionalized terrain-following, hydrostatic-pressure model that is fully compressible and runs on an Arakawa C-grid (Skamarock et al., 2005). The NCAR developed the original model with the flexibility to change the forcing or boundary conditions to be made easily for sensitivity studies. Thus, modifying different variables such as topography in one part of the domain (Madagascar in this thesis) for sensitivity analyses is straightforward (e.g., Hill and Lackmann, 2009; Barimalala et al., 2018; 2020; 2021). The specific version of WRF used in this thesis is the Advanced Research WRF version 3.8.1 (Skamarock et al., 2005), configured at a 10km horizontal resolution over the domain 10 - 100°E, 0 - 40°S with 49 levels extending from the surface to 200hPa. This domain includes the southern African mainland, Madagascar, and the full SWIO TC region. The model was run at 00 UTC on September 1, 2000, and ran until April 30th, 2001, with the first month of the run (i.e., September) being regarded as a model spin-up. The same integration procedure was used each summer for 16 years, as by Barimalala et al. (2018). Unfortunately, computational constraints prevented the winter half of the year from being included in the simulations. Since the TC season in the region only begins in November, not having model output available until October 1st of each year is acceptable. As previously discussed, the CFSRV2

boundary conditions were applied every 6 hours. Due to computational constraints, WRF output analyzed in the TRACK algorithm (Hodges et al., 1994,1995) used data for 00 UTC only.

The physics parameterizations for the model are as follows. The convection scheme for the atmospheric model was run using the Betts-Miller-Janjic cumulus parameterization (Betts and Miller, 1986; Janjic, 1994). The sea and ice models utilized the WRF single-moment 3-class ice microphysics scheme (Hong et al., 2004) and the Noah land surface scheme (Chen and Dudhia, 2001). Through the cloud cover, the Rapid Radiative Transfer Model for longwave radiation (Mlawer et al., 1997) and the cloud-interactive shortwave radiation scheme (Dudhia, 1989) were used. Finally, the Yonsei University planetary boundary layer scheme (Hong et al., 2006). These schemes are ideal for conditions calibrated with southern Africa.

3.3 WRF Model Simulations

The WRF model created two additional runs (FLAT and SEA) on top of the CNTRL run. Each model was run with the same conditions, duration, and schemes as the CNTRL, with each only varying on the topography of Madagascar. Each model setup and criteria are discussed as follows:

1. Control (CNTRL) shows Madagascar's full topography, reasonably representing the regional atmospheric circulation and equivalent to the original Barimalala et al. (2018) study.
2. The second run, FLAT, is the same as CNTRL, but with Madagascar, topography leveled off to 300m. The coastal topography is unchanged and therefore decreases as it approaches sea level over the east and west coasts of the island. Although the topographic features have changed, the experiment replicates all land, surface characteristics, and vegetation types as in CNTRL.
3. The third run, SEA, is similar to the CNTRL but completely removes Madagascar island from the model, creating an uninterrupted ocean basin. Each point is allocated an SST, zonally interpolated using the real Indian Ocean basin surrounding the island.

Figure 3.1 shows the topographical difference between the three experiments. Variations in maximum and average FLAT topography (**Fig. 3.1**; solid/dashed blue) come from large-scale features surrounding the island, such as deep valleys near 16°S and 13°S. The 75% topography (**Fig. 3.1**; dashed black) was run under the original Barimalala et al. (2018) paper. However, as discussed, the 75% topographical experiment is not utilized in either study due to the patterns of the results being too similar to both the FLAT and SEA runs, with even fewer differences when compared to CNTRL.

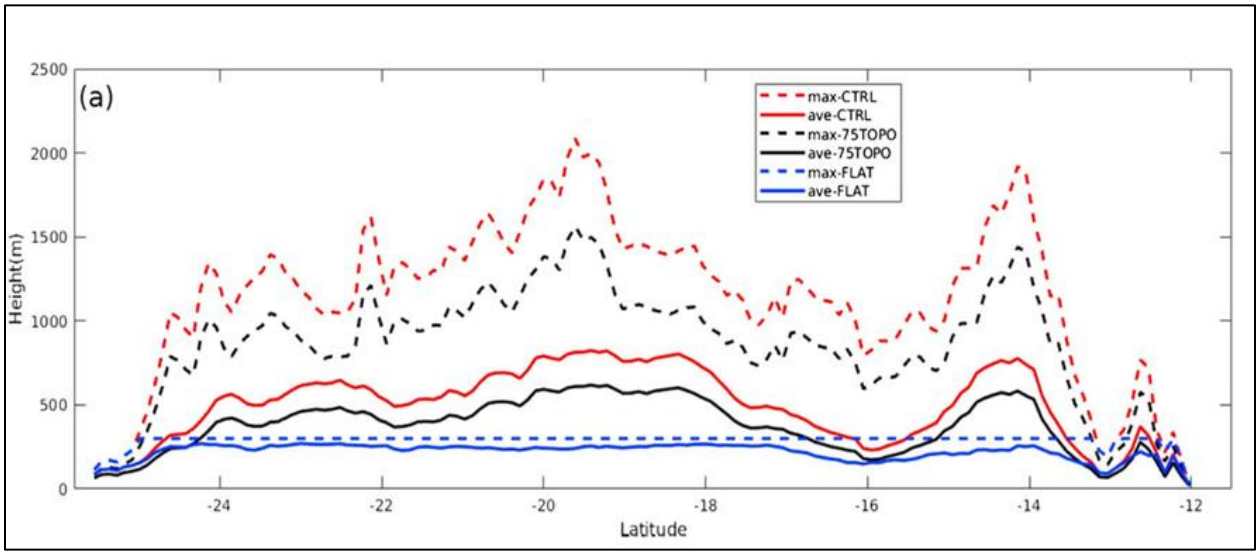

Figure 3.1: South-north transect of the topography of Madagascar throughout the three scenarios (12 - 23°S). The dashed lines represent the max topography surrounding the island, with the solid line being the average topography. (Sourced from Barimalala et al., 2018)

3.4 TRACK Algorithm

TC track patterns have previously been found to have uncertainties when run in regional models such as WRF. Many of these inaccuracies come from uncertainties in physics parameterizations and conditions of the model creating unrealistic environments (Cha and Wang, 2013). Previous studies, such as Cha and Wang (2013), have found that calibrating the conditions and physics parameterizations to the boundary area improves the accuracy of the atmospheric environment. With this study being run within the SWIO, previous literature had been acquired in order to represent the atmospheric environment as accurately as possible (Crétat et al., 2012; Ratnam et al.,

2012; Ratnam et al., 2013; Desbiolles et al., 2018). This calibration then allows TC genesis, track, and lysis to follow the patterns of the real environment as closely as possible.

The tracking methodology utilized in this study is found through Hodges (1994, 1995) TRACK 1.5.2 program. The algorithm runs on a lagrangian mechanic system tracking TCs over global or regional model outputs. TC tracks use relativity vorticity (ξ), which is vertically averaged, allowing for longer storm tracking by improving the temporal coherence when a vorticity maximum shifts between levels. Due to this relative vorticity not being a direct output of WRF, the program calculates relative vorticity using horizontal wind components u and v ($m \cdot s^{-1}$) winds in spherical coordinates taken from the WRF model. The relative vorticity is then calculated using the following:

$$\xi = \frac{1}{a \cos\theta}\left(\frac{\partial v}{\partial \lambda} - \frac{\partial (u \cos\theta)}{\partial \theta}\right) \quad \ldots\ldots\ldots\ldots\ldots\ldots (1)$$

The equation outlines that Theta (Θ) is latitude, Lambda (λ) is longitude, u is the zonal wind, v is meridional wind, and (a) is the radius of the Earth. The equation is run using B-splines from which the first-order derivatives can be obtained analytically rather than using finite differences. Once relative vorticity is calculated, the data is run under a spectral filter on a T63 resolution; this is applied for excessive noise reduction of the full-resolution vorticity and helps to reduce large-scale background allowing for more accurate tracking of each storm's core. The program then applies a tapered spectral coefficient that smooths the data using the same specified filter; these can be further found in Sardeshmukh and Hoskins (1984). Once the filter is applied, the data vertically averages the vorticity (850-600hPa) filtered again to a T63 resolution. Storm centers are then identified by adding a vorticity maximum (minima in the SH but scaled by -1). The minimum vorticity on each level is then added to tracks using a recursive search within the tracked center's 5° radius (geodesic). The use of vorticity minima allows testing for a coherent vertical structure and a warm core of each storm to filter out TC from non-TC. The storm centers are then connected using the nearest-neighbor approach and refined using cost-function minimization to create smoother tracks. To operate with daily data outputs rather than six-hourly, the sensitivity to track smoothness over each storm's track was modified to account for larger jumps in storm cores. The cost function is then subject to adaptive constraints on displacement distance and track smoothness

(Hodges, 1999). Once the tracks have been identified, a 2-day filter is applied to retain those storms that progress longer than a 2-day (2-time steps) period. Although TC can be observed below two days, these filters allow for analyzing the pre- and post-TC tracks over a longer duration. Additional variables, such as maximum 10 m wind speed and mean sea level pressure, are added to apply stricter criteria over the final storm tracking. The max/minimization is performed within a 5° geodesic radius for the pressure, with a 6° geodesic radius for the maximum 10 m wind speed running under full resolution. Each wind and pressure measurement has latitude and longitude values stored along with the intensity at that location. If maxima or minima cannot be found, the value at the T63 center is computed and stored, and the positional values are tagged with a missing value. Optical use of the T63 resolution on the vorticity was done to provide a smoother picture of the vertical structure than the full resolution. Post tracking, the final storm selection is made using a specific set of TC criteria as outlined below:

1. T63 relative vorticity at 850hPa must attain a threshold of at least 6×10^{-5} s^{-1}.
2. The difference in vorticity between 850 and 200hPa (at T63 resolution) must be greater than 6×10^{-5} s^{-1} to provide evidence of a warm core.
3. The T63 vorticity center must exist at each level between 850 and 200hPa to show a coherent vertical structure.
4. Criteria 1 to 3 must be jointly attained for at least one consecutive time step (1-day) and only apply over the oceans.
5. Full vorticity maximum 10 m wind speed must attain a minimum threshold of at least 17 $m \cdot s^{-1}$.

The vorticity threshold is applied simultaneously with the warm core identification to help identify a vertical structure. Tracks are analyzed based on their vorticity fields at the 850, 700, 600, 500, 400, 300, and 250hPa levels to locate vortices with warm core structures. This is done iteratively by starting at 850hPa and using B-spline interpolation and the steepest descent minimization due to TC existing in the Southern Hemisphere. Wind criteria then analyze each storm's track maximum 10 m wind speed. Storms must reach a minimum of 17 $m \cdot s^{-1}$ at any point in their tracking to be considered usable storms. The outputs are then considered the final TC tracks for that specific season.

3.5 Summary

This chapter discusses the boundary conditions and model description for the WRF model, and the TRACK algorithm used in the study. The WRF model was a widely used regional numerical model allowing for the manipulation of various atmospheric variables at a high-resolution output. This straightforward data manipulation made it an optimal model for the investigation of Madagascar terrain on TC tracks. The model's initial physics parameters were taken from the previous literature to calibrate the model's climate to the SWIO. This model was then used to compare two sensitivity runs to the CNTRL model. In the FLAT experiment, Madagascar's topography was modified to feature a 300-meter plateau, while the SEA model incorporated an interpolated representation of Madagascar based on the surrounding SST. The output of these simulations was subsequently subjected to the TRACK algorithm to track the TC generated within each model run. This algorithm was found to use the calculated relative vorticity of each storm to identify a warm core and subject the track to stricter criteria to pull only the TC present in that season. The following sections delve into the investigation of these tracks, in conjunction with the background climatology, with the aim of identifying any significant differences associated with the changing terrain toward TC trajectories.

Chapter 4

4. Results

4.1 Model Comparison

4.1.1 ERA5

The CNTRL runs atmospheric circulation was compared to a high-resolution reanalysis data set to observe any significant difference between the CNTRL model output whose boundary condition was run using CFSRV2. The ERA5 is one of the latest re-analysis products from the European Centre for Medium-Range Weather Forecasts and was created by combining historical and observational data sets that run through an Integrated Forecasting System Cy41r2 (Hersbach et al., 2020). This high-resolution (0.25 x 0.25°) reanalysis was pulled from Copernicus Climate Change Services at a daily output (00 UTC) over the WRF CNTRL domain (10 - 100°E, 0 - 40°S).

4.1.2 850hPa winds

Figures 4.1a-b show the CNTRL run (**Fig. 4.1a**) and the ERA5 reanalysis data (**Fig. 4.1b**) using zonal (u) and meridional (v) winds and geopotential height (GPH) (shaded; m) at the 850hPa pressure level. Monthly data was used in creating a December through March (DJFM) climatology from 2000-2016. The DJFM selection was to focus on the atmospheric conditions within the primary TC season. **Figures 4.1a-b** both show a relatively common circulation pattern with an established SIHP, strong easterly flow, and northeast monsoonal flow towards northern Madagascar.

Figure 4.1c shows anomaly outputs, subtracting the WRF CNTRL model from the ERA5 reanalysis data to observe large-scale changes between the products (**Fig. 4.1a-b)**. **Figure 4.1c** displays a negative cyclonic anomaly located at the southern edge of Madagascar (~14 m) with a slightly less negative anomaly in the SWIO between 70-75°E (~9 m). These anomalies represent the WRF CNTRL run to show an overestimated intensity and westward migration of SIHP when

compared to ERA5 reanalysis. This overestimation is found to simulate enhanced easterly flow into Madagascar, leading to a stronger MCT as well as reducing the monsoonal flow moving into the northeastern edge of the island. These features could be found to lead to an enhanced zonal flow of TC as well as precipitation surrounding the Island, as found in studies such as Vitart et al. (2003) and Ash and Matyas (2012)

4.1.3 500hPa winds

Figure 4.2a-b shows the CNTRL and ERA5 zonal (u) and meridional (v) winds (vectors; $m \cdot s^{-1}$) and GPH (shaded; m) at the 500hPa pressure level. This data was similarly run at a DJFM climatology over the 2000-2016 period. **Figure 4.2a-b** both show a defined Botswana High (BH) pressure centered over 15-25°E and 10-20°S along with mid-level westerlies off southern Africa and easterlies on the northeastern edge of Madagascar.

Figure 4.2c shows differences in 500hPa winds in CNTRL and ERA5 outputs. A predominantly negative cyclonic anomaly sitting at 15-25°E and 10-20°S indicates a relatively stronger (+20 m) BH pressure within the CNTRL when compared to ERA5 reanalysis. The BH is a mid-tropospheric feature that dictates much of southern African rainfall. The overrepresentation of the BH could then simulate dryer conditions over the southern African region, leading to lower inland convection within the model (Reason, 2019). However, the SWIO showed to reasonably be represented, having small variations in GPH (~4-5 m) as well as a relatively well represented mid-level westerly and easterly flow over southern Africa with the CNTRL model showing slightly higher westerlies over central Madagascar.

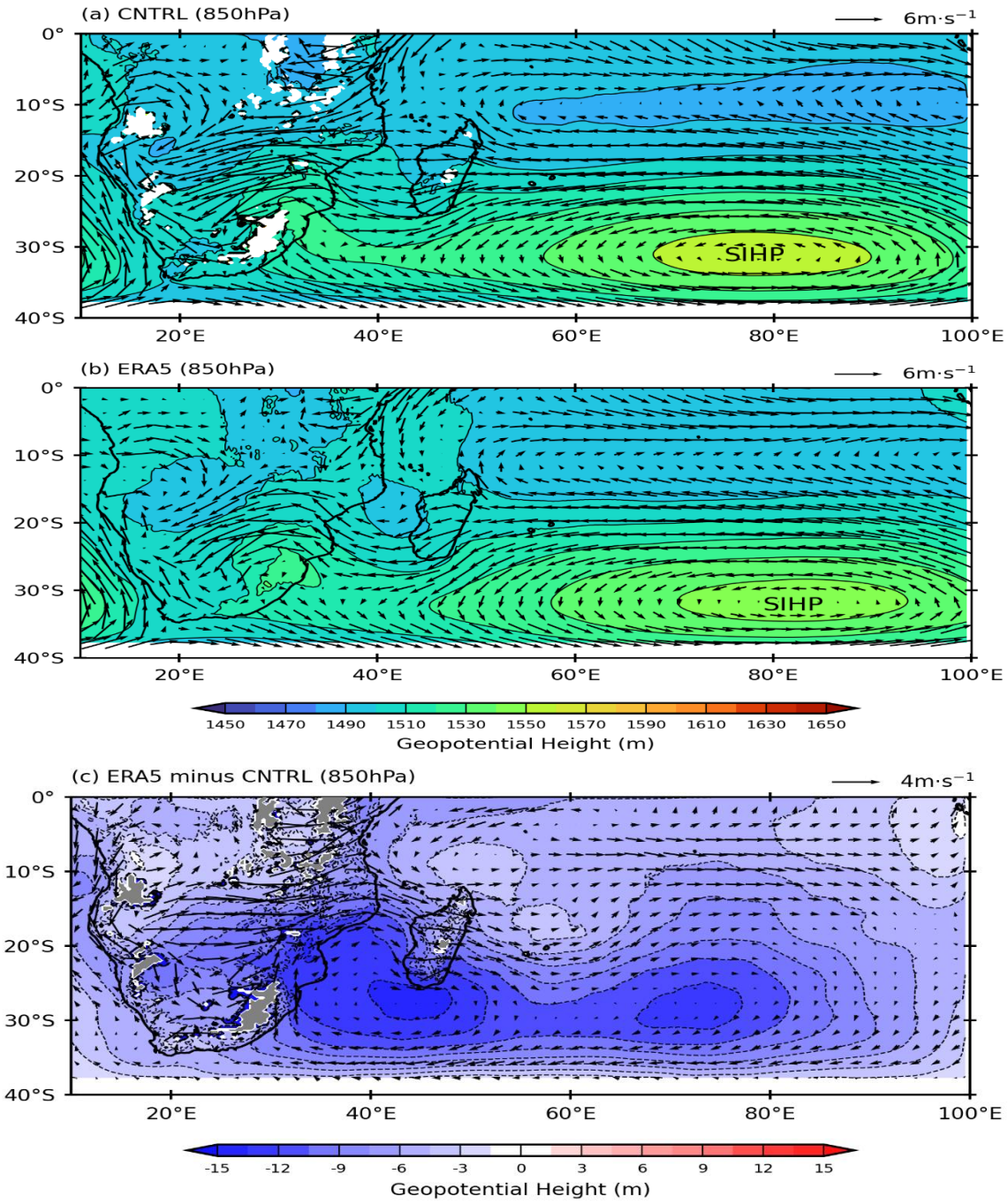

Figure 4.1: Shows 850-hPa wind (vectors; $m \cdot s^{-1}$) and GPH (shaded; m) taken over 2000-2016, December through March. The following shows (a) the WRF CNTRL run re-gridded to a 0.25 x 0.25° resolution (b), the ERA5 reanalysis data ran at 0.25 x 0.25° resolution (c), and the WRF CNTRL model subtracted from the ERA5 reanalysis data. Both show positive anomalies (red) as higher ERA5 GPH and negative (blue) as higher CNTRL GPH. Data below 1450m in (a) and above 14m in (c) represent topography above the 850hPa boundary.

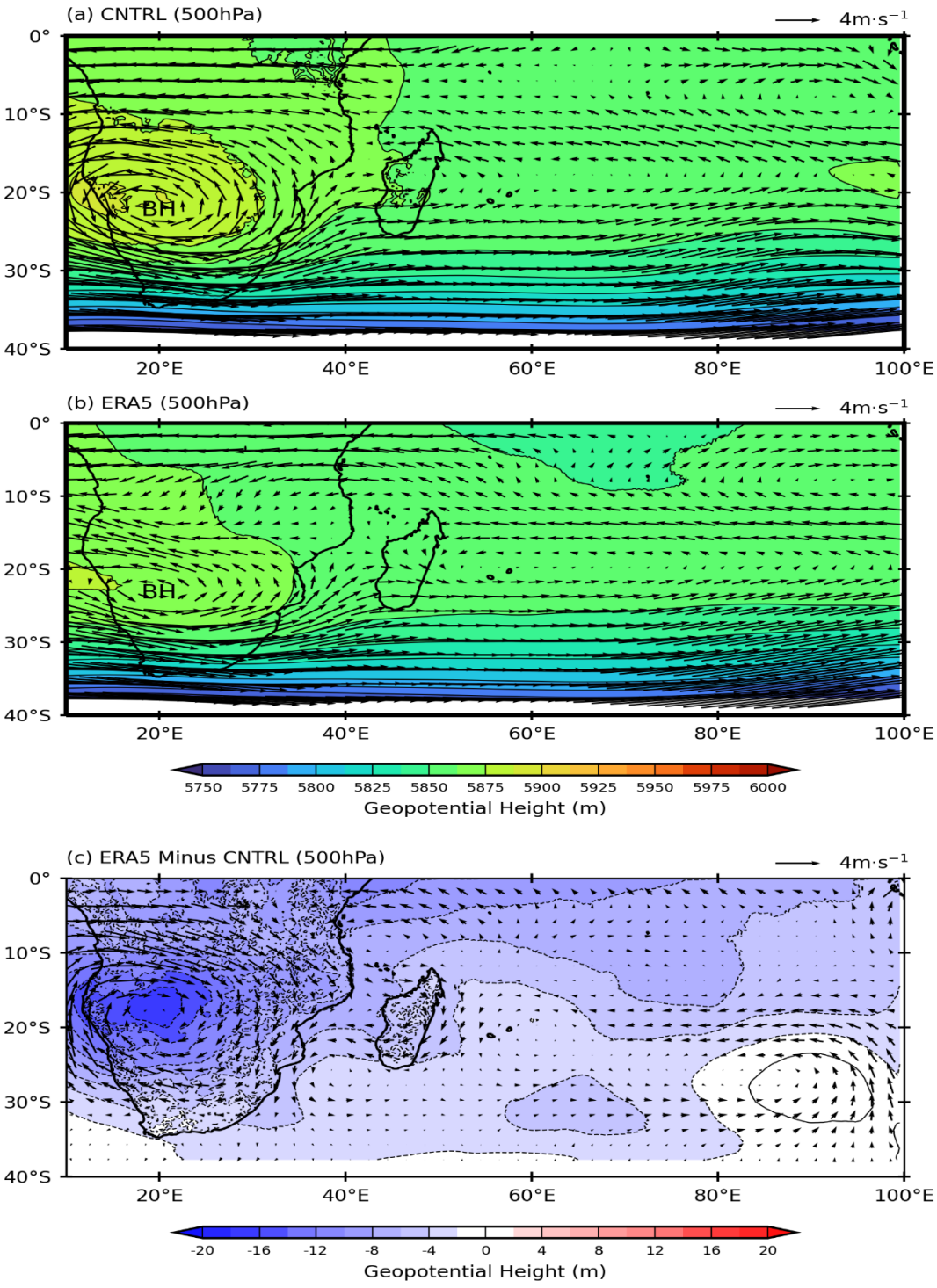

Figure 4.2: Shows 500-hPa wind (vectors; $m \cdot s^{-1}$) and GPH (shaded; m) taken over 2000-2016, December through March. The following shows (a) the WRF CNTRL run re-gridded to a 0.25 x 0.25° resolution (b), the ERA5 reanalysis data ran at 0.25 x 0.25° resolution (c), and the WRF CNTRL model subtracted from the ERA5 reanalysis data. Both show positive anomalies (red) as higher ERA5 GPH and negative (blue) as higher CNTRL GPH.

4.1.4 IBTrACS

Figures 4.3 and 4.4 show the CNTRL run's track and genesis density compared to the IBTrACS data set (Knapp et al., 2010). IBTrACS is a global collection of recent and historical TC track data provided by multiple organizations worldwide to allow for accessible and accurate observational comparisons. This study utilizes the most recently produced version of the IBTrACS data set (v04r00) to show an observed track and genesis density analysis compared to the CNTRL. In studies such as this, individual storm tracks are difficult to compare to model-derived TC due to the model's struggle to produce every storm track correctly. Therefore, a spherical kernel density method provided by Hodges (1996) is used to indicate the relative accuracy of genesis and track patterns of the CNTRLs TCs compared to the observed TCs of IBTrACS over the 2000-2016 period. **Figures 4.3 and 4.4** are calculated under number density per unit area per month, where the unit area is equivalent to a 5° spherical cap (~ 10^6 km^2).

4.1.5 Genesis Density

Figure 4.3 shows the TCs genesis anomalies of the CNTRL model compared to IBTrACS. A negative anomaly sits over the SWIO between 90-95°E (~ 4-4.5 x 10^6 km^2), with a slightly less negative anomaly extending from 70-80°E and into the northeastern edge of Madagascar (~2-3 x 10^6 km^2). These anomalies indicate the CNTRL run to show a northern bias in storm genesis, with a significant number of storms concentrating 5-10°S compared to the IBTrACS. Although TC genesis further north is not uncommon inside the SWIO, more TC genesis is seen north of 20°S in CNTRL than observed in IBTrACS, suggesting a slight northern bias in storm formation with the CNTRL run. Although this bias is evident, many storm formations over the seasons developed further south, agreeing with the observed IBTrACS data set. Therefore, the genesis locations were found to be reasonably accurate compared to IBTrACS, indicating only a few dozen storms tracking further north. Finally, the positive anomaly sitting over the center of the MC (~1-2 x 10^6 km^2) shows IBTrACS to have a slightly stronger storm genesis within the channel when compared to CNTRL.

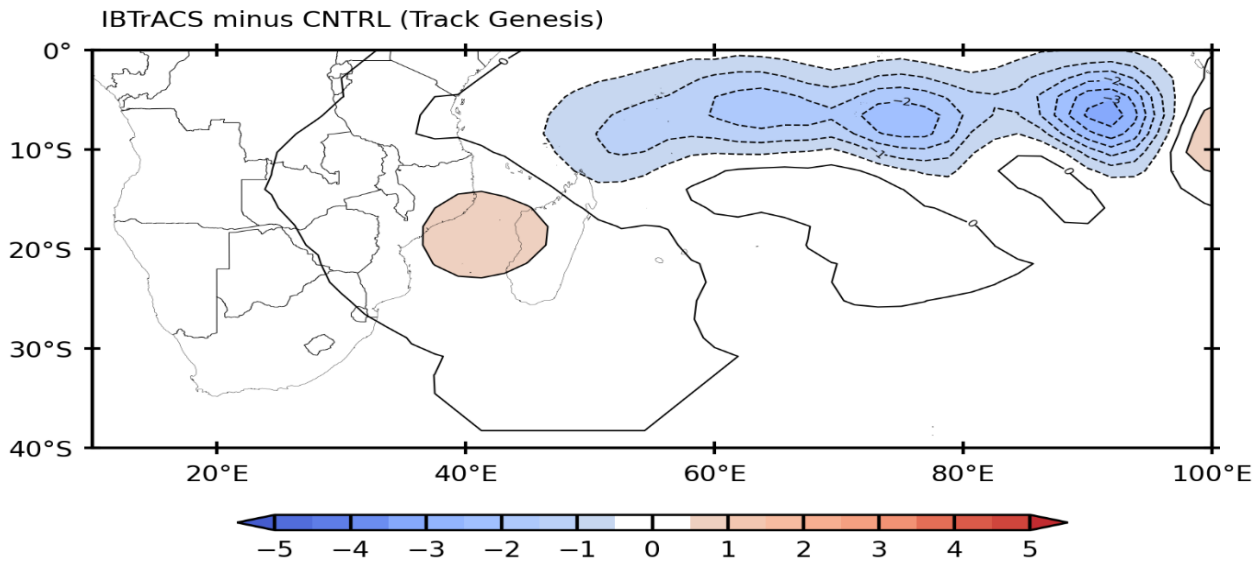

Figure 4.3: The genesis density is computed using the origin point of each storm track. Genesis densities are the number density per unit area per month where the unit area is equivalent to a 5° spherical cap (~ 10^6 km^2).

4.1.6 Track Density

Figure 4.4 shows the track anomalies of the CNTRL model compared to the IBTrACS data set. The negative anomaly from 40-90°E and 5-15°S indicates the CNTRL run to have a westward trajectory bias of storm tracks compared to the observed IBTrACS (6-7 x 10^6 $km^{2)}$. The CNTRL model suggests a relative accuracy among TCs general trajectory south of 20°S, with most storms following a southwestward trajectory. However, the positive anomaly south of 20°S indicates a larger number of storms tracking further south in the observed IBTrACS than the CNTRL run. This could equate to the northern genesis bias of the CNTRL model storms limiting the number of storms tracking as far south as observed. However, this small positive density anomaly (1-2 x 10^6 km^2) could equate to only a few dozen storms tracking that far south, showing the CNTRL to reasonably represent the general track movements of TCs compared to IBTrACS.

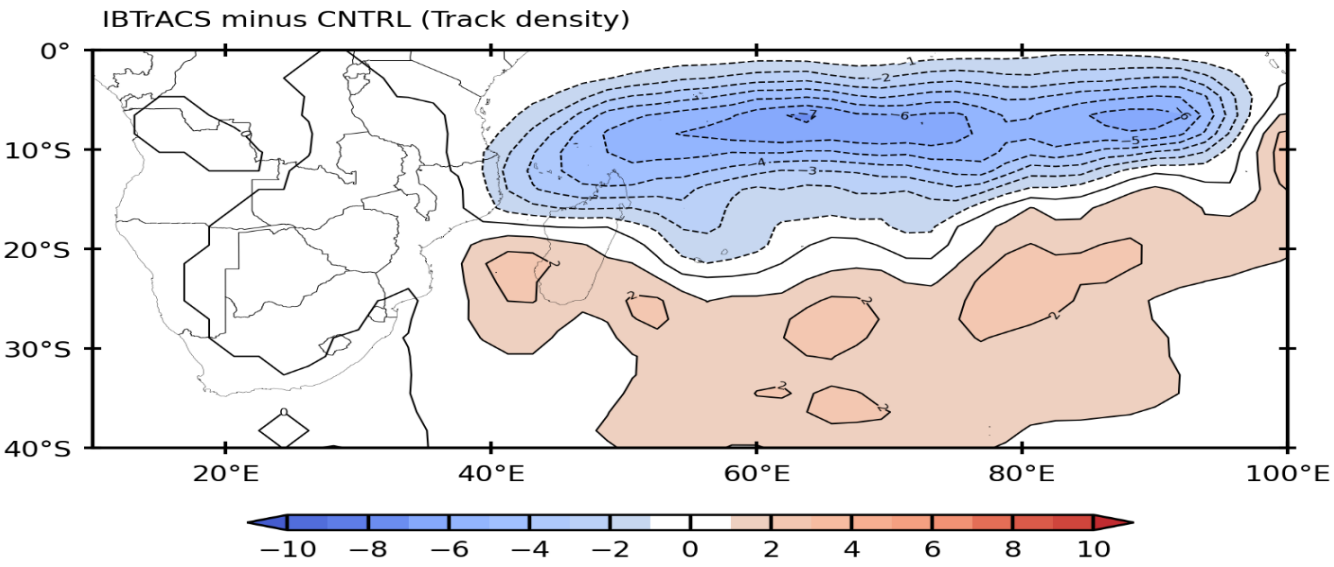

Figure 4.4: The track density is calculated using a single point from each track closest to the estimation point outputting the track density. The raw density statistics are subsequently scaled to number densities per month with a unit area equivalent to a 5° spherical cap (~ 10^6 km^2).

4.2 Tropical Cyclone Tracks

Figure 4.5a-c shows TC trajectories over the SWIO basin from the three WRF runs (CNTRL, FLAT, and SEA) derived from 16 austral summers (2000-2016). Tracks are pulled from September through April to encompass all TCs produced over the austral summer seasons. Since FLAT and SEA have the Madagascan topography flattened or the island replaced by the ocean, analyzing the results along various transects near and through Madagascar itself and far upstream of the changed topography in the open SWIO is useful. Each figure contains five diagonal transects (black lines; **Figure 4.5a-c**) from 5-30°S. Each transect shows the percentage of TCs that pass through it relative to those over the domain, only allowing each storm to be counted once per crossing. The total number of TCs per transect is then divided by the total TCs that occupied the domain, calculating the percentage of TCs that pass through each transect. Due to the different number of TCs produced in the FLAT and SEA runs compared to the CNTRL, data is represented as percentages to allow for comparative analysis.

The CNTRL run was found to have a total of 285 TCs occurring during 2000-2016. Transect one (60-65°E) was created to show storm movement within the middle of the SWIO and indicates that 23.9% of the 285 TCs tracked through this line (**Fig. 4.5a**). Most of these TCs then passed through transect 2, located just east of Madagascar (22.2% of the total). Since TCs very often track

southeastwards as they approach the island's east coast, it is not surprising that transect 3 (located through Madagascar) shows a significant drop in the percentage of total TCs tracking through it (14.1%). Further west, the percentages continue to decrease, with 10.1% of the total passing through transect 4 in the MC and 2.3% through transect 5, located near the Mozambican coast. The latter number is consistent with observations suggesting that about 5% of the total SWIO TCs make landfall on the southern African mainland (Reason and Keibel, 2004).

The FLAT model run (**Fig. 4.5b**) produced 272 TCs in the SWIO, slightly less than in CNTRL. The percentage of TCs passing through transect 1 is very similar to CNTRL (~25%), as are the proportions for transects 2-4 (~21%, 13%, and 10%, respectively). However, a noticeably larger fraction (4%) passes through transect 5 in FLAT, likely because the much-reduced Madagascan topography in this experiment enables TCs approaching the island to continue on a more zonal trajectory than those found in CNTRL. Regarding absolute numbers, 4% represents 11 TCs, whereas, for CNTRL, 2.3% equates to 7 TCs over 16 summers.

For SEA (**Fig. 4.5c**), the total number of TCs within the SWIO increases to 305, substantially larger than in CNTRL. While the proportion tracking through transects 1 and 2 are similar to CNTRL, the island's removal allows a much greater proportion of TCs tracking through transects 3-5. Regarding approximate landfall (transect 5), the 6.2% percentage equates to an average of 19 TCs or more than 1 per summer. As expected, the replacement of Madagascar by ocean grid points in SEA allows a much larger proportion of SWIO TCs to reach the Mozambican coast.

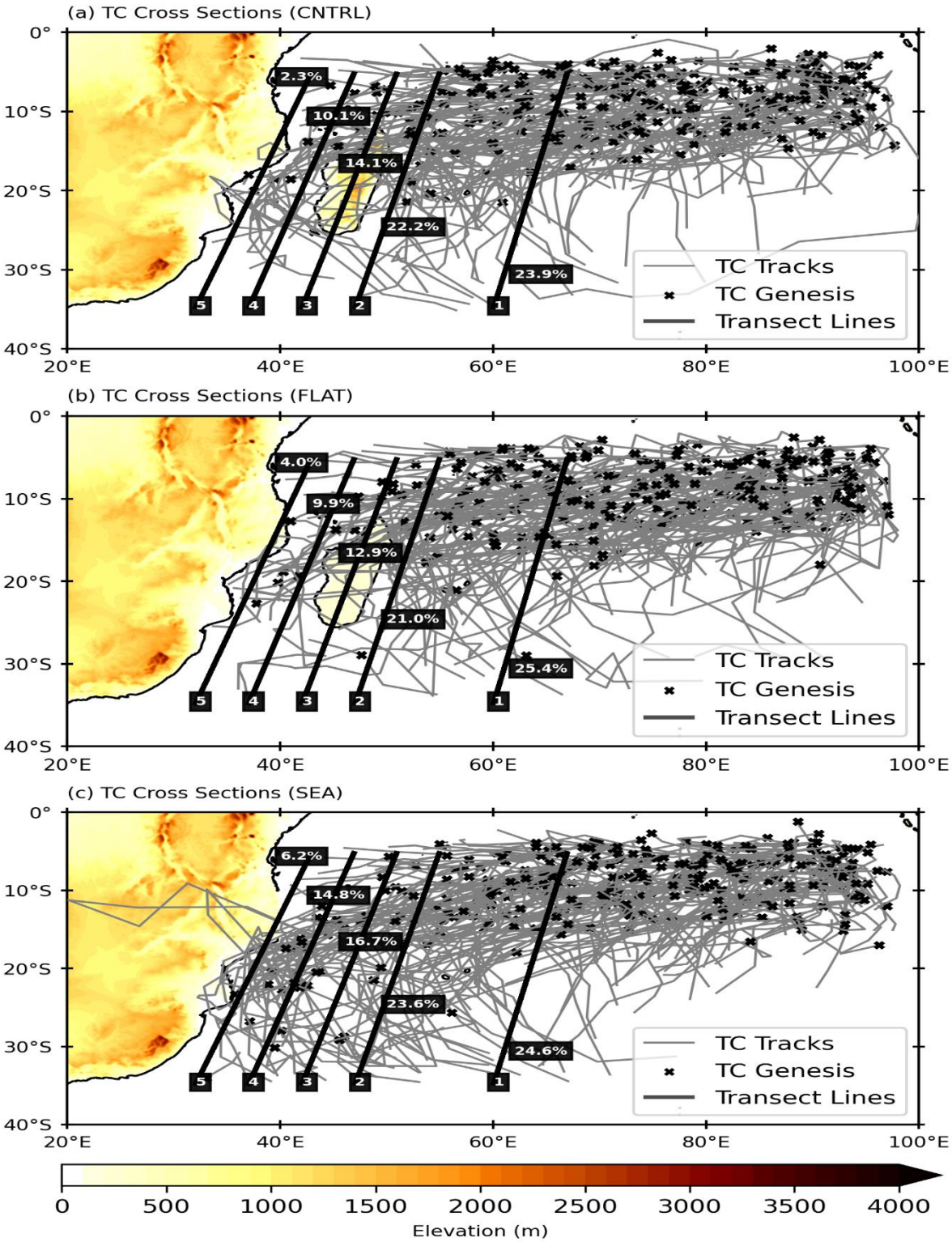

Figure 4.5: TC transect tracks taken over 2000-2016 September through April. The following shows CNTRL (a), FLAT (b), and SEA (c). The number at the bottom of the line represents the transect number, while the percentage value indicates the percentage number of TCs passing through it relative to the total TCs within the full domain.

4.3 Tropical Cyclones in the Mozambique Channel

4.3.1. Frequency

Figure 4.6a-c shows the percentage of the total number of TCs in the SWIO for each model run, which tracks through a box covering the central and southern MC. This box was chosen because relatively few TCs in the observations make landfall on the Mozambique coast north of the box, TC Kenneth in April 2019 being a prominent exception (Mawren et al., 2020). In CNTRL (**Fig. 4.6a**), about 9% of the total number of SWIO TCs occur somewhere in the channel box, and this increases to almost 15% when the ocean replaces Madagascar in the SEA model run (**Fig. 4.6c**). However, in the FLAT run (**Fig. 4.6b**), the result is somewhat unexpected since the proportion of TCs in the box (7.7%) is noticeably less than in CNTRL (9.2%), or absolute terms, only 21 versus 27 TCs. Note that not all the difference will result from TCs tracking from the SWIO across Madagascar itself because there are also differences between the two runs in the number of TCs generated within the MC.

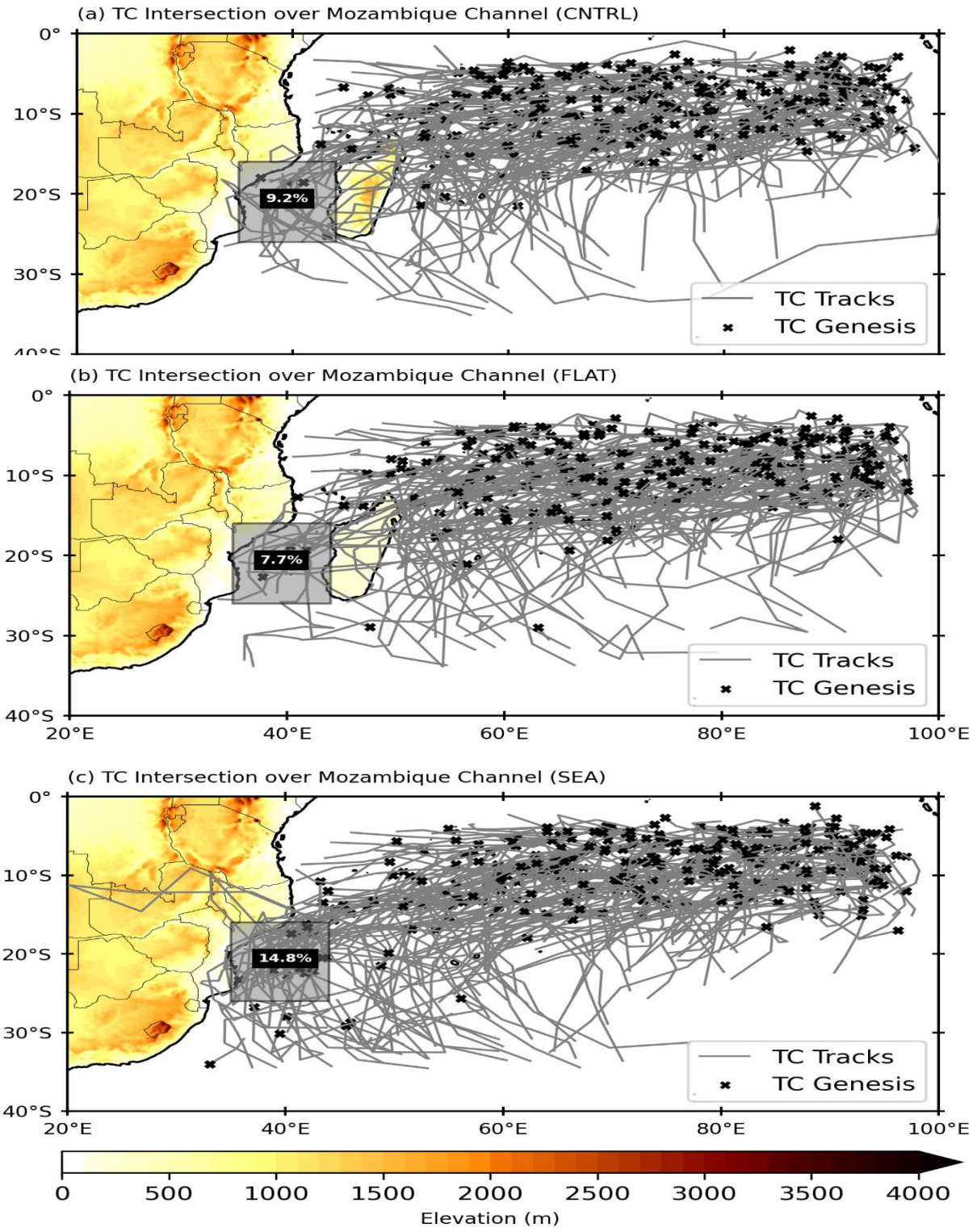

Figure 4.6: TC transect tracks taken over 2000-2016 from September to April. The following show CNTRL (a), FLAT (b), and SEA (c) with the percentage of TCs passing through the grey box in the central and southern MC relative to the total number of SWIO TCs indicated.

4.3.2 Genesis in the Mozambique Channel

Figure 4.7 shows the percentage of the total number of SWIO TCs generated within the central or southern MC in each of the three model runs. Only 1.6% of the total (or 5 TCs) are generated in the box in CNTRL (**Fig. 4.7a**), with somewhat less (4 or 1.5%) in FLAT (**Fig. 4.7b**). Removal of Madagascar in model run SEA allows for a significant amount more TCs to be generated in the area corresponding to the central/southern MC (15 TCs or 4.9%) (**Fig. 4.7c**).

Essentially, the replacement of Madagascar by ocean grid points in SEA run leads to a larger increase in the number of TCs generated in the southern or central channel over CNTRL. Correspondingly, more TCs will be found somewhere in the channel (some of which will have been developed in the SWIO), and a greater percentage making approximate landfall on Mozambique. This result is what would be expected as TCs can maintain themselves over the ocean, whereas they typically weaken quickly over land before dissipating. On the other hand, the differences between FLAT and CNTRL are more subtle. In an attempt to relate these TC differences to the large-scale background circulation, the next section analyses the change in winds (i.e., steering current) between the three model runs.

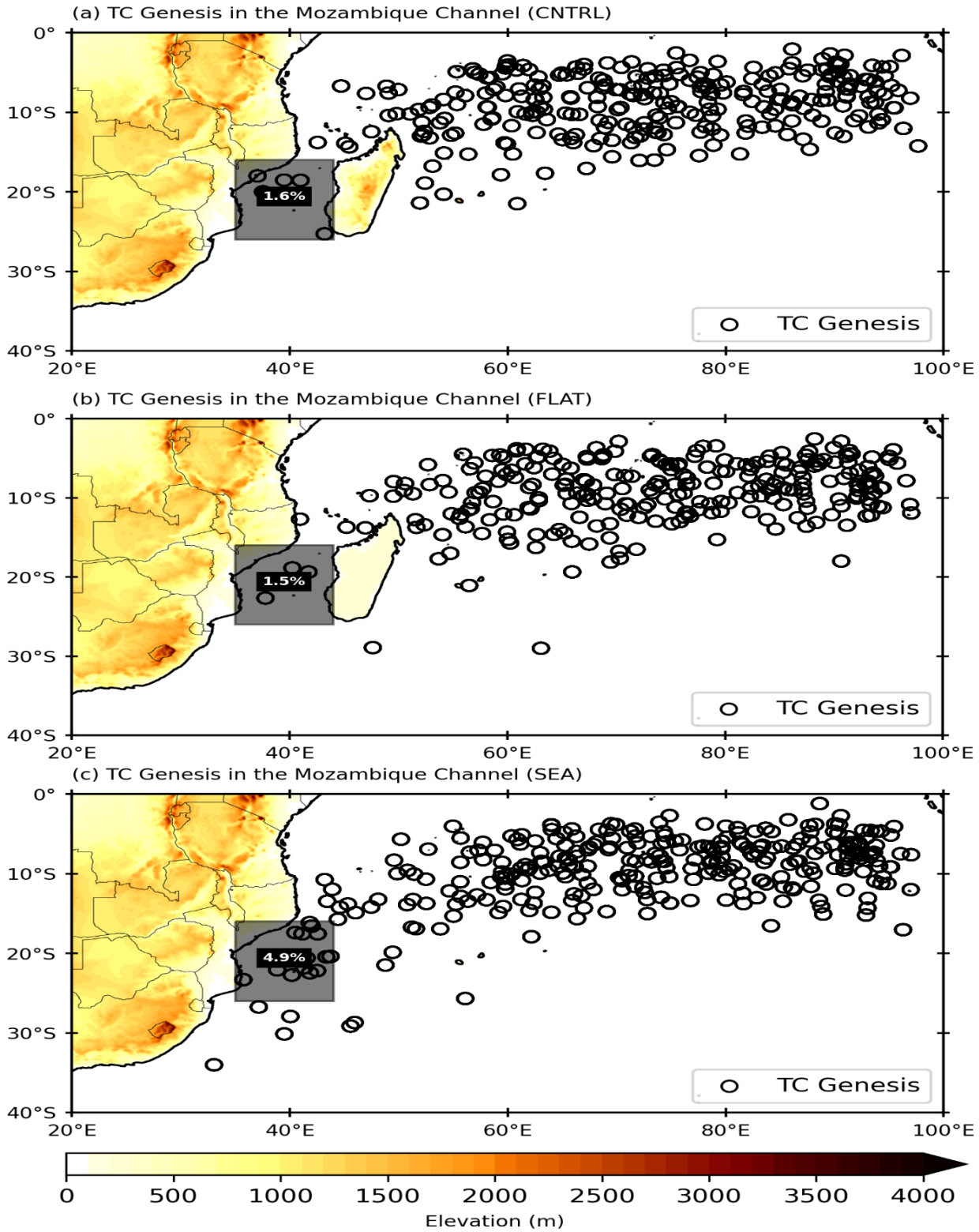

Figure 4.7: TC genesis took over 2000-2016 September through April. The following show CNTRL (a), FLAT (b), and SEA (c). The box shows the percentage of TC genesis within it relative to the full domain.

4.4 Regional Circulation Impacts on Tropical Cyclones

4.4.1. 850hPa Surface-Level Wind Analysis

Figure 4.8a analyzes the CNTRL runs zonal (u) and meridional (v) winds and GPH (shaded; m) at the 850hPa pressure level. Monthly data was used to create a DJFM climatology from 2000-2016 to focus on the peak TC season (unless otherwise noted, the results presented below refer to DJFM). The migration of the SIHP during the summer was a prominent feature in the CNTRL run (100 to 40°E), consistent with previous work based on reanalysis data (Xulu et al., 2020).

Figures 4.9a-b show anomaly outputs, subtracting the original CNTRL run from the FLAT or SEA runs to observe changes between the experiments. The positive anomaly in the FLAT model (**Fig. 4.9a**) runs through the southwestern edge of the MC (~ 4-8 m), with the maximum anomaly sitting on the southwestern edge of Madagascar (+10 m) when compared to the CNTRL. The SEA run (**Fig. 4.9b**) displays a similar positive anomaly location but with smaller differences in magnitude from the CNTRL (maximum 4-6 m). Another but weaker positive anomaly is found to the east of Madagascar. The positive differences in FLAT and SEA relative to CNTRL over southern Madagascar suggest that the reduced topography in these runs allows for a more westward location of the SIHP, causing increased northeasterly winds to flow south of 16°S. However, north of this latitude, a negative difference is apparent in SEA relative to CNTRL (**Fig 4.9b**). This negative difference may occur due to the removal of land in SEA weakening the northwesterly monsoonal flow towards where northern Madagascar is located and strengthening the northeasterly monsoonal flow towards northern Mozambique instead. As seen in Barimalala et al., (2018) "HEAT" experiment, the interpolated grid points over the removed surface (northern Madagascar) show higher surface temperatures (similar to the adjacent SST) than the elevated land surface would have. Hence, there is relative surface heating on the southwestern edge and downstream of Madagascar, relative to CNTRL, and thus an "anomalous heat low" is evident in this region (not shown).

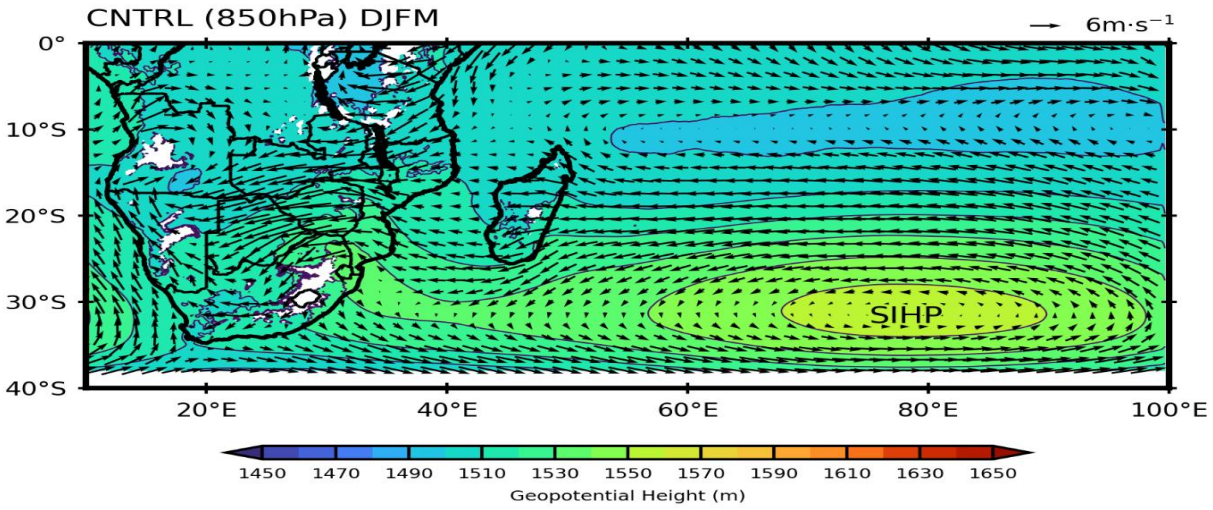

Figure 4.8: CNTRL's 850-hPa wind (vectors; m·s^{-1}) and GPH (shaded; m) taken over 2000-2016, December through March.

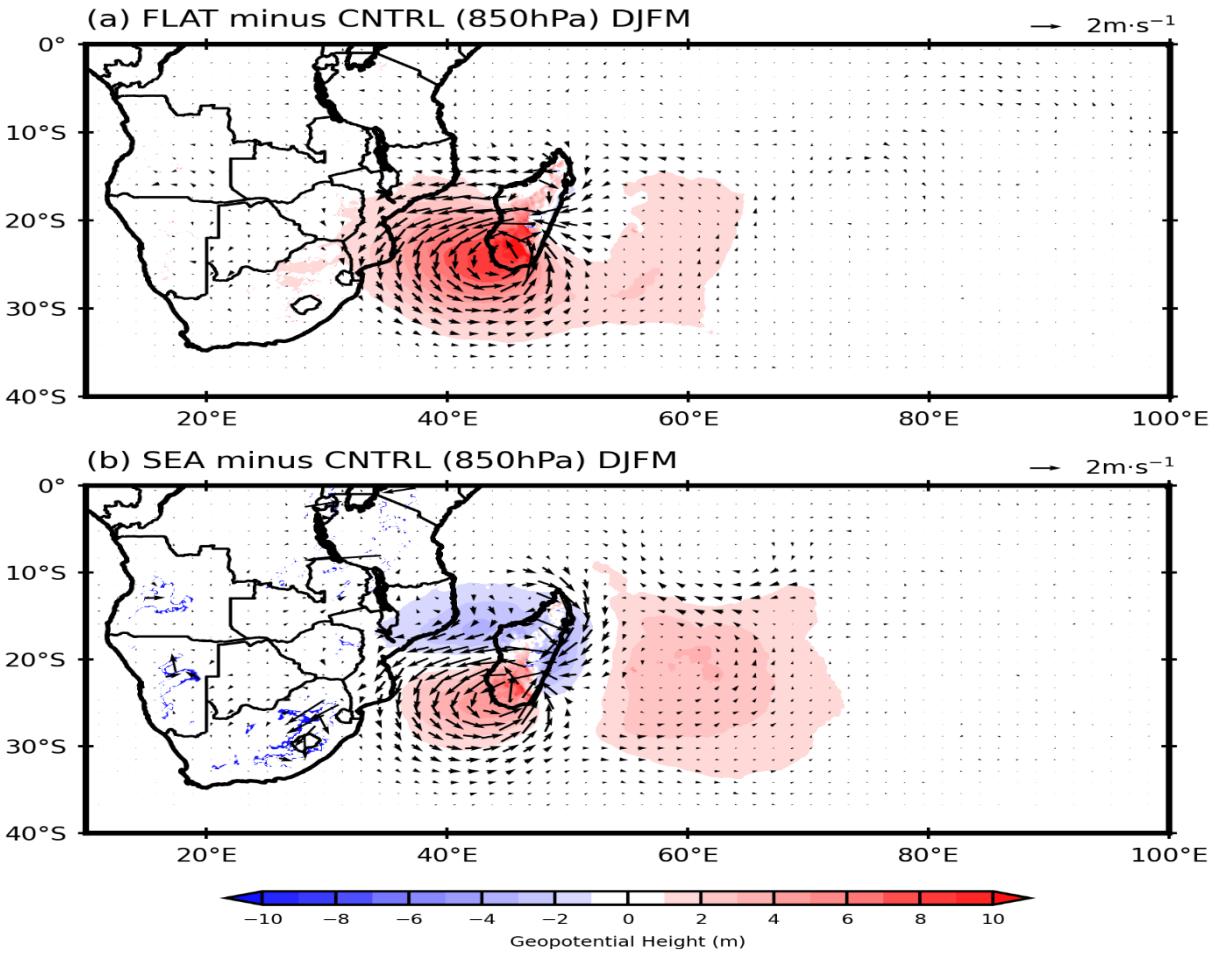

Figure 4.9: Shows 850-hPa wind (vectors; m·s^{-1}) and GPH (shaded; m) taken over 2000-2016, December through March. In (a), the CNTRL run is subtracted from FLAT. In (b), the CNTRL run is subtracted from SEA. Both show positive anomalies (red) as differences in FLAT or SEA and negative (blue) as differences in CNTRL.

4.4.2. 500hPa Mid-Level Wind Analysis

Figure 4.10 shows the CNTRL zonal (u) and meridional (v) winds (vectors; $m \cdot s^{-1}$) and GPH (shaded; m) at the 500hPa pressure level. The subtropical jet is located at the edge of the Hadley cell circulation (25-30°S) over southern Africa / SWIO, with the BH centered over northeastern Namibia / northwestern Botswana.

Figures 4.11a-b show differences in 500hPa winds in CNTRL from FLAT or SEA . As found at the 850hPa level, there are prominent anticyclonic anomalies over and near southern Madagascar, but these are shown to be more spatially extensive. Stronger easterly winds east of northern Madagascar in both FLAT and SEA imply a stronger steering current, allowing for tropical storms generated in the tropical South Indian Ocean to track toward the island. Further north, there are also cyclonic differences from CNTRL in the 500hPa plots, which are mainly confined to the island in the FLAT experiment but extend across the MC and large parts of the mainland in SEA. These cyclonic differences are strongest over the channel and Mozambique.

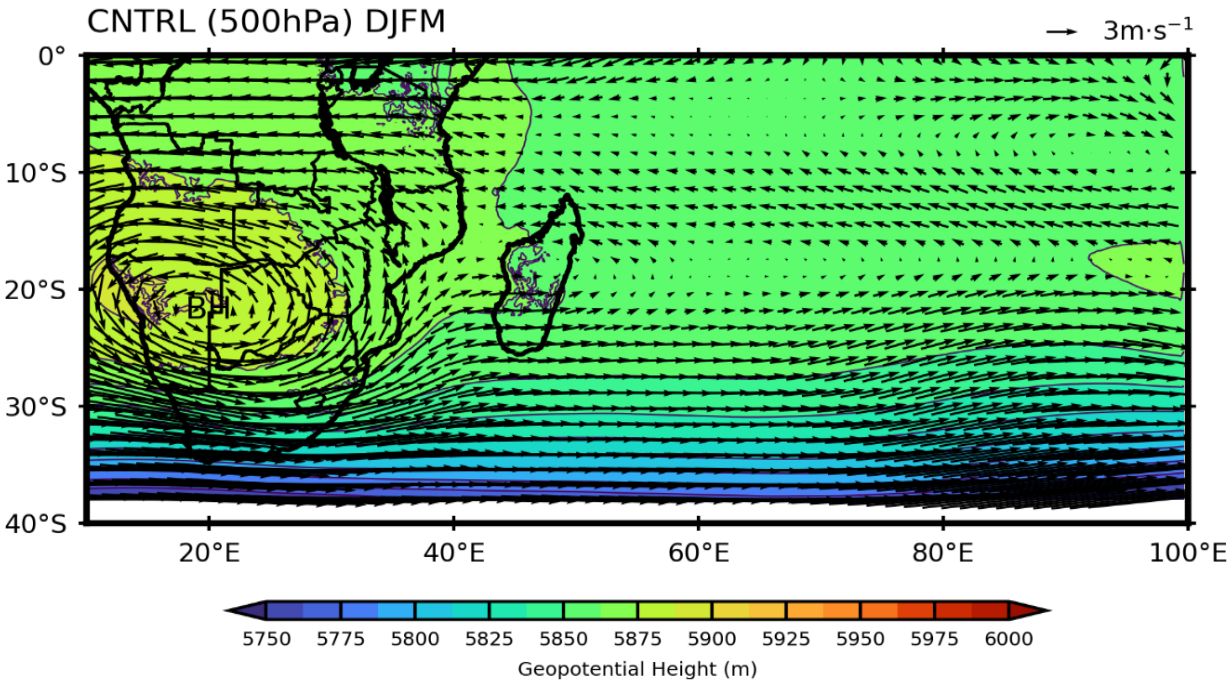

Figure 4.10: CNTRL's 500-hPa wind (vectors; $m \cdot s^{-1}$) and GPH (shaded; m) over the period 2000-2016, December through March

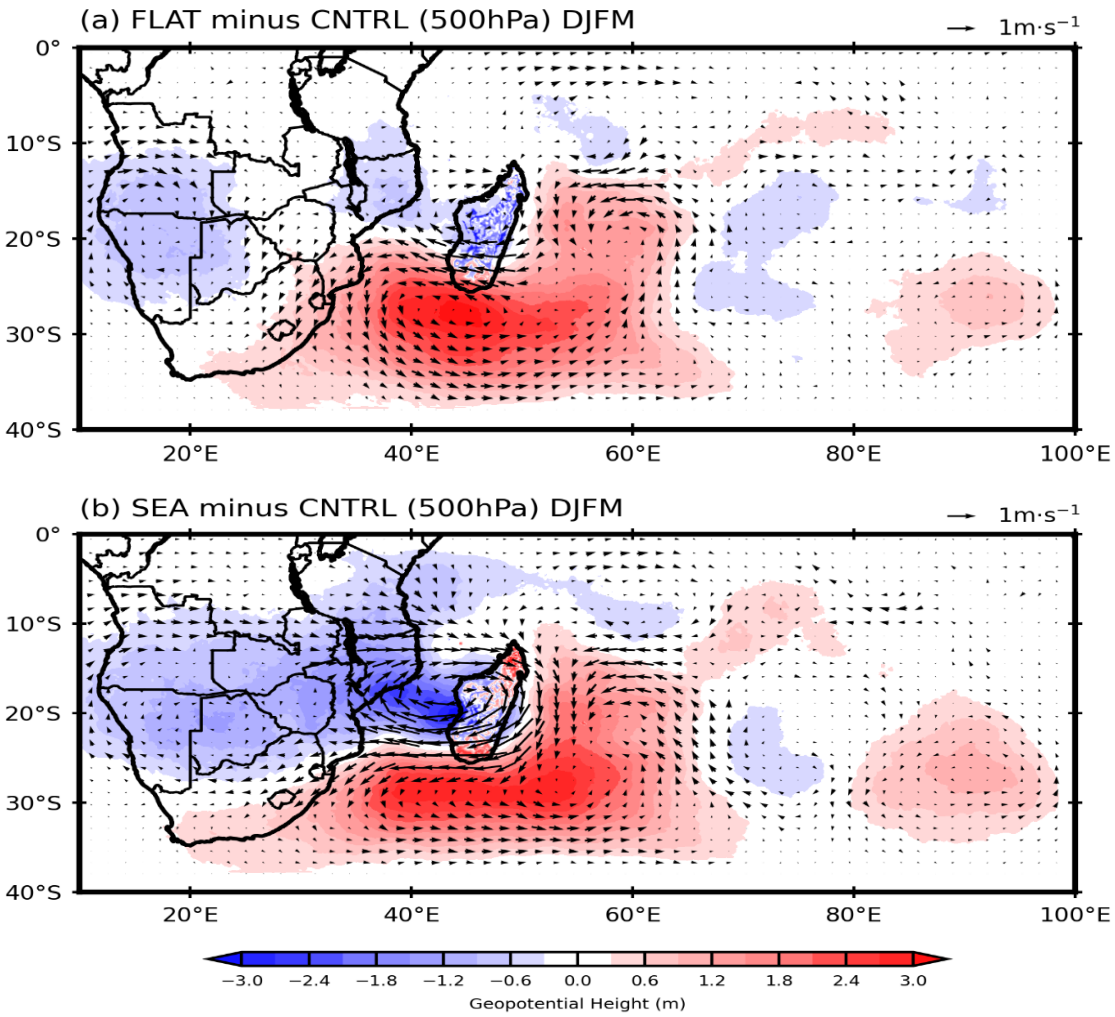

Figure 4.11: 500-hPa wind (vectors; $m \cdot s^{-1}$) and GPH (shaded; m) taken over 2000-2016, December through March. In (a), the CNTRL run is subtracted from FLAT. In (b), the CNTRL run is subtracted from SEA. Both show positive anomalies (red) as differences in FLAT or SEA and negative (blue) as differences in CNTRL.

4.4.3 Vertical Wind Transects

Figure 4.13a-c plots vertical wind cross sections along 43°E and 12-25°S, just off the west coast of Madagascar (red line; **Fig 4.12**). In CNTRL, low-level easterlies are present at about 25-20°S, north of which they weaken and then become weak westerlies, reflecting the location of the MCT in the central channel and the monsoonal flow (westerlies extending up to about 800-850hPa) to its north. As expected, there is not much change from CNTRL to the mid- or upper-level winds in the FLAT or SEA runs; However, clear changes are seen in the lower levels, with the easterlies extending north to about 16°S in FLAT (**Fig. 4.13b**) and throughout the entire channel in SEA

(**Fig. 4.13c**) when the island is replaced by ocean. This northward extension of the easterlies follows due to no island land mass east of southern Africa and no turning of the northeasterly monsoonal winds into monsoonal westerlies across the northern channel as in CNTRL or the real world. Instead, the northeasterly monsoon in SEA penetrates northern Mozambique (**Fig. 4.14a**). In FLAT, the low-level flow in the northern channel still shows evidence of the northwesterly monsoonal winds towards the north of the island (**Fig. 4.14b**). However, the reduced topography weakens the monsoon circulation in the region. The stronger low-level easterlies in FLAT, particularly SEA, are conducive to a greater likelihood of TC landfall in Mozambique (Vitart et al., 2003; Klinman and Reason, 2008). **Figure 4.13d-f** displays a vertical wind cross section spanning the entire domain (0-40°S) west of Madagascar (43°E). Both the CNTRL (**Fig. 4.13d**), FLAT (**Fig. 4.13e**), and SEA (**Fig. 4.13f**) runs on top of the enhanced easterly winds are found to show representations of the STJ-S (200-300hPa) and AEJ-S (500-600hPa). Compared to CNTRL, both sensitivity runs showed enhancements (1-3m·s^{-1}) of both jet features through the reduced topography along with a northward shift in the lower-level easterly winds (**Fig. 4.13c-d**). The enhancement of these jets, along with the northward shift of easterly winds, are found because of variations among variables such as wind shear and moisture flux (Jackson et al., 2008; Astier et al., 2015)

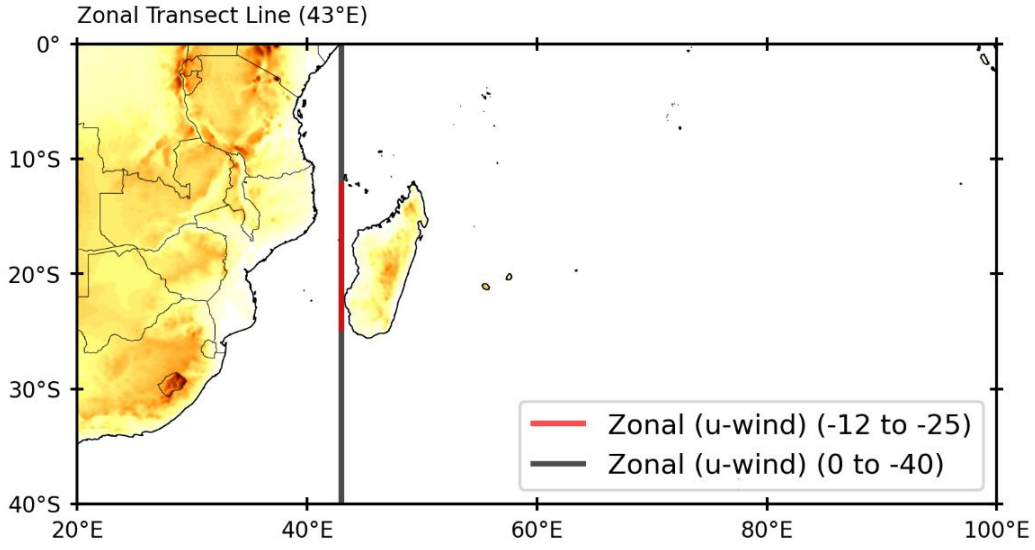

Figure 4.12: The transect is taken from the red line (12-25°S) and black line (0-40°S) from 1000-200hPa.

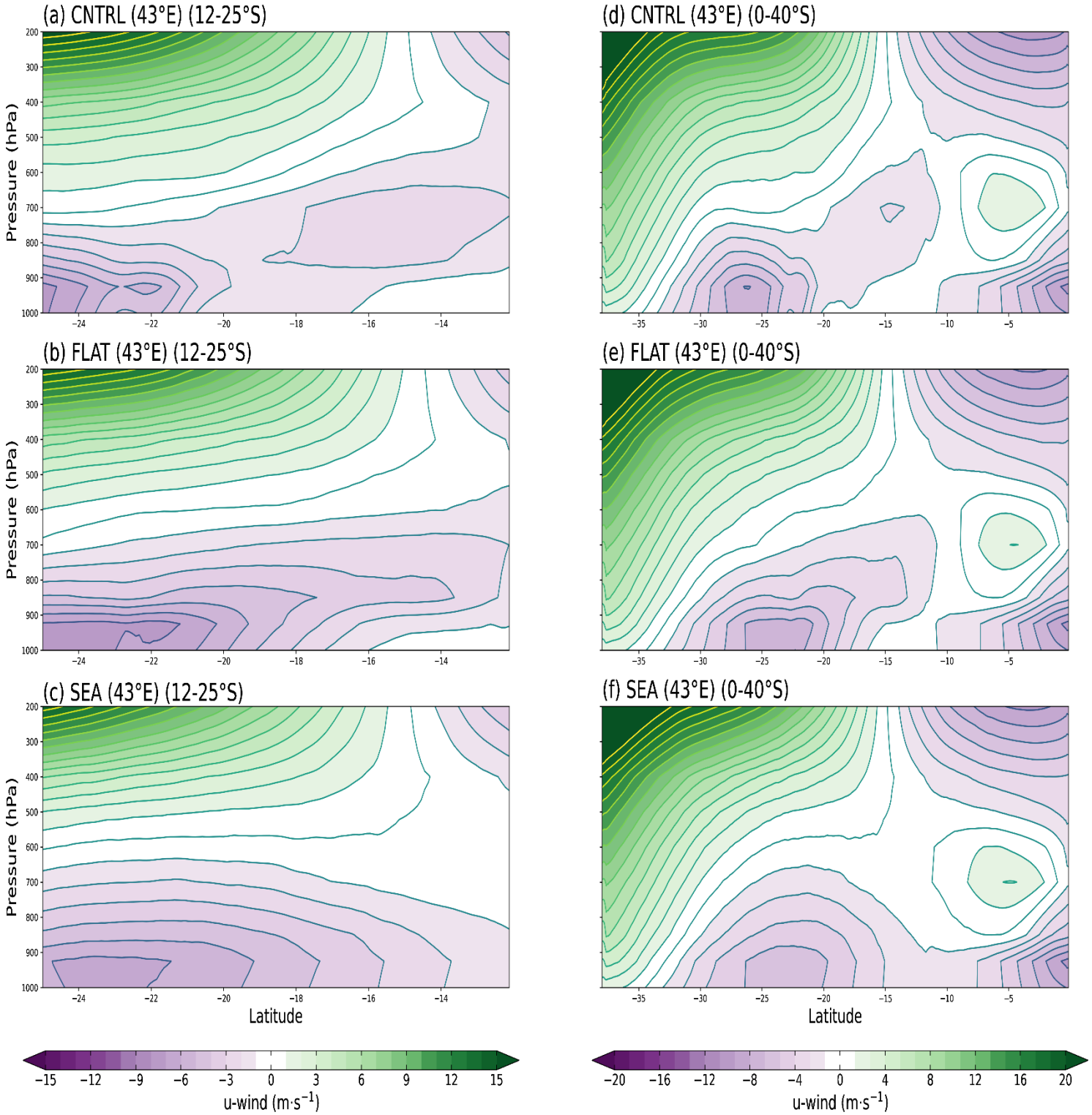

Figure 4.13: Vertical Wind Transect zonal (u-wind) (vectors; m·s-1) located at 43°S just off Madagascan west coast averaged from December Through March. Each figure represents the zonal wind running from 12-25°S or 0-40°S, representing the CNTRL (a, d), FLAT (b, e), and SEA (c, f) runs.

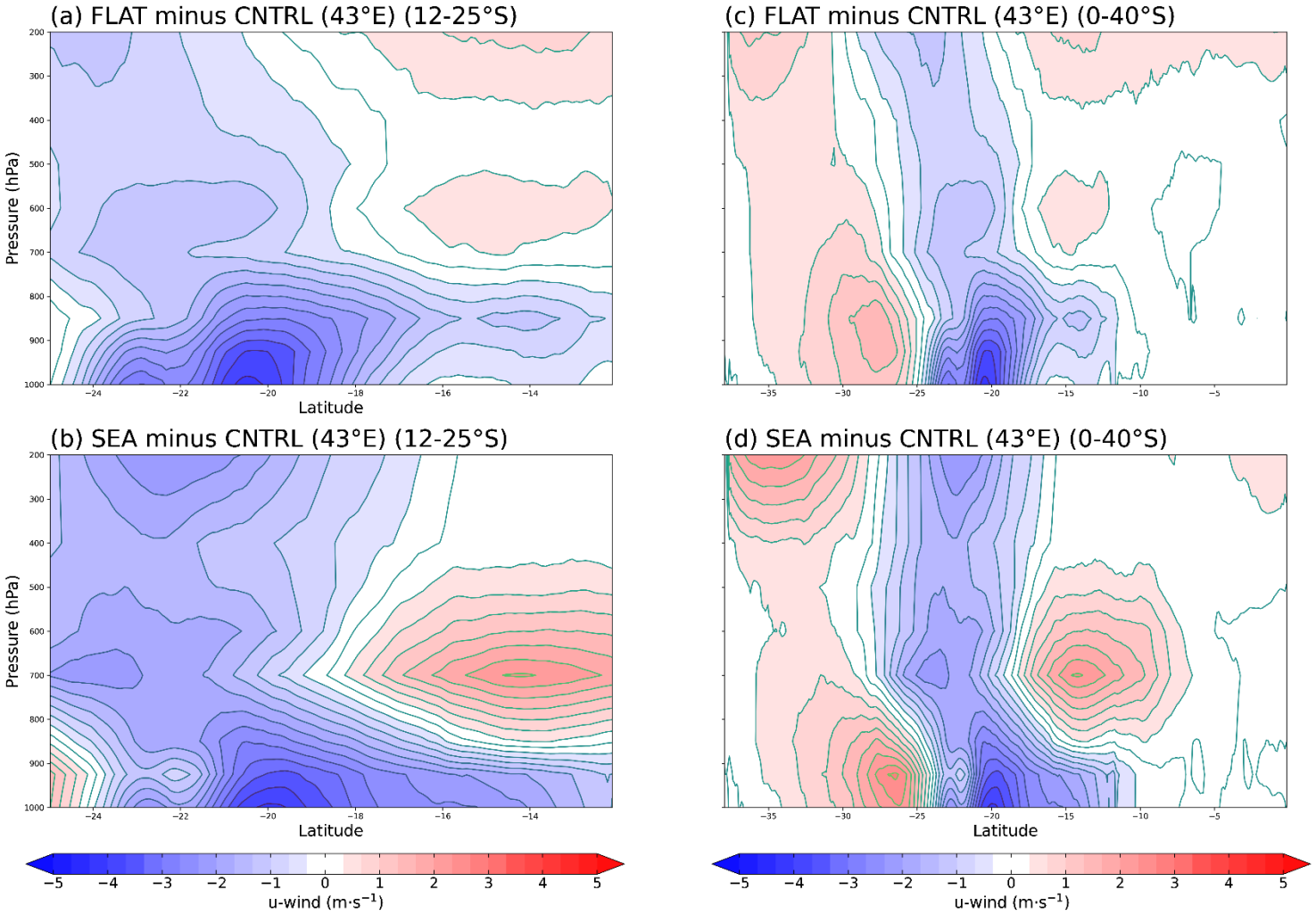

Figure 4.14: Anomalies of zonal (u-wind) (vectors; m·s-1) located 43°S of Madagascar, averaging through December Through March. Each figure represents either the transect 12-25°S or 0-40°S, showing either the FLAT minus CNTRL (a, c) or SEA minus CNTRL (b, d). Color bars show anomalies, with blue indicating a change in the FLAT or SEA run and red indicating a change in CNTRL.

4.4.4 Outgoing Longwave Radiation

A useful proxy of convective cloud cover is given by Outgoing Longwave Radiation (OLR), where low values indicate an increase in deep convective cloud cover. Thus, differences in OLR from CNTRL indicate changes in convective cloud and associated rainfall for the FLAT and SEA runs (**Fig. 4.15a-b**). In FLAT, the northwesterly monsoon is weaker than CNTRL, with reduced cloud cover leading to positive OLR over most of the island and northern channel. As discussed above, the northwesterly monsoon is absent in SEA, resulting in a considerably less convective cloud cover over the island and northeastern channel and hence large positive anomalies in OLR (**Fig. 4.15b**). On the other hand, most of the central and southern channels show substantially lower values of OLR than in CNTRL in both cases, particularly in SEA (**Fig. 4.15b**). These negative OLR differences in the southern and central channels in FLAT and SEA indicate increased convection relative to CNTRL, some of which result from increased TC activity. **Figures 4.5-4.7** show that FLAT and particularly SEA exhibit increased TC track and genesis numbers in these parts of the channel relative to what occurs in the CNTRL run.

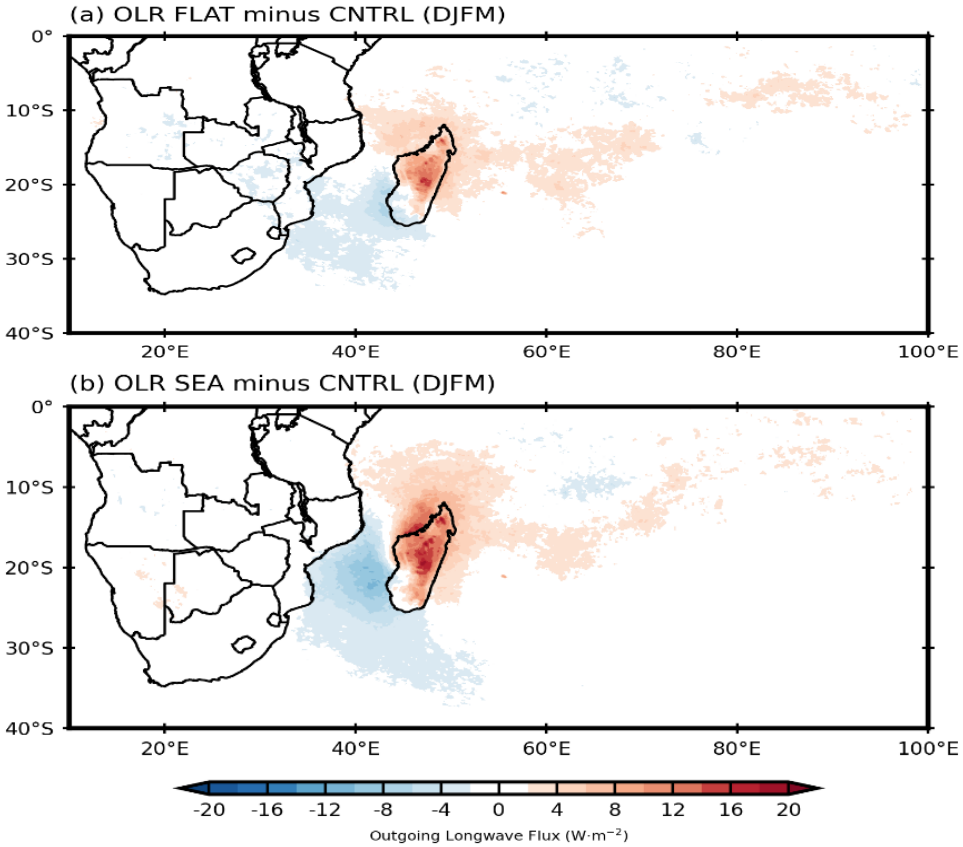

Figure 4.15: OLR differences (shading, $W \cdot m^{-2}$) for FLAT minus CNTRL (a) SEA minus CNTRL (b). Negative (positive) differences imply more (less) convective clouds relative to CNTRL.

4.5. Tropical Cyclone Characteristics

4.5.1. Duration

Changes in storm duration between the three runs are determined for both the full SWIO domain (0-100°E,10-40°S) as well as a sub-domain that focuses on the Madagascan region (32-60°E, 5-35°S) (Black box; **Fig. 4.16**). The results for each duration category are presented as the percentage of the total TCs from September to April in the respective domain shown.

4.5.2. Southwest Indian Ocean Domain

Figure 4.17a shows storm duration starting with short-lived storms, two days or less, with the following categories broken down into four-day increments. In CNTRL over the full domain, the two shortest categories account for about 26% of cases, after which the frequencies of longer-lasting storms drop off quickly to fall to 5% or less for the cases lasting at least 15 days. On the other hand, both FLAT and SEA show the highest frequencies in the second duration category (3-6 days), beyond which the numbers decrease rapidly for the longer-lasting cases. It is not obvious why FLAT and SEA do not also show relatively higher numbers in the shortest duration category. Still, it may relate to the flattened or removed topography allowing storms approaching Madagascar from the south Indian Ocean to last longer than would be the case when the mountains of this island are present. Note that compared to the real world, CNTRL shows too many TCs in the longest-lasting category (> 22 days) (4% or 12 TC) TC Eline is one observed case that has lasted about this long (~ 29 days), but there are few if any other such cases in the real world (Reason and Keibel, 2004). The bias towards too many longer-lasting storms in the model may result from the over-sensitivity of the TRACK algorithm to TC propagation.

4.5.3. Madagascan Sub-Domain

While the bias towards too many long-lasting storms remains for the sub-domain (**Fig. 4.17b**), CNTRL has a clear drop off from the highest numbers in the shortest duration category to longer-lasting cases. FLAT and SEA again show a displaced peak to the second shortest category (3-6 days) with much greater percentages of storms of this duration type than in CNTRL. Thus, the general increase in TC activity in FLAT and SEA in the channel relative to CNTRL likely results from more storms lasting 3-6 days than from storms of other duration categories.

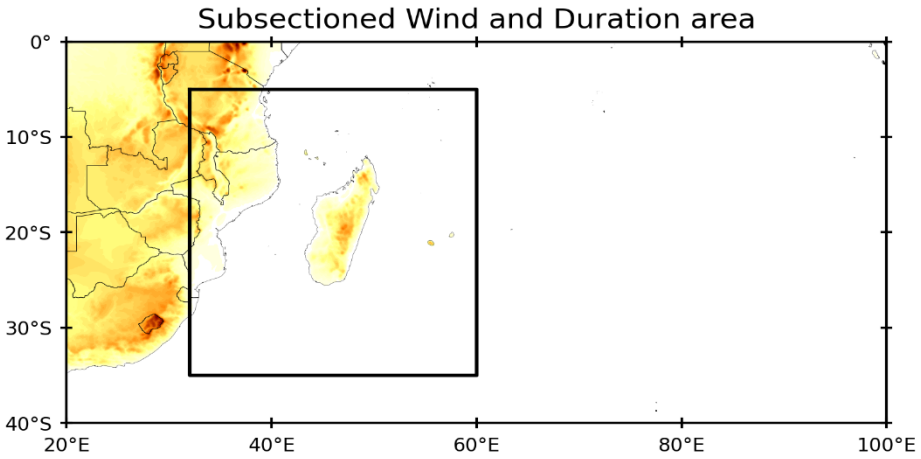

Figure 4.16: A subdomain box that encompasses the MC and Madagascar (32-60°E, 5-35°S)

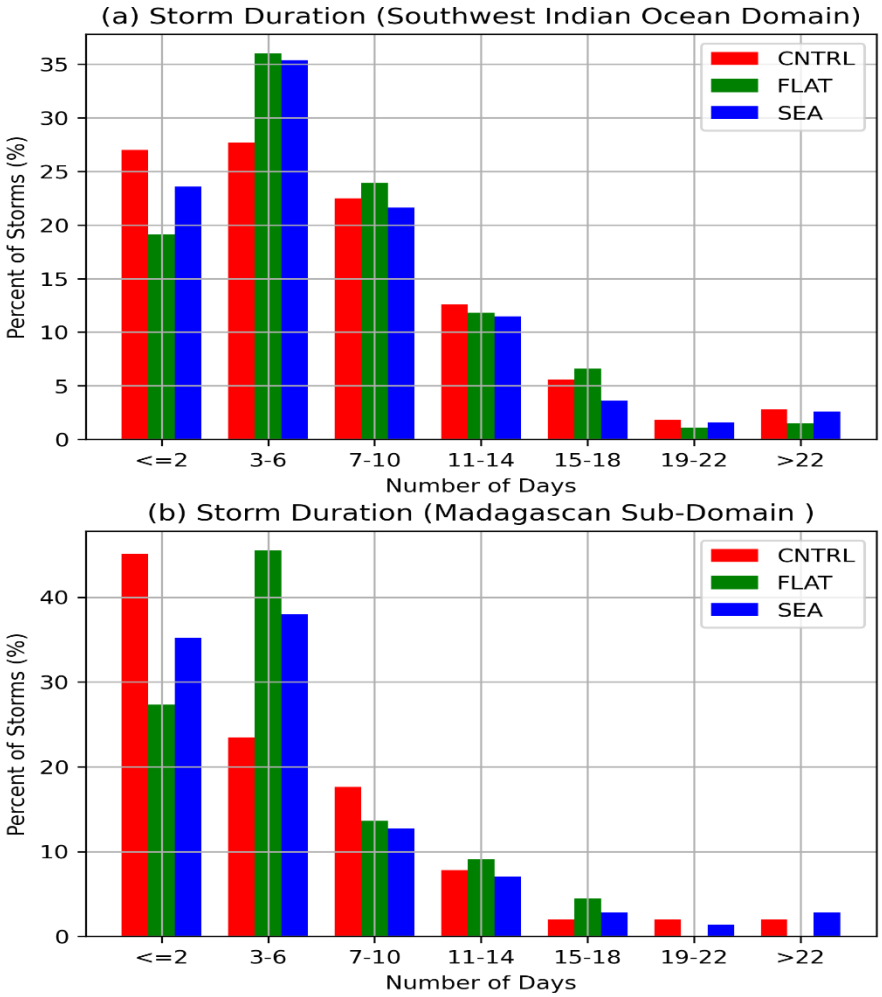

Figure 4.17: Storm duration breakdown of TCs created within the SWIO Domain (0-100°E,10-40°S) (a) and the Madagascan sub-domain (32-60°E, 5-35°S) (b). Each category is divided into four days intervals, with the runs being broken down into CNTRL (Red), FLAT (Green), and SEA (Blue).

4.5.4 Tropical Cyclone Intensity

The previous section shows how Madagascar's topography has been found to play a role in the duration of TC. In the following section, a look at TC intensity is examined by inspecting TC's maximum wind speed found at 10m (**Fig. 4.18a-b**). The following figures display the same boundaries as discussed in Section 4.4.1, outlining the SWIO domain as well as a subdomain located around the Madagascan region. Each intensity category is then presented as the percentage of the total TCs in the respective domain.

4.5.5 Southwest Indian Ocean Domain

Figure 4.18a shows intensity categories following the SWIO tropical cyclone intensity scale created through the Météo-France's La Réunion TC center, which monitors the region. The three scenarios are all found to start with <5% of storms peaking as Tropical Disturbances (TD) (<50 km/h), with the CNTRL and SEA runs showing <1%. All three models are then found to jump by 15-25% in the following two categories with a peak intensity as Moderate Tropical Storms (MTS) (63-88km/h). This is consistent with previous studies showing that the majority of storms created within the Southwest Indian domain peak at a Tropical storm intensity (Leroux et al., 2018). The following two categories are then found to show storm intensity decreasing in frequency by 15-25% in both Severe Tropical Storm (STS) (89–117 km/h) and Tropical Cyclone (TC) (118–165 km/h). Although storm frequencies decreased amongst higher intensity storms in CNTRL and FLAT, the SEA run produced the highest number of TC developments (12% or 37 TC) out of all three runs, showing the model to produce more intense storms throughout the domain compared to the CNTRL. This TC increase within the SEA run could be attributed to added latent heat release and atmospheric moisture caused by the additional SST over Madagascar. Storm frequency past TC intensity shows to be nonexistent in all three models indicating a bias towards weaker storm tracks. Although it is unclear why storm frequencies with higher intensities than TC are not represented in all three runs, this lack of representation could be attributed to the WRF model's initial setup.

4.5.6 Madagascan Sub-Domain

Although a storm bias towards weaker storm tracks remains (**Fig. 4.18b**), the subdomain allows for investigating storm track intensities surrounding the MC. All three models were again found

to peak in the MTS category, with the CNTRL and FLAT showing 15-20% more storms than the SEA run. This peak in tropical storms could be attributed to the CNTRL and FLAT runs topography affecting the intensity of incoming storms as they approach land. The SEA model continues to show a higher frequency of TC surrounding the MC, with the SEA run being almost 15% higher than CNTRL and FLAT. This higher frequency of intense storm tracks indicates that the lack of island topography allows for a better environment for storm intensification closer to land.

In summary, storm duration and intensity showed subtle variations among the three models. The SWIO domain was found to show storm tracks to peak between 3 to 6 days in all three runs as well as reach a maximum of MTS intensity. However, the SEA model continued to show a higher percentage of TC storms when compared to CNTRL in both domains. This indicates that the added SST in SEA allowed for higher-intensity storms to be produced but not necessarily for tracks to have a longer duration.

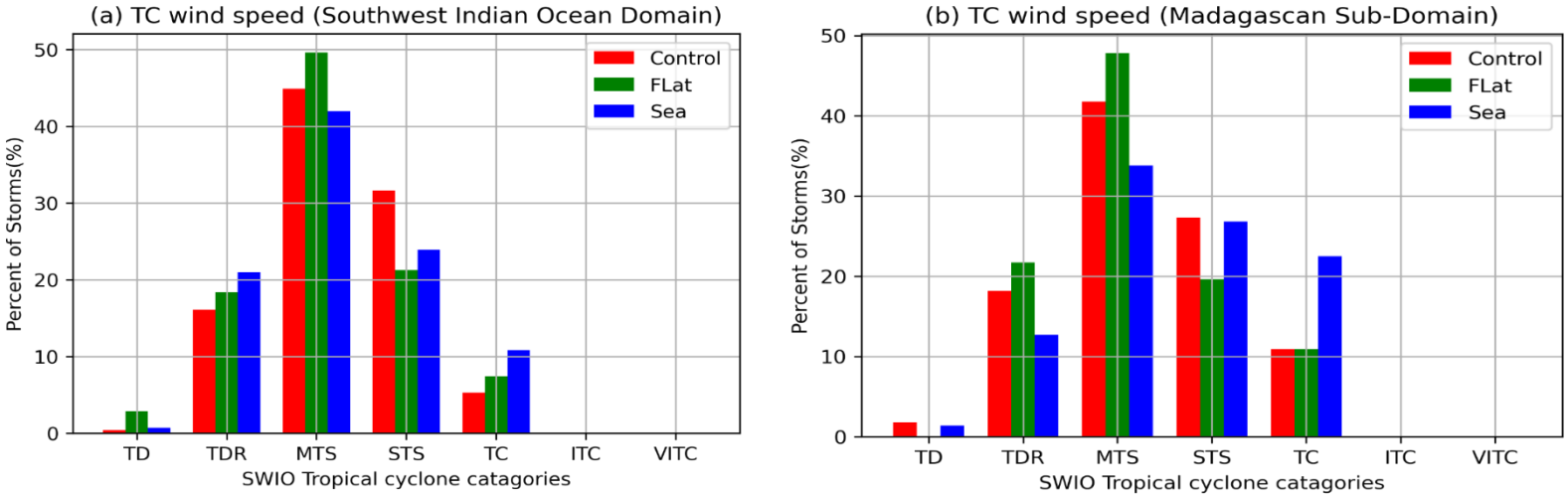

Figure 4.18: Storm intensity breakdown of TCs created within the full domain (0-100°E,10-40°S) (a) and subsection domain (32-60°E, 5-35°S) (b). Each category is broken down based on the TC Intensity Scale created through the Météo-France's La Réunion Tropical Cyclone Center. The following runs are then broken down into CNTRL (Red), FLAT (Green), and SEA (Blue).

4.6. Summary

This chapter analyzed the CNTRL model and sensitivity tests FLAT and SEA, focusing on TC genesis, trajectory, background climatology, and overall storm characteristics. Although there was a slight overestimation of certain features, such as the SIHP and BH in ERA5, and a bias towards northern TC genesis and tracks compared to IBTrACS, the CNTRL model demonstrated relatively accurate background climatology and storm trajectories representing key atmospheric features and general storm tracks seen previously in the SWIO.

The CNTRL run was then tested against the FLAT and SEA sensitivity runs, whose track outputs, particularly SEA, were found to produce a stronger zonal trajectory of TC towards land. The SEA run showed a 3.9% increase in TCs making landfall compared to the CNTRL run, along with a 3.3% increase in storm genesis within the channel. However, despite its flattened topography, the FLAT run still led to most storms recurving out to the SWIO with only a 1.7% (4 storms) increase in storms hitting land.

Through the background climatology, both the FLAT and SEA run was found to exhibit a stronger SIHP and enhanced easterly flow indicative of more zonal storm tracks. However, the flatting and interpolated topography were found to weaken features such as the STJ-S and AEJ, leading to enhanced moisture flux and low vertical shear surrounding the channel creating a more optimal environment for storm genesis. The combined latent heat release from the added SST allowed for an increase in OLR and enhanced convection surrounding the MC.

Both the FLAT and SEA showed similar storm characteristics with small variations between CNTRL, FLAT, and SEA. However, the SEA run showed a higher representation of TC over the entire basin when compared to both FLAT and CNTRL, showing a stronger intensity storm to be created but not necessarily a longer duration of TC.

In the upcoming section, Discussions and Conclusions, the significance and relevance of these results will be discussed in regard to the relevant literature.

Chapter 5

5. Discussion and Conclusion

5.1 Overview

This study explored how the topography of Madagascar potentially influences the incoming path of TCs in the SWIO. This was done by running a set of sensitivity experiments using a regional climate model. Previous research has indicated that topographical features, such as Madagascar, significantly impact the regional climate, particularly regarding precipitation and moisture flux towards southern Africa (e.g., Munday and Washington, 2017; Barimalala et al., 2018; 2020). Although there has been research on the role of Madagascar's topography on regional climate, there is little understanding of how this relates to TCs.

Within the SWIO, TCs are found to form roughly 8-9°S off the equator during the austral summer (November – April). In each season, around 12- 14, storms are created, with only a small amount penetrating southern Africa (Mavume et al., 2009). Most storms in the SWIO are found to follow a southwestward trajectory, following a recurve southeastward once interacting with Madagascar topography. Within the MC, very few storms are found to form due to relatively weak wind shear, SST, and moisture flux, which is needed for TC formation (Jury and Pathack, 1991; Gray, 1998; Mavume et al., 2009). Although, storms that do form in the MC are found further south and generally follow a south-southeastward trajectory out of the channel (Matays, 2015). However, TCs formed on the eastward side of the MC during days of higher GPHs were then found to have a higher probability of tracking southwestward into Mozambique (Matays, 2015).

Intense storms such as TC Eline (February–March 2000), TC Favio (February 2007), and the recent TC Freddy (March 2023) have shown uncharacteristic tracks, whereby these systems penetrated further inland (westwards) than was normal for an average TC. It remains unclear as to what exact factors may result in these unusual tracks around southern Africa and highlights the need to better understand TC frequency, location, and tracks in the SWIO.

5.2 Model Setup and TRACK Analysis

5.2.1. The WRF Model and Input

This study's initial CNTRL run was run at a 10 km horizontal resolution over the SWIO basin (10-100°E, 0-40°S) with 49 vertical layers and up to 200hPa. The model was forced by CFSRV2 reanalysis data every 6 hours starting September 1st, 2000, and running until April 30th, 2001. This process was then done for 16 austral summers up to 2016. The models' physics parameterizations were all found to be the optimal parameters for the SWIO region, simulating the southern African climate relatively accurately according to previous literature. Due to computational restraints, each model's output was then pulled at 00 UTC and used as inputs for the Hodges TRACK algorithm (Hodges 1994,1995)

As previously discussed, the boundary condition for each model run was provided by CFSRV2 reanalysis data. CFSRV2 is a global atmospheric reanalysis dataset that comprehensively describes the Earth's climate system by assimilating a wide range of observations into a numerical weather prediction model (Saha et al., 2010, 2014). CFSRV2 was chosen due to its relatively high horizontal resolution (~38 km) and general performance in simulating Southern Hemisphere TCs, including MSLP, vertical structure, and 10-meter wind speeds (Saha et al., 2010, 2014; Hodges et al., 2017). CFSRV2 was also found to utilize a technique to perfect TC tracks by adjusting the location of the TC vortex to the observed coordinates before assimilating the observational data into the numerical model (Saha et al., 2010). Due to its ability to produce reasonable storm tracks, WRF has previously been used with this reanalysis data as a boundary condition to simulate storms such as TC Dineo in February 2017 (Meyiwa, 2019). However, it is recognized that more modern reanalysis data, such as ERA5, could produce a more realistic simulation of TCs (Gualtieri, 2022; Donkin and Abiodun, 2023). This could be due to better resolving key TC development and intensity features, such as ERA5's improved estimation of latent heat release associated with the Agulhas Current (Nkwinkwa et al., 2019).

Another key factor in simulating the TCs is the horizontal resolution of the experiments. The selected resolution for this study of 10km has previously been found as an acceptable resolution for TC climatological studies (Rapolaki and Reason, 2018; Meyiwa, 2019). However, future work could investigate running at a higher resolution (<10km), allowing for a possibly better

representation of TC vertical structure, location, timing, and intensity. A finer model resolution, specifically in the Northern Hemisphere, has contributed to the accuracy of TC vertical structure, tracks, and time of genesis occurrences (Done et al., 2004; Kain et al., 2006; Weisman et al., 2008). However, little research has been done on the optimal resolution within the SWIO. Using the Model for Prediction Across Scales-Atmosphere (MPAS-A) data, Donkin and Abiodun (2023) tested the influence of horizontal resolution on a few TC case study events in the SWIO. Through the case studies of TCs Idai and Kenneth, a higher resolution (anywhere from 10km to 3km) allowed for an optimal environment for accurate TC tracking and intensity (Lui et al., 2021). It was also found that a change in the physical parametrization, such as running a convection-permitting parameterization at a higher resolution (i.e., 3km), did not show TC Kenneth's rapid intensification, as seen in reality. This was found to be due to the convective parameterization, as well as the higher resolution, not accurately capturing the transport of heat and moisture up to the upper troposphere, which in turn did not simulate the rapid intensification of TC Kenneth properly. It should be noted that MPAS-A has been found to compare similarly to the WRF model in comparison of storm tracks and the underestimation of TC intensity (Lui et al., 2021).

5.2.2. TRACK Analysis

Outside of the initial WRF model setup, the TRACK algorithm (Hodges 1995, 1996) was used to identify and track TCs. This algorithm is found to be used in a significant amount of storm tracking studies in both the Northern (Hodges and Emerton, 2015; Redmond et al., 2015; Manganello et al., 2012) and Southern (Hoskins and Hodges, 2005; Gleixner et al., 2014) Hemispheres. Input data for TRACK was the WRF daily (00 UTC) output due to computation constraints. A limited test on 6 hourly input data was performed, and it was found to be slightly more advantageous than the daily data (not shown). When comparing the daily to the 6 hourly inputs, it was found that the daily is more likely to produce inaccurate storm tracks due to large shifts in storm location, intensity, and structure between 24-hour periods. Therefore, running this tracking model with 6-hourly input would perhaps then allow for higher accuracy of storm tracking, creating a more realistic tracking record when compared to IBTrACS, which is discussed in more detail below.

5.3 Comparison Between CNTRL and Observed

The background climatology and TC tracks of the CNTRL model were assessed by comparing them with observations from the ERA5 reanalysis dataset and identified TCs from the IBTrACS database. The comparisons indicated that the CNTRL run reasonably simulated the regional climate. However, there were some clear differences between the two outputs, such as ERA5 showing a stronger westward migration of the SIHP as well as a stronger BH pressure when compared to CNTRL. These systems account for variations in easterly wind flow, moisture flux, and inland convection within southern Africa (Xulu et al., 2020; Driver and Reason, 2017) These changes could account for variations in TC within the CNTRL being simulated differently than observed, particularly when it came to the timing, genesis location and tracking of individual systems (e.g., TC Favio – February 2007). Further to that, it was found that the WRF model's CNTRL simulation of TCs contained a slight bias toward weaker storm developments. Previous studies have found that a weaker-than-observed storm bias can be attributed to the model's initial setup, such as physical parameterizations, model resolution, and boundary conditions (Cha and Wang, 2013).

Overall, CNTRL was found to provide relatively accurate storm trajectories towards Madagascar (i.e., westward migration and southeastward recurve) as well as produced a relatively accurate number of TCs per season, with an average of 12-14 per year (e.g., Mavume et al., 2000). As a result, the TCs simulated in the CNTRL indicated that the model is a suitable data input to study TC sensitivity toward Madagascar's topography.

5.4 The Sensitivity Experiments

There were two sensitivity runs performed using the WRF model, namely, (1) a flattened topography with the Madagascan topography being smoothed down to a 300m plateau (FLAT) and (2) where the ocean replaced the Madagascar land mass through interpolating the surrounding SST (SEA). As previously discussed, the sensitivity simulations were subjected to the same conditioning as CNTRL to assess how the modified terrain affected the behavior of approaching storms.

Within the FLAT run, it was initially observed that there was a decrease in the number of storms generated in comparison to the CNTRL. However, the storms that were produced were found to show a stronger zonal trajectory approaching Madagascar from the northeastern edge. It was observed that most TC originating from the SWIO approached Madagascar similarly to the CNTRL (southwestward trajectory); however, upon interacting with Madagascar's flattened topography, a decrease of 9% in storm progression was seen similar to that of CNTRL, suggesting that despite the flattened topography, most storms continued to recurve on a poleward trajectory as they approached and were pushed further southeastward after their interaction with the terrain. Following landfall in Mozambique, the FLAT run indicated a rise of around 2% in the number of storms that penetrated inland compared to CNTRL. Since there was no significant change in the number of genesis storms being created within the MC between FLAT and CNTRL, the 2% increase was equated towards a slightly higher number of TCs zonally progressing towards land.

Regarding the SEA run, the model was found to have an increase in both storms tracking inland as well as genesis occurrences. Although the initial SWIO storm trajectories were found to be like that of CNTRL, the removal of land allowed storms to have a stronger zonal (westward) trajectory contributing to a around a 4% increase in storms tracking into the mainland and a 5.6% increase in storms passing through the channel when compared the CNTRL. By removing the island, it was also discovered that there was a 3.3% rise in the occurrence of TC formation in the MC region, in contrast to the CNTRL, indicating optimal conditions for TC genesis with the added SST surrounding Mozambique.

Due to a greater frequency of storms making landfall, the baseline climate was then subsequently examined across the three runs. For both (FLAT and SEA), the easterly winds over the South Indian Ocean were found to be substantially stronger than in CNTRL, leading to a doubling in lower-level moisture flux towards Madagascar. The strengthening of the low-level easterlies was related to the SIHP in the South Indian Ocean being stronger and located closer to southern Africa in FLAT and SEA relative to CNTRL. These changes in moisture fluxes in the Madagascan region result in greater penetration of South Indian Ocean moisture over the southern African mainland and hence increased summer rainfall there (but decreased over Madagascar) in FLAT and SEA relative to CNTRL (Barimalala et al., 2018).

As previously discussed, storms generated around the eastern edge of the SIHP in the FLAT and SEA were found to progress on a zonal trajectory over the northeastern part of the flattened or interpolated Madagascar before exhibiting a strong southeastward recurve back into the open South Indian Ocean. In general, the storms in FLAT and SEA appear to be generated further north than is typical in observation and have stronger zonal tracking compared to CNTRL and IBTrACS. Although in the real South Indian Ocean, tropical storms can sometimes generate an equatorward of 8-9^{o}S, all three model runs show many storms developing in the 5-8°S band, which is unrealistic. Similarly, too many model storms track mainly westward and for too long. In reality, systems often track more in a southward or southwestward direction, as seen in studies such as Mavume et al. (2009) and Ash and Matyas (2012). However, as seen in Ash and Matyas, 2012 further westward and southwestward tracking, similar to that of FLAT and SEA, was found through a neutral ENSO and a positive SIOD. Although influential, these features were not found to be soul initiators toward a westward trajectory.

Although genesis further north is common outside of the run, the majority of storms were found to start in the northern SWIO and then progress on a westward trajectory tracking towards the northern edge of Madagascar. However, as observed, the FLAT run showed a stronger recurve once reaching the island's northeastern edge compared to SEA, which tracked more zonally. These TCs tracks are different from the more common poleward trajectories observed storms forming further north in the SWIO are found to take (Ash and Matyas, 2012; Ho et al., 2006; Ramsay et al., 2012). The model bias towards a too westwardly track appears to be greater in SEA than in FLAT, perhaps because the removal of the island in SEA results in the easterly winds north of 16°S strengthening compared to CNTRL as well as added latent heat flux due to the additional SST. However, there are cases in the real world where intense TCs can track for great distances in a more or less completely westward direction, as seen in TC Eline in February 2000 (Reason and Keibel, 2004), TC Kenneth in April 2019 (Mawren et al., 2020) and most recently TC Freddy in March 2023. It is not obvious why the model tends to generate too many tropical storms in low latitudes compared to observations. Still, it may be related to model bias in the location of SIHP and the TRB. For example, the model SIHP is stronger and extends further west than reality and hence is less favorable for the monsoonal northwesterly to penetrate over northern Madagascar and the ocean to its northeast, thereby shifting the TRB northwards in the model. Such a bias

allows model tropical storms to generate north of where they would realistically and track more easily in a westward direction.

Within the Madagascan Sub-Domain, storm tracks in FLAT show a southwest recurve once approaching the flattened topography compared to CNTRL. This result seems counter-intuitive since the lower and flatter topography would present less of a barrier to storm passage near and over the island. However, Barimalala et al. (2018) showed that the Rossby / Froude number ratio, appropriate for rotating, stratified flow approaching a mountain barrier, is still well within the blocking category in FLAT (Ro/Fr = 1.4, in order for blocking not to occur, Ro/Fr << 1 is needed). FLAT, therefore, presents a plateau barrier of 300m above sea level, which appears to be effective at encouraging approaching storms to recurve back into the open South Indian Ocean rather than continuing westwards over the island. Further research is needed to better understand the mechanisms by which the large-scale topography interacts with the background flow and influences the storm's track.

Storm genesis in the MC relative to the total number of model storms in the South Indian Ocean does not vary significantly between FLAT and CNTRL. However, as previously stated, for SEA, there is a substantial increase (3.3%) in the number of storms generated in the channel relative to the whole model domain. This increase in SEA may be related to the increase in surface latent heat flux since a warm SST grid point in that experiment has now replaced Madagascar. Quasigeostrophic theory (e.g., Fandry and Leslie, 1984) implies that a lowering of topography can be thought of as adding artificial heating over the area. As a result, such a lowering might be favorable for moisture concentration over the channel and storm development. A latent heat analysis was then performed during the TC season (DJFM) on FLAT and SEA compared to CNTRL to observe how much additional heat was added through the flatting and removal of the island (**Appendix; Fig. 6.1a-b**). The FLAT run showed no addend latent heat over Madagascar compared to CNTRL, as the experiment replicated all land, surface characteristics, and vegetation types used in the CNTRL run (**Fig. 6.1a**). However, a small increase (20-30 $W \cdot m^{-2}$) in latent heat surrounding the island was seen, possibly due to variations in SST and enhanced easterly flow toward the surface. In contrast, the SEA run exhibited an extra inflow of latent heat (180-240 $W \cdot m^{-2}$) throughout the entire island and into the MC due to the interpolated SST now replacing the land (**Fig. 6.1b**). This supplementary heat source encompassing the island and the continuous easterly

trade winds leading to an enhanced moisture flux indicates an optimal environment for a greater occurrence of TCs generated in the SEA run, particularly in the vicinity of the MC.

Storm trajectories within the channel are found further north in both FLAT and SEA relative to CNTRL, with a strong south-eastward trajectory back into the South Indian Ocean. Those storms forming further south in the channel are found to have a strong poleward trajectory out in the ocean areas east of South Africa. The observed trajectory of storms, particularly as they near land such as Mozambique, could be linked to the presence of intensified easterly trade winds causing a westerly zonal flow. This aligns with the findings of Matyas (2015), which suggested that more powerful easterly winds were associated with a more severe SIHP and a positive Indian Ocean Subtropical Dipole leading to a strong recurve of storms out of the channel. Climate modes such as the Indian Ocean Subtropical Dipole, Southern Annular Mode, and ENSO have also all been found to lead to anomalies in the anticyclonic circulation over the subtropical South Indian Ocean (Reason et al., 2000). Such anomalies may then influence the number of storms generated and their tracks over the South Indian Ocean (Ash and Matyas, 2012)

Through the analysis of the mid-level 500hPa winds, strong easterly winds are present north of 25°S with weaker westerlies south of 19°S. During the FLAT (SEA) runs, smaller anticyclonic pressure systems are observed on Madagascar's southwestward (eastward) side. These systems have relatively minor variations in pressure when compared to the CNTRL run (contour intervals +-3 m). However, during the FLAT run, the high-pressure system was positioned along the southwestern edge of Madagascar between 35-45°E, possibly resulting in the increase of TCs having a zonal trajectory oriented toward Madagascar. It was found that many of these tracks closely resembled the path of TC Favio and TC Eline, which both had mid-level pressure systems situated south of Madagascar during their progression inland. As a result, the storms did not follow a southward trajectory as is common and instead followed a strong east-west trajectory towards Mozambique (Reason and Keibel, 2004; Klinman and Reason, 2008). Similarly, the SEA run showed a high-pressure system situated southeast of Madagascar. This shift and the uninterrupted easterly flow resulted in an even stronger east-west steering flow, facilitating the zonal trajectory of outer ocean storms toward land. Both runs also depicted a cyclonic anomaly showing a higher pressure within the CNTRL run. Compared to FLAT, the pressure anomaly is observed across the entire island; however, in SEA, it extends into the MC.

Additional factors also found to affect the regional climate included the STJ-S, situated at 30-35°S and approximately 200hPa, and the AEJ-S, located at 5-15°S and 600hPa. Using vertical transect plots, these jet features were both found to be slightly enhanced in FLAT and SEA runs, possibly due to the reduced surface friction created through the flatting or removal of the Madagascar terrain. Variations in these features, specifically the strengthen or latitudinal movement of the STJ-S toward the equator or poles, can then be found to impact factors such as moisture flux and VWS over the channel, contributing to or hindering cyclogenesis. Within an unaltered environment, the strengthened or lateral movement towards the equator of the STJ-S is found to cause a stronger VWS over the channel leading to a decrease in cyclogenesis (Astier et al., 2015). Studies have shown that the most effective VWS for the formation of TC is in the range of 5-10 $m \cdot s^{-1}$. This range facilitates the formation of the "ventilation" effect in the TC's core, creating optimal conditions for its development (Gray, 1968; Demaria, 1996; Bracken and Bosart, 2000). Therefore, a shear analysis was done over the DJFM period between the 500-850hPa levels on both the SEA and FLAT runs compared to the CNTRL to investigate the altered shear environments. Both runs showed an increase of 1-3 $m \cdot s^{-1}$ in VWS over the MC; however, the original CNTRL run only showed VWS originally averaging at 1-1.5 $m \cdot s^{-1}$, and therefore both the FLAT and SEA runs only peaked at 4.5-5 $m \cdot s^{-1}$ (**Appendix; Fig. 6.2a-b**). With the VWS staying within the optimal range, additional variables such aslatent heat flux and moisture flux become more influential towards storm developments within the channel.

Additionally, moisture concentration was also found to shift in accordance with Madagascar's topography. This caused a variation within TC genesis, intensity, and duration surrounding the island. OLR was used in the representation for precipitation and convection for the SWIO and showed to be consistent with Barimalala et al. (2018) paper indicating that both the FLAT and SEA runs have higher precipitation running over the MC when compared to the CNTRL. Barimalala et al. (2018) originally found moisture shift to be connected to the MCT's weakening (strengthening), causing a strengthening (weakening) of the SICZ. This confirms an increase (decrease) of moisture transport towards southeast Africa, causing an increase (decrease) in mainland rainfall. As described earlier, the combination of an increased moisture flux into the land and an undisturbed easterly flow within the SEA run creates a more conducive environment for TC genesis within the MC (Matyas, 2015).

5.5 Conclusion

The initial reason for conducting this study was to better understand the sensitivity of TC, whose courses were affected by the terrain of Madagascar. Storms like TC Eline (February 2000), TC Favio (February 2007), and TC Idai (March 2019) all demonstrated changes in their path or strength as they approached or crossed the island topography. Although many of the TC were considered atypical among the previous storms in the SWIO, more recent events, such as the very intense TC Freddy, demonstrated a comparable zonal trajectory into Madagascar's topography. Very intense TC Freddy was found to impact the region a total of three times, with continued recurving between Madagascar and Mozambique. This impact was found to allow for a significant amount of damage to the countries that were already found to be impacted by TC Batsirai and TC Cheneso in the previous months (Flash Update No. 1,2023). Once hitting land, TC Freddy was found to drop over six months' worth of rain in over six days, leaving over 1000 people either deceased or missing from multiple counties (Flash Update No. 12) This storm alone was also found to create significant flooding and housing damage causing over 874,000 people to suffer from hunger after the impact (Flash Update No. 1,2023).

This idealized sensitivity study allowed one to explore the potential influences of Madagascar and its topography on TC characteristics and trajectories toward land using different simulated terrain heights. While this study allowed for a first order understanding of Madagascar influences, it was found to be limited due to the lack of feedback from the altered Madagascan surface on the boundary conditions (i.e., CFSR). This limited feedback would not have been seen as a problem had the study been run using a global circulation model. However, using a regional circulation model helped concentrate on the essential storm statistics and regional circulation response of TC. Note that this study did not perform any statistical analysis or spatial examination of TC intensity across the various model runs. While this would have provided a more comprehensive understanding of the results, it would have required additional ensemble runs for each case, which were not computationally feasible during the scope of this study. However, this analysis is recommended for future work. Although this study did not delve into the specifics of how changes in topography affect the dynamics of flow as it adjusts to the changes in topography and its effects on cyclogenesis or movement, it offers valuable insights that complement actual simulations of

specific TC events. Similar findings to this study regarding TC sensitivity to a manipulated island topography could also be seen in other islands worldwide, such as Tawain and the Philippines. Studies conducted on these islands have shown that TCs tend to interact with their mountainous topography before hitting the mainland. For instance, Yang et al. (2008) observed the atmospheric and tracking changes of TC Nari under multiple topographical conditions, ranging from full topography to a fully replaced ocean run, showing liner intensity and track changes within the storm as it approached the reduced topographical island. This study, as well as others conducted in this area, were found to have demonstrated that these topographical variations in both Taiwan and the Philippines can affect both the overall amount of wind speed and moisture flow in the region as well as specific aspects of TC behavior, such as with changes in intensity and trajectory towards land (Yang et al., 2008; Tang and Chan, 2014). However, it's important to note that size comparison should be considered when comparing results due to varying atmospheric factor changes that are largely based on the overall size and height of the island (Vitart et al., 2003). Madagascar, the fourth largest island in the world, has a large north-south extent close to the southern African mainland, which leads to rather unique impacts on the regional climate (as discussed in Mawren et al., 2023). Therefore, results from these studies are not directly comparable to the present results due to the varying size and height of the island. By highlighting the significance of Madagascan topography in the evolution of weather systems in the MC and SWIO region, it serves as a useful reference for future diagnostic studies using observations and reanalysis data products (Mawren et al., 2023).

References

Adebiyi, A. A., and Zuidema, P. (2016). The role of the southern African easterly jet in modifying the southeast Atlantic aerosol and cloud environments. *Quarterly Journal of the Royal Meteorological Society*, *142*(697), 1574–1589. https://doi.org/10.1002/qj.2765

Archer, C. L., and Caldeira, K. (2008). Historical trends in the jet streams. *Geophysical Research Letters*, *35*(8), L08803. https://doi.org/10.1029/2008GL033614

Arivelo, T. A., and Lin, Y.-L. (2016). Climatology of Heavy Orographic Rainfall Induced by Tropical Cyclones over Madagascar: From Synoptic to Mesoscale Perspectives. *Earth Science Research*, *5*(2), 132. https://doi.org/10.5539/esr.v5n2p132

Ash, K. D., and Matyas, C. J. (2012). The influences of ENSO and the subtropical Indian Ocean Dipole on tropical cyclone trajectories in the southwestern Indian Ocean. *International Journal of Climatology*, *32*(1), 41–56. https://doi.org/10.1002/joc.2249

Astier, N., Plu, M., and Claud, C. (2015). Associations between tropical cyclone activity in the Southwest Indian Ocean and El Niño Southern Oscillation: Tropical cyclone activity in the Southwest Indian Ocean and ENSO. *Atmospheric Science Letters*, *16*(4), 506–511. https://doi.org/10.1002/asl.589

Banzon, V. F., Reynolds, R. W., Stokes, D., and Xue, Y. (2014). A 1/4°-Spatial-Resolution Daily Sea Surface Temperature Climatology Based on a Blended Satellite and in situ Analysis. *Journal of Climate*, *27*(21), 8221–8228. https://doi.org/10.1175/JCLI-D-14-00293.1

Barimalala, R., Blamey, R. C., Desbiolles, F., and Reason, C. J. C. (2020). Variability in the Mozambique Channel Trough and Impacts on Southeast African Rainfall. *Journal of Climate*, *33*(2), 749–765. https://doi.org/10.1175/JCLI-D-19-0267.1

Barimalala, R., Blamey, R. C., Desbiolles, F., and Reason, C. J. C. (2021). The influence of southeastern African river valley jets on regional rainfall. *Climate Dynamics*, *57*(9–10), 2905–2920. https://doi.org/10.1007/s00382-021-05846-1

Barimalala, R., Desbiolles, F., Blamey, R. C., and Reason, C. (2018). Madagascar Influence on the South Indian Ocean Convergence Zone, the Mozambique Channel Trough and southern African Rainfall. *Geophysical Research Letters*, *45*(20). https://doi.org/10.1029/2018GL079964

References

Bengtsson, L., Botzet, M., and Esch, M. (1995). Hurricane-type vortices in a general circulation model. *Tellus A*, *47*(2), 175-196.

Berry, G., and Reeder, M. J. (2014). Objective Identification of the Intertropical Convergence Zone: Climatology and Trends from the ERA-Interim. *Journal of Climate*, *27*(5), 1894–1909. https://doi.org/10.1175/JCLI-D-13-00339.1

Betts, A. K., and Miller, M. J. (1986). A new convective adjustment scheme. Part II: Single column tests using GATE wave, BOMEX, ATEX and arctic air-mass data sets. *Quarterly Journal of the Royal Meteorological Society*, *112*(473), 693–709. https://doi.org/10.1002/qj.49711247308

Bluestein, H. B. (1992). *Synoptic-dynamic Meteorology in Midlatitudes: Observations and theory of weather systems* (Vol. 2). Taylor and Francis.

Bracken, W. E., and Bosart, L. F. (2000). The Role of Synoptic-Scale Flow during Tropical Cyclogenesis over the North Atlantic Ocean. *Monthly Weather Review*, *128*(2), 353. https://doi.org/10.1175/1520-0493(2000)128<0353:TROSSF>2.0.CO;2

Broccoli, A. J., and Manabe, S. (1990). Can existing climate models be used to study anthropogenic changes in tropical cyclone climate? *Geophysical Research Letters*, *17*(11), 1917–1920. https://doi.org/10.1029/GL017i011p01917

Brown, K. A., Carter Ingram, J., Flynn, D. F. B., Razafindrazaka, R., and Jeannoda, V. (2009). Protected Area Safeguard Tree and Shrub Communities from Degradation and Invasion: A Case Study in Eastern Madagascar. *Environmental Management*, *44*(1), 136–148. https://doi.org/10.1007/s00267-008-9257-5

Byrne, M. P., Pendergrass, A. G., Rapp, A. D., and Wodzicki, K. R. (2018). Response of the Intertropical Convergence Zone to Climate Change: Location, Width, and Strength. *Current Climate Change Reports*, *4*(4), 355–370. https://doi.org/10.1007/s40641-018-0110-5

Cha, D.-H., and Wang, Y. (2013). A Dynamical Initialization Scheme for Real-Time Forecasts of Tropical Cyclones Using the WRF Model*. *Monthly Weather Review*, *141*(3), 964–986. https://doi.org/10.1175/MWR-D-12-00077.1

Chang-Seng, D. S., and Jury, M. R. (2010). Tropical cyclones in the SW Indian Ocean. Part 2: Structure and impacts at the event scale. *Meteorology and Atmospheric Physics*, *106*(3–4), 163–178. https://doi.org/10.1007/s00703-010-0059-y

References

Chen, F., and Dudhia, J. (2001). Coupling an advanced land-surface hydrology model with the Penn State-NCAR MM5 modeling system. Part I: model implementation and sensitivity. Monthly Weather Review, 129, 569–585

Chikoore, H., Vermeulen, J. H., and Jury, M. R. (2015). Tropical cyclones in the Mozambique Channel: January–March 2012. *Natural Hazards*, *77*(3), 2081–2095. https://doi.org/10.1007/s11069-015-1691-0

Cook, C., Reason, C., and Hewitson, B. (2004). Wet and dry spells within particularly wet and dry summers in the South African summer rainfall region. *Climate Research*, *26*, 17–31. https://doi.org/10.3354/cr026017

Crétat, J., Pohl, B., Richard, Y., and Drobinski, P. (2012). Uncertainties in simulating regional climate of southern Africa: Sensitivity to physical parameterizations using WRF. *Climate Dynamics*, *38*(3–4), 613–634. https://doi.org/10.1007/s00382-011-1055-8

Dare, R. A., and McBride, J. L. (2011). The Threshold Sea Surface Temperature Condition for Tropical Cyclogenesis. *Journal of Climate*, *24*(17), 4570–4576. https://doi.org/10.1175/JCLI-D-10-05006.1

Davis, C., Wang, W., Chen, S. S., Chen, Y., Corbosiero, K., DeMaria, M., Dudhia, J., Holland, G., Klemp, J., Michalakes, J., Reeves, H., Rotunno, R., Snyder, C., and Xiao, Q. (2008). Prediction of Landfalling

Defforge, C. L., and Merlis, T. M. (2017). Evaluating the Evidence of a Global Sea Surface Temperature Threshold for Tropical Cyclone Genesis. *Journal of Climate*, *30*(22), 9133–9145. https://doi.org/10.1175/JCLI-D-16-0737.1

DeMaria, M. (1996). The effect of vertical shear on tropical cyclone intensity change. *Journal of Atmospheric Sciences*, *53*(14), 2076-2088.

DeMaria, M. (1996). The effect of vertical shear on tropical cyclone intensity change. *Journal of Atmospheric Sciences*, *53*(14), 2076-2088.

Desbiolles, F., Blamey, R., Illig, S., James, R., Barimalala, R., Renault, L., and Reason, C. (2018). Upscaling impact of wind/sea surface temperature mesoscale interactions on southern Africa austral summer climate. *International Journal of Climatology*, *38*(12), 4651–4660. https://doi.org/10.1002/joc.5726

References

Done, J., Davis, C. A., and Weisman, M. (2004). The next generation of NWP: Explicit forecasts of convection using the weather research and forecasting (WRF) model. *Atmospheric Science Letters*, *5*(6), 110–117. https://doi.org/10.1002/asl.72

Donkin, P. T., and Abiodun, B. J. (2023). Capability and sensitivity of MPAS-A in simulating tropical cyclones over the South-West Indian Ocean. *Modeling Earth Systems and Environment*, *9*(1), 527–542. https://doi.org/10.1007/s40808-022-01517-0

Driver, P., and Reason, C. J. C. (2017). Variability in the Botswana High and its relationships with rainfall and temperature characteristics over southern Africa: VARIABILITY IN THE BOTSWANA HIGH AND SOUTHERN AFRICAN RAINFALL. *International Journal of Climatology*, *37*, 570–581. https://doi.org/10.1002/joc.5022

Dudhia, J. (1989). Numerical study of convection observed during the winter monsoon experiment using a mesoscale two-dimensional model. Journal of the Atmospheric Sciences, 46, 3077–3107. https://doi.org/10.1175/1520-0469

Emanuel, K. (2003). Tropical cyclones. *Annual review of earth and planetary sciences*, *31*(1), 75-104.

Fandry, C. B., Leslie, L. M., and Steedman, R. K. (1984). Kelvin-type coastal surges generated by tropical cyclones. *Journal of physical oceanography*, *14*(3), 582-593.

Feba, F., Ashok, K., and Ravichandran, M. (2019). Role of changed Indo-Pacific atmospheric circulation in the recent disconnect between the Indian summer monsoon and ENSO. *Climate Dynamics*, *52*, 1461-1470.

Feng, J., Hu, D., and Yu, L. (2014). How does the Indian Ocean subtropical dipole trigger the tropical Indian Ocean dipole via the Mascarene high? *Acta Oceanologica Sinica*, *33*(1), 64–76. https://doi.org/10.1007/s13131-014-0425-6

Fink, A. H., and Speth, P. (1998). Tropical cyclones. *Naturwissenschaften*, *85*, 482-493.

Fitchett, J. M., and Grab, S. W. (2014). A 66-year tropical cyclone record for south-east Africa: Temporal trends in a global context. *International Journal of Climatology*, *34*(13), 3604–3615. https://doi.org/10.1002/joc.3932

Gallego, D., Ribera, P., Garcia-Herrera, R., Hernandez, E., and Gimeno, L. (2005). A new look for the Southern Hemisphere jet stream. *Climate Dynamics*, *24*(6), 607–621. https://doi.org/10.1007/s00382-005-0006-7

References

Giorgi, F., and Mearns, L. O. (1999). Introduction to special section: Regional Climate Modeling Revisited. *Journal of Geophysical Research: Atmospheres*, *104*(D6), 6335–6352. https://doi.org/10.1029/98JD02072

Gleixner, S., Keenlyside, N., Hodges, K. I., Tseng, W.-L., and Bengtsson, L. (2014). An inter-hemispheric comparison of the tropical storm response to global warming. *Climate Dynamics*, *42*(7–8), 2147–2157. https://doi.org/10.1007/s00382-013-1914-6

Gray, W. M. (1968). GLOBAL VIEW OF THE ORIGIN OF TROPICAL DISTURBANCES AND STORMS. *Monthly Weather Review*, *96*(10), 669–700. https://doi.org/10.1175/1520-0493(1968)096<0669:GVOTOO>2.0.CO;2

Gray, W. M. (1998). The formation of tropical cyclones. *Meteorology and Atmospheric Physics*, *67*(1–4), 37–69. https://doi.org/10.1007/BF01277501

Gualtieri, G. (2022). Analysing the uncertainties of reanalysis data used for wind resource assessment: A critical review. *Renewable and Sustainable Energy Reviews*, *167*, 112741. https://doi.org/10.1016/j.rser.2022.112741

Held, I. M., and Hou, A. Y. (1980). Nonlinear axially symmetric circulations in a nearly inviscid atmosphere. *Journal of the Atmospheric Sciences*, *37*(3), 515-533.

Hersbach, H., Bell, B., Berrisford, P., Hirahara, S., Horányi, A., Muñoz-Sabater, J., Nicolas, J., Peubey, C., Radu, R., Schepers, D., Simmons, A., Soci, C., Abdalla, S., Abellan, X., Balsamo, G., Bechtold, P., Biavati, G., Bidlot, J., Bonavita, M., … Thépaut, J. (2020). The ERA5 global reanalysis. *Quarterly Journal of the Royal Meteorological Society*, *146*(730), 1999–2049. https://doi.org/10.1002/qj.3803

Hill, K. A., and Lackmann, G. M. (2009). Analysis of Idealized Tropical Cyclone Simulations Using the Weather Research and Forecasting Model: Sensitivity to Turbulence Parameterization and Grid Spacing. *Monthly Weather Review*, *137*(2), 745–765. https://doi.org/10.1175/2008MWR2220.1

Ho, C.-H., Kim, J.-H., Jeong, J.-H., Kim, H.-S., and Chen, D. (2006). Variation of tropical cyclone activity in the South Indian Ocean: El Niño–Southern Oscillation and Madden-Julian Oscillation effects. *Journal of Geophysical Research*, *111*(D22), D22101. https://doi.org/10.1029/2006JD007289

References

Hodges, K. I. (1994). A general method for tracking analysis and its application to meteorological data. *Monthly Weather Review*, *122*(11), 2573-2586.

Hodges, K. I. (1995). Feature tracking on the unit sphere. *Monthly Weather Review*, *123*(12), 3458-3465.

Hodges, K. I. (1996). Spherical nonparametric estimators applied to the UGAMP model integration for AMIP. *Monthly Weather Review*, *124*(12), 2914-2932.

Hodges, K. I. (1999). Adaptive Constraints for Feature Tracking. *Monthly Weather Review*, *127*(6), 1362–1373. https://doi.org/10.1175/1520-0493(1999)127<1362:ACFFT>2.0.CO;2

Hodges, K. I., and Emerton, R. (2015). The Prediction of Northern Hemisphere Tropical Cyclone Extended Life Cycles by the ECMWF Ensemble and Deterministic Prediction Systems. Part I: Tropical Cyclone Stage*. *Monthly Weather Review*, *143*(12), 5091–5114. https://doi.org/10.1175/MWR-D-13-00385.1

Hodges, K. I., Hoskins, B. J., Boyle, J., and Thorncroft, C. (2003). A Comparison of Recent Reanalysis Datasets Using Objective Feature Tracking: Storm Tracks and Tropical Easterly Waves. *Monthly Weather Review*, *131*(9), 2012–2037. https://doi.org/10.1175/1520-0493(2003)131<2012:ACORRD>2.0.CO;2

Hodges, K., Cobb, A., and Vidale, P. L. (2017). How Well Are Tropical Cyclones Represented in Reanalysis Datasets? *Journal of Climate*, *30*(14), 5243–5264. https://doi.org/10.1175/JCLI-D-16-0557.1

Hong, S. Y., Dudhia, J., and Chen, S. H. (2004). A revised approach to ice microphysical processes for the bulk parameterization of clouds and precipitation. Monthly Weather Review, 132(1), 103–120. https://doi.org/10.1175/1520-0493(2004)132<0103:ARATIM>2.0.CO;2

Hong, S. Y., Noh, Y., and Dudhia, J. (2006). A new vertical diffusion package with an explicit treatment of entrainment processes. Monthly Weather Review, 134(9), 2318–2341. https://doi.org/10.1175/Mwr3199.1

Hoskins, B. J., and Hodges, K. I. (2005). A new perspective on Southern Hemisphere storm tracks. *Journal of Climate*, *18*(20), 4108-4129.

References

Hurricanes with the Advanced Hurricane WRF Model. *Monthly Weather Review*, *136*(6), 1990–2005. https://doi.org/10.1175/2007MWR2085.1

Imbol Nkwinkwa N, A. S., Rouault, M., and Johannessen, J. A. (2019). Latent heat flux in the Agulhas Current. *Remote Sensing*, *11*(13), 1576.

Jackson, B., Nicholson, S. E., and Klotter, D. (2008). Mesoscale Convective Systems over Western Equatorial Africa and Their Relationship to Large-Scale Circulation. *Monthly Weather Review*, *137*(4), 1272–1294. https://doi.org/10.1175/2008MWR2525.1

Janjic, Z. (1994). The step-mountain eta coordinate model: Further developments of the convection, viscous sublayer and turbulence closure schemes. Monthly Weather Review, 122(5), 927–945. https://doi.org/10.1175/1520-0493(1994)122<0927:TSMECM>2.0.CO;2

Jury, M. R. (1993). A preliminary study of climatological associations and characteristics of tropical cyclones in the SW Indian Ocean. *Meteorology and Atmospheric Physics*, *51*(1–2), 101–115. https://doi.org/10.1007/BF01080882

Jury, M. R., and Pathack, B. (1991). A study of climate and weather variability over the tropical southwest Indian Ocean. *Meteorology and Atmospheric Physics*, *47*(1), 37–48. https://doi.org/10.1007/BF01025825

Jury, M. R., Pathack, B., and Parker, B. (1999). Climatic Determinants and Statistical Prediction of Tropical Cyclone Days in the Southwest Indian Ocean. *Journal of Climate*, *12*(6), 1738–1746. https://doi.org/10.1175/1520-0442(1999)012<1738:CDASPO>2.0.CO;2

Kain, J. S., Weiss, S. J., Levit, J. J., Baldwin, M. E., and Bright, D. R. (2006). Examination of Convection-Allowing Configurations of the WRF Model for the Prediction of Severe Convective Weather: The SPC/NSSL Spring Program 2004. *Weather and Forecasting*, *21*(2), 167–181. https://doi.org/10.1175/WAF906.1

Kim, D., Jin, C.-S., Ho, C.-H., Kim, J., and Kim, J.-H. (2015). Climatological features of WRF-simulated tropical cyclones over the western North Pacific. *Climate Dynamics*, *44*(11–12), 3223–3235. https://doi.org/10.1007/s00382-014-2410-3

Klinman, M. G., and Reason, C. J. C. (2008). On the peculiar storm track of TC Favio during the 2006–2007 Southwest Indian Ocean tropical cyclone season and relationships to ENSO. *Meteorology and Atmospheric Physics*, *100*(1–4), 233–242. https://doi.org/10.1007/s00703-008-0306-7

References

Knapp, K. R., Kruk, M. C., Levinson, D. H., Diamond, H. J., and Neumann, C. J. (2010). The International Best Track Archive for Climate Stewardship (IBTrACS): Unifying Tropical Cyclone Data. *Bulletin of the American Meteorological Society*, *91*(3), 363–376. https://doi.org/10.1175/2009BAMS2755.1

Kossin, J. P., Knapp, K. R., Vimont, D. J., Murnane, R. J., and Harper, B. A. (2007). A globally consistent reanalysis of hurricane variability and trends. *Geophysical Research Letters*, *34*(4), L04815. https://doi.org/10.1029/2006GL028836

Krishnamurti, T. N. (1961). The subtropical jet stream of winter. *Journal of the Atmospheric Sciences*, *18*(2), 172-191.

Kuete, G., Pokam Mba, W., and Washington, R. (2020). African Easterly Jet South: Control, maintenance mechanisms and link with Southern subtropical waves. *Climate Dynamics*, *54*(3–4), 1539–1552. https://doi.org/10.1007/s00382-019-05072-w

L'Heureux, M. L., and Thompson, D. W. J. (2006). Observed Relationships between the El Niño–Southern Oscillation and the Extratropical Zonal-Mean Circulation. *Journal of Climate*, *19*(2), 276–287. https://doi.org/10.1175/JCLI3617.1

Landman, W. A., Seth, A., and Camargo, S. J. (2005). The Effect of Regional Climate Model Domain Choice on the Simulation of Tropical Cyclone–Like Vortices in the Southwestern Indian Ocean. *Journal of Climate*, *18*(8), 1263–1274. https://doi.org/10.1175/JCLI3324.1

Leroux, M.-D. (2018). *Recent Advances in Research and Forecasting of Tropical Cyclone Track, Intensity, and Structure at Landfall*. *7*(2).

Lui YS, Tse LKS, Tam CY, Lau KH, Chen J (2021) Performance of MPAS-A and WRF in predicting and simulating western North Pacific tropical cyclone tracks and intensities. Theor Appl Climatol 143:505–520. https://doi.org/10.1007/s00704-020-03444-5

Malawi: Tropical Cyclone Freddy - Flash Update No. 1 (16 March 2023) - Malawi. (2023, March 16). ReliefWeb. https://reliefweb.int/report/malawi/malawi-tropical-cyclone-freddy-flash-update-no-1-16-march-2023

Malawi: Tropical Cyclone Freddy - Flash Update No. 12 (7 April 2023) - Malawi. (2023, April 7). ReliefWeb.https://reliefweb.int/report/malawi/malawi-tropical-cyclone-freddy-flash-update-no-12-7-april-2023

References

Manatsa, D., Morioka, Y., Behera, S. K., Matarira, C. H., and Yamagata, T. (2014). Impact of Mascarene High variability on the East African 'short rains.' *Climate Dynamics*, *42*(5–6), 1259–1274. https://doi.org/10.1007/s00382-013-1848-z

Manganello, J. V., Hodges, K. I., Kinter, J. L., Cash, B. A., Marx, L., Jung, T., Achuthavarier, D., Adams, J. M., Altshuler, E. L., Huang, B., Jin, E. K., Stan, C., Towers, P., and Wedi, N. (2012). Tropical Cyclone Climatology in a 10-km Global Atmospheric GCM: Toward Weather-Resolving Climate Modeling. *Journal of Climate*, *25*(11), 3867–3893. https://doi.org/10.1175/JCLI-D-11-00346.1

Matyas, C. J. (2015). Tropical cyclone formation and motion in the Mozambique Channel: TROPICAL CYCLONES IN THE MOZAMBIQUE CHANNEL. *International Journal of Climatology*, *35*(3), 375–390. https://doi.org/10.1002/joc.3985

Mavume, A., Rydberg, L., Rouault, M., and Lutjeharms, J. (2009). Climatology and Landfall of Tropical Cyclones in the South- West Indian Ocean. *Western Indian Ocean Journal of Marine Science*, *8*(1). https://doi.org/10.4314/wiojms.v8i1.56672

Mawren, D., Blamey, R., Hermes, J., and Reason, C. J. C. (2023). On the importance of the Mozambique Channel for the climate of southeastern Africa. *Climate Dynamics*, *60*(1–2), 279–299. https://doi.org/10.1007/s00382-022-06334-w

Mawren, D., Hermes, J., and Reason, C. J. C. (2020). Exceptional Tropical Cyclone Kenneth in the Far Northern Mozambique Channel and Ocean Eddy Influences. *Geophysical Research Letters*, *47*(16). https://doi.org/10.1029/2020GL088715

Mearns, L. O., Arritt, R., Biner, S., Bukovsky, M. S., McGinnis, S., Sain, S., Caya, D., Correia, J., Flory, D., Gutowski, W., Takle, E. S., Jones, R., Leung, R., Moufouma-Okia, W., McDaniel, L., Nunes, A. M. B., Qian, Y., Roads, J., Sloan, L., and Snyder, M. (2012). The North American Regional Climate Change Assessment Program: Overview of Phase I Results. *Bulletin of the American Meteorological Society*, *93*(9), 1337–1362. https://doi.org/10.1175/BAMS-D-11-00223.1

Mearns, L. O., Bogardi, I., Giorgi, F., Matyasovszky, I., and Palecki, M. (1999). Comparison of climate change scenarios generated from regional climate model experiments and statistical downscaling. *Journal of Geophysical Research: Atmospheres*, *104*(D6), 6603–6621. https://doi.org/10.1029/1998JD200042

References

Meyiwa, S. (2019). *Numerical modelling of Tropical Cyclone Dineo and its rainfall impacts over north-eastern South Africa* (Master's thesis, Faculty of Science).

Mich, B. (2022). *National Hurricane Operations Plan*.

Mlawer, E., Taubman, S., Brown, P., Iacono, M., and Clough, S. (1997). Radiative transfer for inhomogeneous atmospheres: RRTM. A validated correlated-k model for the longwave. Journal of Geophysical Research, 102(D14), 16,663–16,682. https://doi.org/10.1029/97JD00237

Moses, O., and Ramotonto, S. (2018). Assessing forecasting models on prediction of the tropical cyclone Dineo and the associated rainfall over Botswana. *Weather and Climate Extremes*, *21*, 102–109. https://doi.org/10.1016/j.wace.2018.07.004

Munday, C., and Washington, R. (2017). Circulation controls on southern African precipitation in coupled models: The role of the Angola Low: ANGOLA LOW AND RAINFALL IN MODELS. *Journal of Geophysical Research: Atmospheres*, *122*(2), 861–877. https://doi.org/10.1002/2016JD025736

Munday, C., and Washington, R. (2018). Systematic Climate Model Rainfall Biases over southern Africa: Links to Moisture Circulation and Topography. *Journal of Climate*, *31*(18), 7533–7548. https://doi.org/10.1175/JCLI-D-18-0008.1

Naeraa, M., and Jury, M. R. (1998). Tropical cyclone composite structure and impacts over eastern Madagascar during January?March 1994. *Meteorology and Atmospheric Physics*, *65*(1–2), 43–53. https://doi.org/10.1007/BF01030268

Nicholson, S. E. (2009). A revised picture of the structure of the "monsoon" and land ITCZ over West Africa. *Climate Dynamics*, *32*, 1155-1171.

Nicholson, S. E., and Grist, J. P. (2003). The seasonal evolution of the atmospheric circulation over West Africa and equatorial Africa. *Journal of climate*, *16*(7), 1013-1030.

Ogwang, B. A., Ongoma, V., Xing, L., and Ogou, K. F. (2015). Influence of Mascarene high and Indian Ocean dipole on East African extreme weather events. *Geographica Pannonica*, *19*(2), 64-72.

Olivier, J. (1993). Flood producing weather systems: Tropical cyclones. In W. J. R. Alexander (Ed.), Flood Risk Reduction Measures (pp. 23-34). University of Pretoria.

References

Parker, B. A., and Jury, M. R. (1999). Synoptic environment of composite tropical cyclones in the South-West Indian Ocean. *South African Journal of Marine Science*, *21*(1), 99–115.https://doi.org/10.2989/025776199784126105

Pezza, A. B., and Simmonds, I. (2005). The first South Atlantic hurricane: Unprecedented blocking, low shear and climate change. *Geophysical Research Letters*, *32*(15). https://doi.org/10.1029/2005gl023390

Pielke, R. A. (1990). The Hurricane Routledge. *NY, NY*.

Pillay, M. T., and Fitchett, J. M. (2021). On the conditions of formation of Southern Hemisphere tropical cyclones. *Weather and Climate Extremes*, *34*, 100376. https://doi.org/10.1016/j.wace.2021.100376

Potty, J., Oo, S. M., Raju, P. V. S., and Mohanty, U. C. (2012). Performance of nested WRF model in typhoon simulations over West Pacific and South China Sea. *Natural Hazards*, *63*(3), 1451–1470. https://doi.org/10.1007/s11069-011-0074-4

Ramsay, H. A., Camargo, S. J., and Kim, D. (2012). Cluster analysis of tropical cyclone tracks in the Southern Hemisphere. *Climate Dynamics*, *39*(3–4), 897–917. https://doi.org/10.1007/s00382-011-1225-8

Rapolaki, R. S., and Reason, C. J. C. (2018). Tropical storm Chedza and associated floods over south-eastern Africa. *Natural Hazards*, *93*(1), 189–217. https://doi.org/10.1007/s11069-018-3295-y

Ratnam, J. V., Behera, S. K., Masumoto, Y., Takahashi, K., and Yamagata, T. (2012). A simple regional coupled model experiment for summer-time climate simulation over southern Africa. *Climate Dynamics*, *39*(9–10), 2207–2217. https://doi.org/10.1007/s00382-011-1190-2

Ratnam, J. V., Behera, S. K., Ratna, S. B., Rautenbach, C. J. D. W., Lennard, C., Luo, J.-J., Masumoto, Y., Takahashi, K., and Yamagata, T. (2013). Dynamical Downscaling of Austral Summer Climate Forecasts over southern Africa Using a Regional Coupled Model. *Journal of Climate*, *26*(16), 6015–6032. https://doi.org/10.1175/JCLI-D-12-00645.1

Reason, C. J. C. (2007). Tropical cyclone Dera, the unusual 2000/01 tropical cyclone season in the Southwest Indian Ocean and associated rainfall anomalies over southern Africa. *Meteorology and Atmospheric Physics*, *97*(1–4), 181–188. https://doi.org/10.1007/s00703-006-0251-2

References

Reason, C. J. C. (2017). Climate of southern Africa. In C. J. C. Reason, *Oxford Research Encyclopedia of Climate Science*. Oxford University Press. https://doi.org/10.1093/acrefore/9780190228620.013.513

Reason, C. J. C. (2019). Low-frequency variability in the Botswana High and southern African regional climate. *Theoretical and Applied Climatology*, *137*(1–2), 1321–1334. https://doi.org/10.1007/s00704-018-2661-8

Reason, C. J. C., Allan, R. J., Lindesay, J. A., and Ansell, T. J. (2000). ENSO and climatic signals across the Indian Ocean Basin in the global context: Part I, interannual composite patterns. *International Journal of Climatology*, *20*(11), 1285–1327. https://doi.org/10.1002/1097-0088(200009)20:11<1285::AID-JOC536>3.0.CO;2-R

Reason, C. J. C., and Keibel, A. (2004). Tropical Cyclone Eline and Its Unusual Penetration and Impacts over the southern African Mainland. *Weather and Forecasting*, *19*(5), 789–805. https://doi.org/10.1175/1520-0434(2004)019<0789:TCEAIU>2.0.CO;2

Reason, C. J. C., Landman, W., and Tennant, W. (2006). Seasonal to Decadal Prediction of southern African Climate and Its Links with Variability of the Atlantic Ocean. *Bulletin of the American Meteorological Society*, *87*(7), 941–956. https://doi.org/10.1175/BAMS-87-7-941

Redmond, G., Hodges, K. I., Mcsweeney, C., Jones, R., and Hein, D. (2015). Projected changes in tropical cyclones over Vietnam and the South China Sea using a 25 km regional climate model perturbed physics ensemble. *Climate Dynamics*, *45*(7–8), 1983–2000. https://doi.org/10.1007/s00382-014-2450-8

Reynolds RW, Smith TM, Liu C, Chelton DB, Casey KS, Schlax MG (2007) Daily high-resolution-blended analyses for sea surface temperature. J Clim 20:5473–5496. https://doi.org/10.1175/JCLI-D-14-00293.1

Roberts, M. J., Camp, J., Seddon, J., Vidale, P. L., Hodges, K., Vannière, B., Mecking, J., Haarsma, R., Bellucci, A., Scoccimarro, E., Caron, L., Chauvin, F., Terray, L., Valcke, S., Moine, M., Putrasahan, D., Roberts, C. D., Senan, R., Zarzycki, C., … Wu, L. (2020). Projected Future Changes in Tropical Cyclones Using the CMIP6 HighResMIP Multimodel Ensemble. *Geophysical Research Letters*, *47*(14). https://doi.org/10.1029/2020GL088662

Rossby, C.-G. (1949). On the Dispersion of Planetary Waves in a Barotropic: Atmosphere. *Tellus*, *1*(1), 54–58. https://doi.org/10.1111/j.2153-3490.1949.tb01928.x

References

Saha, S., Moorthi, S., Pan, H.-L., Wu, X., Wang, J., Nadiga, S., Tripp, P., Kistler, R., Woollen, J., Behringer, D., Liu, H., Stokes, D., Grumbine, R., Gayno, G., Wang, J., Hou, Y.-T., Chuang, H., Juang, H.-M. H., Sela, J., … Goldberg, M. (2010). The NCEP Climate Forecast System Reanalysis. *Bulletin of the American Meteorological Society*, *91*(8), 1015–1058. https://doi.org/10.1175/2010BAMS3001.1

Saha, S., Moorthi, S., Wu, X., Wang, J., Nadiga, S., Tripp, P., Behringer, D., Hou, Y.-T., Chuang, H., Iredell, M., Ek, M., Meng, J., Yang, R., Mendez, M. P., Van Den Dool, H., Zhang, Q., Wang, W., Chen, M., and Becker, E. (2014). The NCEP Climate Forecast System Version 2. *Journal of Climate*, *27*(6), 2185–2208. https://doi.org/10.1175/JCLI-D-12-00823.1

Sardeshmukh, P. D., and Hoskins, B. I. (1984). Spatial smoothing on the sphere. *Monthly weather review*, *112*(12), 2524-2529.

Schade, L. R., and Emanuel, K. A. (1999). The Ocean's Effect on the Intensity of Tropical Cyclones: Results from a Simple Coupled Atmosphere–Ocean Model. *Journal of the Atmospheric Sciences*, *56*(4), 642–651. https://doi.org/10.1175/1520-0469(1999)056<0642:TOSEOT>2.0.CO;2

Schneider, T., Bischoff, T., and Haug, G. H. (2014). Migrations and dynamics of the intertropical convergence zone. *Nature*, *513*(7516), 45–53. https://doi.org/10.1038/nature13636

Schreck, C. J., Knapp, K. R., and Kossin, J. P. (2014). The Impact of Best Track Discrepancies on Global Tropical Cyclone Climatologies using IBTrACS. *Monthly Weather Review*, *142*(10), 3881–3899. https://doi.org/10.1175/MWR-D-14-00021.1

Seager, R., Murtugudde, R., Naik, N., Clement, A., Gordon, N., and Miller, J. (2003). Air–sea interaction and the seasonal cycle of the subtropical anticyclones. *Journal of climate*, *16*(12), 1948-1966.

Skamarock, W. C., Klemp, J. B., Dudhia, J., Gill, D. O., Barker, D. M., Wang, W., and Powers, J. G. (2005). *A description of the advanced research WRF version 2*. National Center For Atmospheric Research Boulder Co Mesoscale and Microscale Meteorology Div.

Suzuki R, Behera SK, Iizuka S, Yamagata T (2004) Indian Ocean subtropical dipole simulated using coupled general circulation model. J Geophys Res 109. doi:10.1029/2003JC001974

Suzuki, T. (2011). Seasonal variation of the ITCZ and its characteristics over central Africa. *Theoretical and Applied Climatology*, *103*(1–2), 39–60. https://doi.org/10.1007/s00704-010-0276-9

References

Takong, R. R., and Abiodun, B. J. (2022). *Simulating widespread extreme rainfall events over the Drakensberg with WRF and MPAS models.* [Preprint]. In Review. https://doi.org/10.21203/rs.3.rs-2049862/v1

Tang, Chi Kit, and Johnny C.L. Chan. 2014. "Idealized Simulations of the Effect of Taiwan and Philippines Topographies on Tropical Cyclone Tracks." *Quarterly Journal of the Royal Meteorological Society* 140(682): 1578–89.

Tropical Cyclones. (2021, April 12). World Meteorological Organization. https://public.wmo.int/en/our-mandate/focus-areas/natural-hazards-and-disaster-risk-reduction/tropical-cyclones

Vitart, F., Anderson, D., and Stockdale, T. (2003). Seasonal Forecasting of Tropical Cyclone Landfall over Mozambique. *Journal of Climate*, *16*(23), 3932–3945. https://doi.org/10.1175/1520-0442(2003)016<3932:SFOTCL>2.0.CO;2

Waliser, D. E., Li, J.-L. F., L'Ecuyer, T. S., and Chen, W.-T. (2011). The impact of precipitating ice and snow on the radiation balance in global climate models: PRECIPITATING ICE, RADIATION AND GCMs. *Geophysical Research Letters*, *38*(6), n/a-n/a. https://doi.org/10.1029/2010GL046478

Walsh, K., and Watterson, I. G. (1997). Tropical Cyclone-like Vortices in a Limited Area Model: Comparison with Observed Climatology. *Journal of Climate*, *10*(9), 2240–2259. https://doi.org/10.1175/1520-0442(1997)010<2240:TCLVIA>2.0.CO;2

Watterson, I. G., Evans, J. L., and Ryan, B. F. (1995). Seasonal and interannual variability of tropical cyclogenesis: Diagnostics from large-scale fields. *Journal of Climate*, *8*(12), 3052-3066.

Weatherford, C. L. (1989). *Structural evolution of typhoons, The* (Doctoral dissertation, Colorado State University. Libraries).

Weisman, M. L., Davis, C., Wang, W., Manning, K. W., and Klemp, J. B. (2008). Experiences with 0–36-h Explicit Convective Forecasts with the WRF-ARW Model. *Weather and Forecasting*, *23*(3), 407–437. https://doi.org/10.1175/2007WAF2007005.1

Xulu, N. G., Chikoore, H., Bopape, M.-J. M., and Nethengwe, N. S. (2020). Climatology of the Mascarene High and Its Influence on Weather and Climate over southern Africa. *Climate*, *8*(7), 86. https://doi.org/10.3390/cli8070086

References

Yang, M., Zhang, D., and Huang, H. (2008). A modeling Study of Typhoon Nari (2001) at Landfall. Part I: Topographic Effects. *Journal of the Atmospheric Sciences*, *65*(10), 3095–3115. https://doi.org/10.1175/2008jas2453.1

Žagar, N., Skok, G., and Tribbia, J. (2011). Climatology of the ITCZ derived from ERA Interim reanalyses. *Journal of Geophysical Research*, *116*(D15), D15103. https://doi.org/10.1029/2011JD015695

Appendix

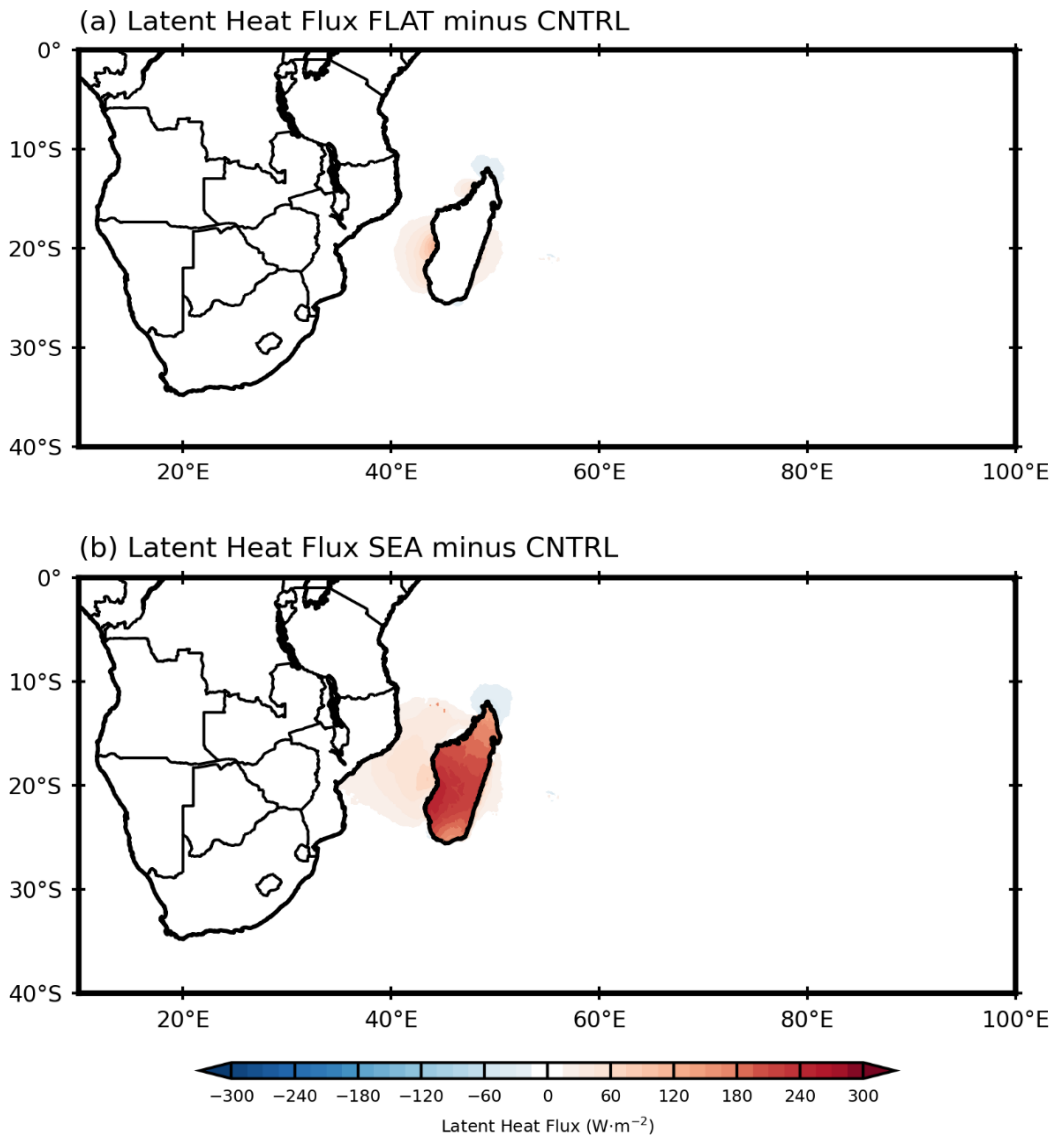

Figure 6.1: Latent Heat Flux differences (shading, $W \cdot m^{-2}$) for FLAT minus CNTRL (a) SEA minus CNTRL (b). Positive (negative) differences imply more (less) latent heat release in FLAT or SEA relative to CNTRL

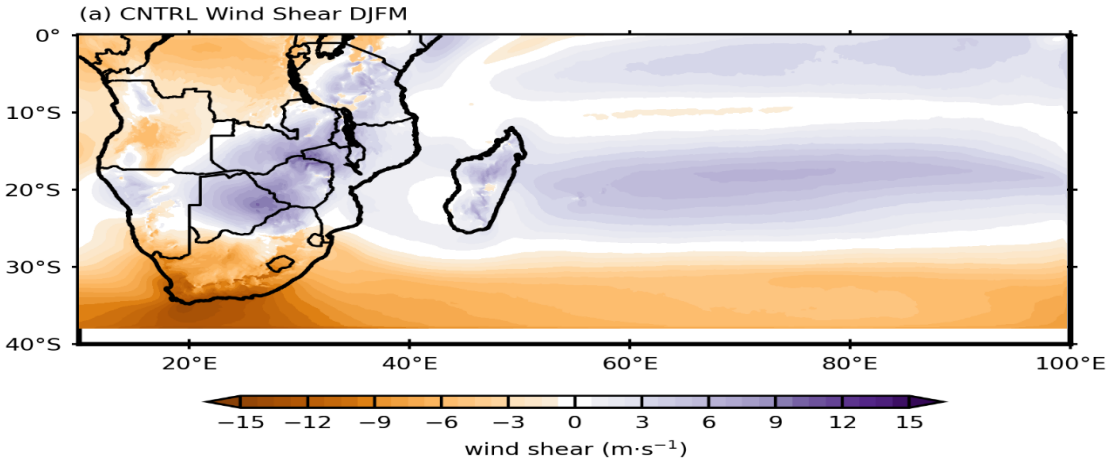

Figure 6.2: 850–500hPa CNTRL shear vector (vector; $m \cdot s^{-1}$). Positive (negative) differences imply stronger (weaker) wind shear over the CNTRL run.

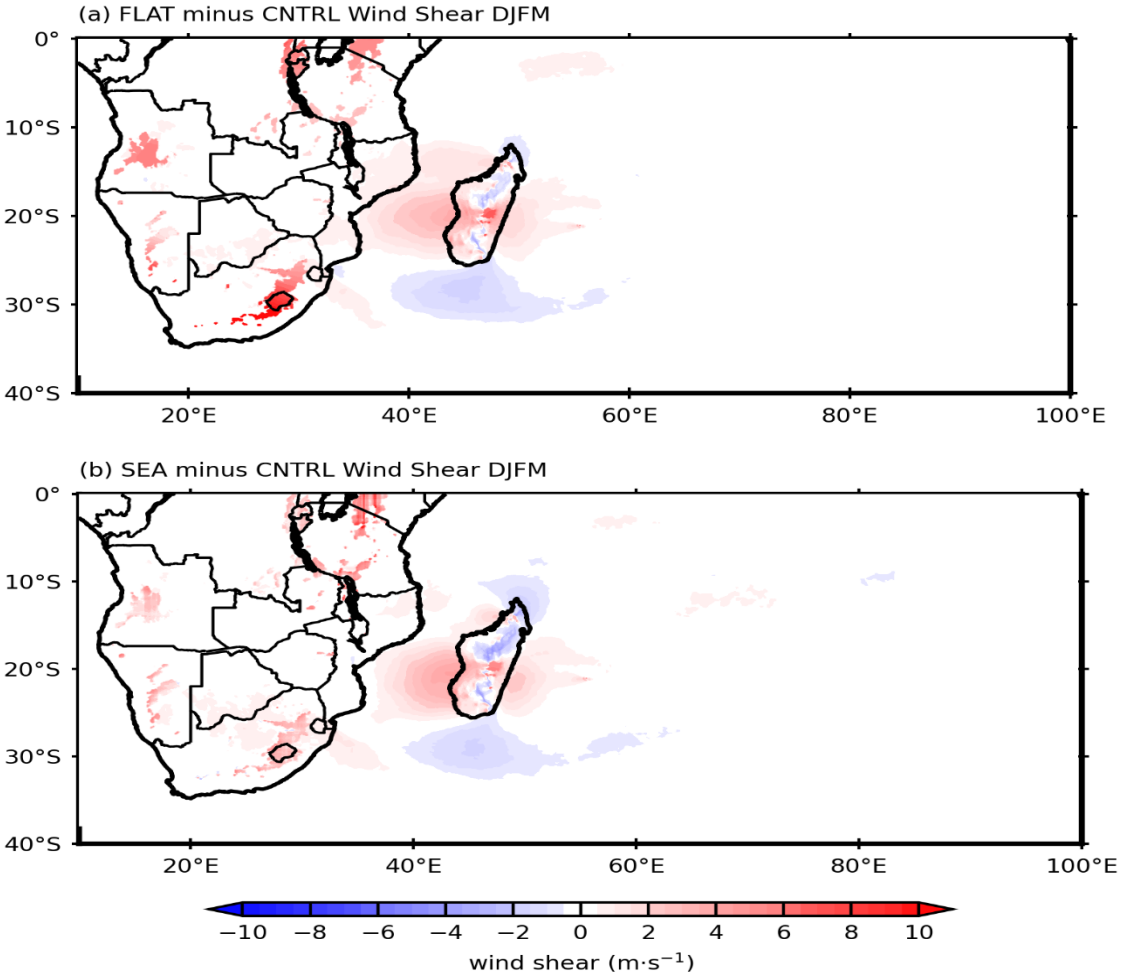

Figure 6.3: 850–500hPa shear vector anomalies (vector; $m \cdot s^{-1}$) for FLAT minus CNTRL (a) SEA minus CNTRL (b). Positive (negative) differences imply stronger (weaker) wind shear in FLAT or SEA relative to CTRL.